NASA Contractor Report 2979

Experimental Investigation of Effect of Jet Decay Rate on Jet-Induced Pressures on a Flat Plate

John M. Kuhlman, Don S. Ousterhout,
and Ronald W. Warcup

GRANT NGL-47-003-039
APRIL 1978

NASA

NASA Contractor Report 2979

Experimental Investigation of Effect of Jet Decay Rate on Jet-Induced Pressures on a Flat Plate

John M. Kuhlman, Don S. Ousterhout, and Ronald W. Warcup
Old Dominion University Research Foundation
Norfolk, Virginia

Prepared for
Langley Research Center
under Grant NGL-47-003-039

NASA
National Aeronautics
and Space Administration

Scientific and Technical Information Office

1978

EXPERIMENTAL INVESTIGATION OF EFFECT OF JET DECAY RATE ON JET-INDUCED PRESSURES ON A FLAT PLATE

By

John M. Kuhlman, Don S. Ousterhout, and Ronald W. Warcup

Old Dominion University

SUMMARY

An experimental study of the interaction between a lift jet and an aircraft wing for a jet VTOL aircraft was performed for the simplified model of an unheated, subsonic, circular jet exiting at right angles to a flat plate into a uniform subsonic crosswind. The effects of jet dynamic pressure decay rate upon the jet location and jet-induced pressure distribution on the plate were studied over a range of jet-to-crossflow velocity ratios of $2.2 \leq R \leq 10$. Jet decay rate was varied through use of cylindrical centerbodies with flat or hemispherical tips submerged in the jet nozzle at various depths below the jet exit plane.

Quicker jet dynamic pressure decay, caused by the presence of a centerbody, resulted in reductions in the jet-induced lift loss by as much as 45 percent relative to values for jets with no centerbody at larger values of crossflow velocity. Jet dynamic pressure decay rate slightly decreased the pitching moment. Also, the jet centerline trajectory was found to turn in the crossflow direction more rapidly as jet decay rate increased. Thus, future VTOL model studies must attempt to simulate as accurately as possible the anticipated jet exhaust nozzle geometry and the resulting jet decay rate to insure proper prediction of the magnitude of the jet interaction induced loads.

INTRODUCTION

The performance of jet powered VTOL aircraft has been the subject of a large amount of recent research effort. Such efforts have been aimed at the development of predictive techniques for use on specific full-scale VTOL configurations using wind tunnel models and/or mathematical models of the flowfield about the aircraft. One particular problem area of great importance is the interaction between the engine exhaust jets and the aircraft wing and fuselage in the vicinity of the jets during transition from a hover configuration to forward flight. It is found that such a jet induces negative pressures on the airframe around the exhaust, and thus an incremental loss in the lift force on the aircraft. Also, during forward flight this jet-induced pressure distribution is highly asymmetrical, with a small positive pressure region ahead of the jet and a larger negative pressure region behind the jet, thereby leading to a nose up pitching moment. Both the lift loss and pitching moment increase as forward flight speed increases.

Many previous wind tunnel studies have measured the performance and interaction effects for specific VTOL aircraft configurations (refs. 1 and 2). Also, other studies have been made of a simplified model, having the essential characteristics of the jet interaction problem; that of a circular jet exiting at right angle to a flat plate aligned parallel with a uniform crossflow. Such studies have reported both the jet-induced load distributions on the flat plate (refs. 3, 4, 5, 6, 7) and the jet trajectory as it deflects in the direction of the crossflow (refs. 8, 9, 10). Fearn and Weston (ref. 3) found the key nondimensional parameter governing the distribution and magnitude of the jet-induced load to be the jet-to-crossflow velocity ratio, R, for jets with very uniform initial dynamic pressure profiles. In another paper the same authors modelled the interaction of a jet and a crosswind as a pair of contrarotating

vortices (ref. 11). Characteristics of this vortex pair have been documented by Kamotani and Greber (ref. 9). This vortex jet model has been utilized by Dietz (ref. 12) in a mathematical model to predict jet-induced plate surface pressures based upon the location and strength of the vortex pair associated with the jet. Work on the jet-crossflow interaction problem related to VTOL aircraft performed before 1970 has been summarized by Margason (ref. 13).

Most of these studies have been made for configurations with essentially uniform jet exit dynamic pressure profiles. This is, however, not the type of initial profile to be expected in actual VTOL aircraft exhaust jets (refs. 14, 15, 16, 17), due to the ducting and slotted nozzle vanes, as well as to the annular nature of the flow through the engine itself. Ziegler and Wooler (ref. 18) and Livingston (ref. 19) have studied some effects of stratified, nonuniform jets and have found different induced pressures than for models with uniform initial jet dynamic pressure profiles. Further, Gentry and Margason (ref. 20) have found for a jet in hover that the lift loss was greatly affected by the jet decay rate, the lift loss being increased as the jet decay rate increased.

The current work is an extension of the work by Livingston (ref. 19), systematically investigating the effects of varying jet decay rate upon the jet-induced pressure distribution and jet centerline location for a circular, subsonic air jet exiting perpendicular to a flat plate into a uniform, subsonic crossflow. Jet decay rate has been varied through use of cylindrical centerbodies submerged in the jet nozzle at various depths below the exit plane. Data has been obtained over a range of jet-to-crossflow velocity ratios of $2.2 \leq R \leq 10$. Results are presented in graphical form for the jet centerline trajectories, jet centerline dynamic pressure decay, integrated lift loss and pitching moment, and pressure coefficient distributions. The

present results have been briefly summarized by Kuhlman and Warcup (ref. 21).

SYMBOLS

Data are presented in nondimensional form, or in both SI Units and U.S. Customary Units where appropriate. Measurements and calculations have been made in U.S. Customary Units.

A	effective jet exit area, m^2 (ft^2)
c_p	pressure coefficient, $\frac{p - p_{no\ jet}}{q_\infty}$
D	effective jet diameter, m (ft)
D_n	nominal jet diameter (jet orifice diameter), m (ft)
ΔL	jet-induced lift loss, N (lb)
ΔM	jet-induced pitching moment, m-N (ft-lb)
p	static pressure, N/m^2 (lb/ft^2)
q	dynamic pressure, N/m^2 (lb/ft^2)
q_∞	crossflow dynamic pressure, N/m^2 (lb/ft^2)
r	radius, m (ft)
R	$\frac{V_e}{V_\infty}$ jet-to-crossflow velocity ratio
s	arc length measured along jet trajectory, m (ft)
T	jet thrust, N (lb)
V_e	effective jet exit velocity, m/s (ft/s)
V_∞	crossflow velocity, m/s (ft/s)
x	streamwise coordinate, origin at center of jet orifice, m (ft)
y	transverse coordinate, origin at center of jet orifice, m (ft)

z coordinate perpendicular to plate, origin on plate surface, m (ft)

Subscripts:

∞ free stream

e effective

max maximum

n nominal

no jet value measured with zero jet velocity

APPARATUS

The experimental study was conducted in the low speed closed circuit wind tunnel located at Old Dominion University, which has a test section 0.915 m by 1.22 m (3 ft by 4 ft). Crossflow airspeeds ranged from 13.7 m/s to 62 m/s (45 ft/s to 203 ft/s), corresponding to free stream Mach numbers of 0.04 to 0.18. Jet Mach number based on the jet effective exit velocity was 0.4, and jet Reynolds number based on the jet effective diameter was 2×10^5.

The flat plate was made from hard board sheet 0.915 m or 35.4 D_n wide by 1.22 m or 47.3 D_n long. The plate was 0.019 m (0.062 ft) thick, fitted with a round leading edge, and mounted 0.106 m from the tunnel test section floor. The boundary layer on the flat plate was tripped using a method described by Braslow, Hicks, and Harris (ref. 22). A view of the plate mounted in the test section appears in figure 1.

The jet exited perpendicular to the plate through a circular orifice 0.0258 m (0.085 ft) in diameter. The nozzle center was located 0.6 m (2 ft) back from the plate leading edge on the plate centerline.

The plate was fitted with 226 static pressure taps located on rays emanating from the center of the jet as shown in figure 2. These ports were made of 0.061 cm diameter stainless steel tubing. The distances from the nozzle centerline to the various static pressure tap locations are listed in table 1.

The air jet was created by an air compressor connected to a 0.14 m (0.466 ft) diameter plenum chamber and a smoothly contoured 30:1 area contraction ratio nozzle. A section view of the plenum and nozzle is shown in figure 3. Jet air flow rates were measured using a turbine type flowmeter. Jet mass flow rate was held constant on any one test run, using an electronic feedback control, to within ±0.2 percent.

Also shown in figure 3 is an example of the type of centerbody, or plug, used to vary the jet dynamic pressure decay rate. The centerbody shown is cylindrical, with a diameter of 0.019 m (0.062 ft, or 0.75 D_n), having a hemispherical tip pointed in the jet flow direction. Also utilized in some tests was a second cylindrical plug of the same diameter with a flat, or square, end. Jet decay rate was varied by varying the submergence depth of the plug tip beneath the jet exit plane.

The plate static pressure ports were connected by plastic tubing through four scanning type valves to a capacitance type pressure transducer and digital readout device. The pressure transducer was calibrated using a dead weight tester.

A motorized, three degrees of freedom traversing mechanism was mounted to the top of the tunnel test section; this traverse is shown in figure 1. Pitot static and total head probes were mounted to the traverse to investigate the characteristics of the jet, such as centerline location and dynamic pressure decay.

Temperatures were monitored using 0.025 cm diameter chromel-alumel thermocouples. Tunnel temperature was nominally 310 K (560 R), with the jet exit temperature nominally 15 K (27 R)

below the tunnel temperature. Tunnel temperatures gradually increased during each individual data run, but this temperature increase was generally less than 12 K (22 R).

EXPERIMENTAL PROCEDURE

The plate was initially aligned parallel to the plane of the tunnel test section floor. Flow angularity between the plate and the crossflow was less than 0.5 degrees, based upon measured static pressures on the plate with no jet flow. The plate surface was carefully waxed. The gap between the plate and the nozzle was filled and smoothed. A separation bubble was observed at the plate leading edge which extended 0.08 m in the transverse and 0.05 m in the flow directions. Tufts placed on the plate showed no other flow irregularities. Turbulence intensities in the crossflow were nominally 0.2 percent as measured with a hot wire anemometer. The crossflow was measured to be uniform to within 1 percent in a plane perpendicular to the flow direction over the jet exit.

The jet nozzle and plenum were aligned with the plate to insure axial symmetry of the jet-induced plate pressure distribution for a representative nozzle configuration with no centerbody and no crossflow.

Jet exit plane dynamic pressure profiles were measured in the no crossflow or static case using a pitot static probe. The centerbodies were adjusted in the jet nozzle to insure symmetry of the initial jet profiles with no crossflow. The measured dynamic pressure profiles were used to calculate the jet thrust, since it was not feasible to measure thrust directly. Jet configurations with no centerbody in the nozzle were found to have uniform dynamic pressure profiles (to within 1 percent) with radius, until the nozzle boundary layer was reached. Examples of the effect of the centerbodies on the initial dynamic pressures are shown in nondimensional form in figure 4. Generally, as the centerbody tip was moved toward

the nozzle exit plane the exit dynamic pressure profiles became more nonuniform, with the momentum defect at the jet axis becoming larger.

For the various nozzle configurations calibrated above, the jet-induced pressures on the plate were measured for a range of crossflow velocities. Static pressures were electrically averaged at each port location for a minimum of 5 seconds, to obtain a good mean value, since Fearn and Weston (ref. 3) and Kuhlman (ref. 23) have observed large, low frequency static pressure fluctuations on the plate in the lee of the jet. Static pressure data presented are the difference between jet on and jet off conditions. The jet induced lift loss, ΔL, and pitching moment, ΔM, were obtained by integrating these static pressure differences using a constant pressure panel approximation.

Jet centerline locations were measured for each nozzle configuration over a range of crossflow speeds using a total pressure Kiel probe mounted on the traverse. The jet centerline location was defined to be the locus of points of maximum total pressure in the plane of symmetry of the flow.

Dynamic pressure decay along the jet centerline for these configurations was measured using a pitot static probe. The centerline trajectory data were numerically curve fitted, and used to orient the pitot probe tangent to the local flow direction. These dynamic pressure decay data are the maximum local dynamic pressures at various positions along the arc length of the jet trajectory.

Data for different nozzle configurations or different centerbody locations have been compared at the same value of jet-to-crossflow velocity ratio using a technique described by Ziegler and Wooler (ref. 18) and Livingston (ref. 19). All nozzle configurations have been tested at approximately the same effective jet exit velocity, corresponding to a jet Mach number of 0.4.

The effective velocity has been calculated as that of an equivalent jet with a constant dynamic pressure and circular shape created by an isentropic expansion from the measured stagnation conditions in the plenum to the measured jet exit static pressure. This equivalent jet is also required to have the same mass flow rate and thrust, T, as measured for the actual jet with a nonuniform exit dynamic pressure profile. Also calculated from this procedure is a circular effective jet area, from which an effective jet diameter, D, has been calculated. The effective jet diameter decreases as the centerbody tip is moved toward the jet exit plane. The effective jet diameter has been used to nondimensionalize all dimensions, such as jet centerline location, distance along the jet centerline, and plate surface area. The effective jet velocity has been used to calculate the jet-to-crossflow velocity ratio, R. This is in contrast to the usual procedure where R is defined as the square root of the ratio of jet to crossflow dynamic pressures, but it is estimated that this generally leads to no more than a 5 percent change in the computed velocity ratio. However, uncertainties in D and R of 10 percent are estimated for the flat-ended plug flush configuration due to an inaccuracy in the measured thrust.

It is estimated that flow conditions during any one run were constant to within 1 to 2 percent. Jet centerline locations were repeatable to within 2 percent. Static pressures on the plate were generally repeatable to within 2 percent, and the integrated lift losses and pitching moments and the jet dynamic pressure decay data are estimated to have an accuracy of 5 percent.

PRESENTATION OF RESULTS

Data for the jet-induced plate surface static pressure distribution, jet centerline location, jet-induced lift loss and pitching moment, and jet dynamic pressure decay have been obtained for a range of jet-to-crossflow velocity ratios of

$2.2 \leq R \leq 10$. These data have been obtained for the following jet centerbody configurations:

1. no centerbody

2. round ended centerbody with tip submerged one nominal jet exit diameter, D_n , below nozzle exit plane

3. round ended centerbody submerged 0.5 D_n below nozzle exit

4. round ended centerbody flush with nozzle exit

5. flat ended centerbody submerged 1.375 D_n below nozzle exit

6. flat ended centerbody submerged 0.875 D_n below nozzle exit

7. flat ended centerbody submerged 0.375 D_n below nozzle exit

8. flat ended centerbody flush with nozzle exit

Results of these wind tunnel studies for various configurations and values of R are presented in the following figures:

DATA	FIGURE
Constant pressure contours	5-38
Jet centerline locations	39-47
Jet-induced nondimensional lift loss	48-49
Jet-induced nondimensional pitching moment	50-51
Jet centerline dynamic pressure decay	52-60

DISCUSSION OF RESULTS

As displayed in figures 5 through 38, the jet-induced plate pressure distributions are generally characterized by a small positive pressure region ahead of the jet and a much larger negative pressure region to the side of and behind the jet. As observed by Fearn and Weston (ref. 3), the jet-to-crossflow ratio, R, is a key parameter governing the distribution of the jet-induced loads. As the crossflow increases, corresponding to a decrease in R, the pressures become more asymmetrical fore-to-aft. In figure 9 the present data for a configuration with no centerbody in the nozzle at $R = 3.9$ are compared with data of Fearn and Weston (ref. 3) at the same value of R and a similar jet Mach number. Constant pressure contours generally agree with the data of reference 3 to within the estimated accuracy with which their locations can be determined except in the vicinity directly behind the jet.

Data taken at similar values of R, but with a centerbody in the nozzle, generally show very similar pressure contours ahead of the jet, but greatly changed contours behind the jet. As the centerbody tip is moved toward the jet exit plane, these contours in the lee of the jet are pulled in closer to the jet exit. Thus, the data indicate that the presence of a centerbody in the jet nozzle significantly affects the jet-induced pressure distribution, especially at the lower values of R (higher crossflow). Similar pressure contour shapes have been reported in reference 4.

Jet centerline trajectories for a range of jet-to-velocity ratios for jet configurations with no centerbody are compared in figure 39 with similar data taken by Margason (ref. 8). Results shown are a least squares power law fit to the actual data. As the crossflow increases (R decreasing), the jet is deflected more rapidly in the crossflow direction.

As shown in figures 40 to 47, for fixed values of the velocity ratio, R, the presence of a centerbody in the jet nozzle causes a slight increase in the jet turning. As the plug

tip is moved up towards the nozzle exit, this turning generally becomes more rapid. Hence, jets for configurations with centerbodies lie slightly closer to the plate surface.

Results of numerical integration of the pressure data previously displayed in figures 5 to 38 appear in figure 48 for nozzle configurations with the hemispherical tipped centerbody (round ended plug) and figure 49 for flat ended centerbody configurations. The lift loss has been calculated for a circular area on the plate equal to 43 times the jet effective exit area, and nondimensionalized by the calculated jet thrust. On both figures the current results for nozzles with no plug are displayed for comparison purposes. For each particular nozzle configuration as the crossflow speed increases, moving from left to right on the horizontal axis, the jet-induced lift loss, ΔL , increases greatly, reaching 70 percent of the jet thrust at $(R)^{-1} \simeq 0.4$ for the no plug configuration. Two approximate integrations of the pressure contour results of Fearn and Weston (ref. 3) are shown in figure 48 for comparison with the present results for jets with no centerbodies. The present lift losses for jets with no centerbody are roughly 75 percent as great as results at the same value of R by Fearn and Weston from reference 3.

From the curves for various nozzle configurations in figures 48 and 49 at a fixed value of crossflow-to-jet velocity ratio, it is seen that the presence of a centerbody in the jet nozzle greatly reduces the jet-induced lift loss. This reduction in ΔL increases as either plug tip is moved closer to the nozzle exit plane, reaching a 35 percent reduction over the no plug case at $R^{-1} \simeq 0.4$ for the round ended plug tip flush to the plate surface, and a 45 percent reduction over the no plug case at $R^{-1} \simeq 0.4$ for the flat plug flush.

Figures 50 and 51 show the pitching moment about the transverse axis through the jet origin, nondimensionalized by the

calculated jet thrust times the effective jet diameter for the round ended and flat ended plug configurations respectively. Again, the pitching moment has been calculated for a circular area on the plate equal to 43 times the jet effective exit area. As observed for the lift loss, the nose up induced pitching moment increases as the crossflow is increased, corresponding to increased forward flight speeds. The pitching moment is slightly decreased by the presence of a centerbody in the jet nozzle at higher values of crossflow velocity.

The effect of crossflow on the jet centerline decay is shown in figure 52, for jets with no centerbody in the nozzle. The ratio of the local maximum dynamic pressure minus the free stream q_∞ divided by exit plane maximum q_{max} minus free stream q_∞ is shown as a function of nondimensional arc length along the jet trajectories shown earlier in figures 39 to 47. With no crossflow $(R = \infty)$ the jet was observed to have a potential core that persisted over 5 effective jet diameters from the exit plane. As the crossflow increased, corresponding to decreasing R, the dynamic pressure decay rate increased until it appeared that the maximum dynamic pressure began to decrease within one jet diameter of the jet exit at $R = 2.5$.

Figure 53 compares results for the nondimensional jet centerline dynamic pressure decay at a constant jet-to-crossflow velocity ratio of $R = 8$ for the round ended plug configurations with results shown in the previous figure for the no plug case. As the plug tip is moved upwards toward the jet exit plane, the jet decay to the crossflow q occurs more rapidly. Similar results are seen in figure 54 for nozzle configurations with the flat ended plug at $R = 8$. Again the plug causes quicker jet decay. Figures 55 through 60 show similar results for the various plug locations at values of R of 6, 4, and 2.5. In all cases the jet centerline dynamic pressure decays more rapidly as the centerbody is moved toward the jet exit plane.

The effects of a centerbody in the jet nozzle may be summarized as resulting in:

1. nonuniform initial jet dynamic pressure profiles,
2. more rapid jet turning,
3. more rapid jet centerline dynamic pressure decay, and
4. decreased induced lift loss at high crossflow,

assuming the velocity ratio is held constant. This reduced induced loading on the plate occurs in spite of the fact that the jet is observed to lie closer to the plate. Based on results in reference 11, this indicates that the centerbody causes a weakening of the vortex pair associated with the jet. Also, the current results, where increased jet decay rate leads to a decreased induced lift loss for a jet in a crossflow, show an opposite trend than was observed by Gentry and Margason (ref. 20) for jets with no crossflow.

The current results, where the centerbody causes quicker jet decay and a redistribution of the induced loads, explain discrepancies between data of Ousterhout (ref. 4) and data of other investigators (refs. 3, 5, 6, 7). The jet used in reference 4 was observed to begin to decay much more rapidly than jets used in the other investigations, where a potential jet core generally existed for 4 to 6 diameters beyond the jet exit. This quicker jet decay in reference 4 is believed to be the cause of the observed pinching in of the pressure contours behind the jet exit.

Further, the present results indicate that jet decay rate has a significant effect upon jet-induced loads around the jet. Model jet VTOL studies such as references 1 and 2 must therefore attempt to match prototype jet exit and decay characteristics.

CONCLUSIONS

The current experimental studies into the effect of jet decay rate on jet location and jet-induced loads on a flat plate have shown that:

1. The presence of a centerbody in the jet nozzle leads to nonuniform jet exit dynamic pressure profiles and more rapid decay of the jet dynamic pressure.

2. More rapid jet dynamic pressure decay rates result in slightly more rapid deflection of the jet in the free steam direction.

3. More rapid jet decay rate leads to a change in the jet-induced pressures on the flat plate, where plate constant pressure contours behind the jet move nearer to the jet exit as jet decay rate increases.

4. Increased jet decay rate leads to a large decrease in the jet-induced lift loss, and a slight decrease in pitching moment.

It is therefore recommended that all experimental VTOL model studies and theoretical models attempt to duplicate as nearly as possible the anticipated full scale jet exhaust decay characteristics to insure proper prediction of the jet interference loading on the aircraft.

REFERENCES

1. Vogler, Raymond D.: Interference Effects of Single and Multiple Round or Slotted Jets on a VTOL Model in Transition. NASA TN D-2380, August 1964.

2. Margason, Richard J.; and Gentry, Garl L., Jr.: Aerodynamic Characteristics of a Five-Jet VTOL Configuration in the Transition Speed Range. NASA TN D-4812, 1968.

3. Fearn, Richard L.; and Weston, Robert P.: The Induced Pressure Distribution of a Jet in a Crossflow, NASA TN D-7916, July 1975.

4. Ousterhout, Donald S.: An Experimental Investigation of a Cold Jet Emitting from a Body of Revolution into a Subsonic Free Stream. NASA CR-2089, August 1972.

5. Soullier, A.: Testing at SI. MAS for Basic Investigation on Jet Interactions. Distribution of Pressures Around the Jet Orifice. NASA TTF-14066, April 1968.

6. Bradbury, L. J. S.; and Wood, M. N.: The Static Pressure Distribution Around a Circular Jet Exhausting Normally from a Plane Wall Into an Airstream. British ARC C. P. No. 822, 1965.

7. Vogler, Raymond D.: Surface Pressure Distributions Induced on a Flat Plate by a Cold Air Jet Issuing Perpendicularly from the Plate and Normal to a Low Speed Free-Stream Flow. NASA TN D-1629, March 1963.

8. Margason, Richard J.: The Path of a Jet Directed at Large Angles to a Subsonic Free Stream. NASA TN D-4919, November 1968.

9. Kamotani, Yasuhiro; and Greber, Isaac: Experiments on a Turbulent Jet in a Cross Flow. NASA CR-72893, June 1971.

10. Rudinger, G.; and Moon, L. F.: Laser-Doppler Measurements in a Subsonic Jet Injected into a Subsonic Cross Flow. ASME Journal of Fluids Engineering, September 1976, pp. 516-520.

11. Fearn, Richard; and Weston, Robert P.: Vorticity Associated with a Jet in a Cross Flow. AIAA Journal, Vol. 12, No. 12, December 1974, pp. 1666-1671.

12. Dietz, W. E., Jr.: A Method for Calculating the Induced Pressure Distribution Associated with a Jet in a Crossflow. M.S. Thesis, Florida University, 1975 (also available as NASA CR 146434, 1975).

13. Margason, Richard J.: Review of Propulsion-Induced Effects on Aerodynamics of Jet/STOL Aircraft. NASA TN D-5617, February 1970.

14. Hall, Gordon R.; and Rogers, Kenneth H.: Recirculation Effects Produced by a Pair of Heated Jets Impinging on a Ground Plane. NASA CR-1307, May 1969.

15. Abbott, W. A.: Studies of Flow Fields Created by Vertical and Inclined Jets when Stationary or Moving over a Horizontal Surface. British ARC C. P. No. 911, 1967.

16. Hall, Gordon R.: Recirculation and Injestion Characteristics of a Large-Scale VTOL Lift Engine Pod. NASA CR-72410, August 1968.

17. Ryan, Patrick E.; and Cosgrove, Wayne J.: The Effect of Exhaust Conditions, Surface Winds, and Geometric Scale on Hot Gas Ingestion for Two Jet VTOL Configurations. NASA CR-66965, September 1970.

18. Ziegler, H.; and Wooler, P. T.: Analysis of Stratified and Closely Spaced Jets Exhausting into a Crossflow. NASA CR-132297, November 1973.

19. Livingston, D. K.: An Experimental Investigation of a Cold Jet with Solid Center Body Emitting from a Flat Plate into a Subsonic Free Stream. M.S. Thesis, Old Dominion University, May 1975.

20. Gentry, Garl L.; and Margason, Richard J.: Jet Induced Lift Losses on VTOL Configurations Hovering In and Out of Ground Effect. NASA TN D-3166, February 1966.

21. Kuhlman, J. M.; and Warcup, R. W.: Effects of Jet Decay Rate on Jet Induced Loads on a Flat Plate. AIAA Paper No. 77-596, Proceedings of AIAA/NASA V/STOL Conference, Palo Alto, California, June 6-8, 1977.

22. Braslow, A. L.; Hicks, R. M.; and Harris, R. V., Jr.: Use of Grit-Type Boundary-Layer-Transition Trips. Presented at Conference on Aircraft Aerodynamics, Langley Research Center, May 23-25, 1966, published in NASA SP-124.

23. Kuhlman, J. M.: A Vorticity Shedding Phenomenon in the Wake of an Air Jet in a Crossflow. Virginia Journal of Science, Vol. 26, No. 2, p. 106.

Table 1. Flat plate pressure port locations.

Pressure Port No.	Radial Distance cm	(in.)
1	1.905	(0.750)
2	2.223	(0.875)
3	2.540	(1.000)
4	3.493	(1.375)
5	4.445	(1.750)
6	5.398	(2.125)
7	6.350	(2.500)
8	7.303	(2.875)
9	8.255	(3.250)
10	9.208	(3.625)
11	10.160	(4.000)
12	11.430	(4.500)
13	12.700	(5.000)
14	13.970	(5.500)
15	15.240	(6.000)
16	16.510	(6.500)
17	17.780	(7.000)
18	19.050	(7.500)
19	20.320	(8.000)
20	20.638	(8.125)
21	20.955	(8.250)
22	21.273	(8.375)
23	21.590	(8.500)

Figure 1. Experimental apparatus.

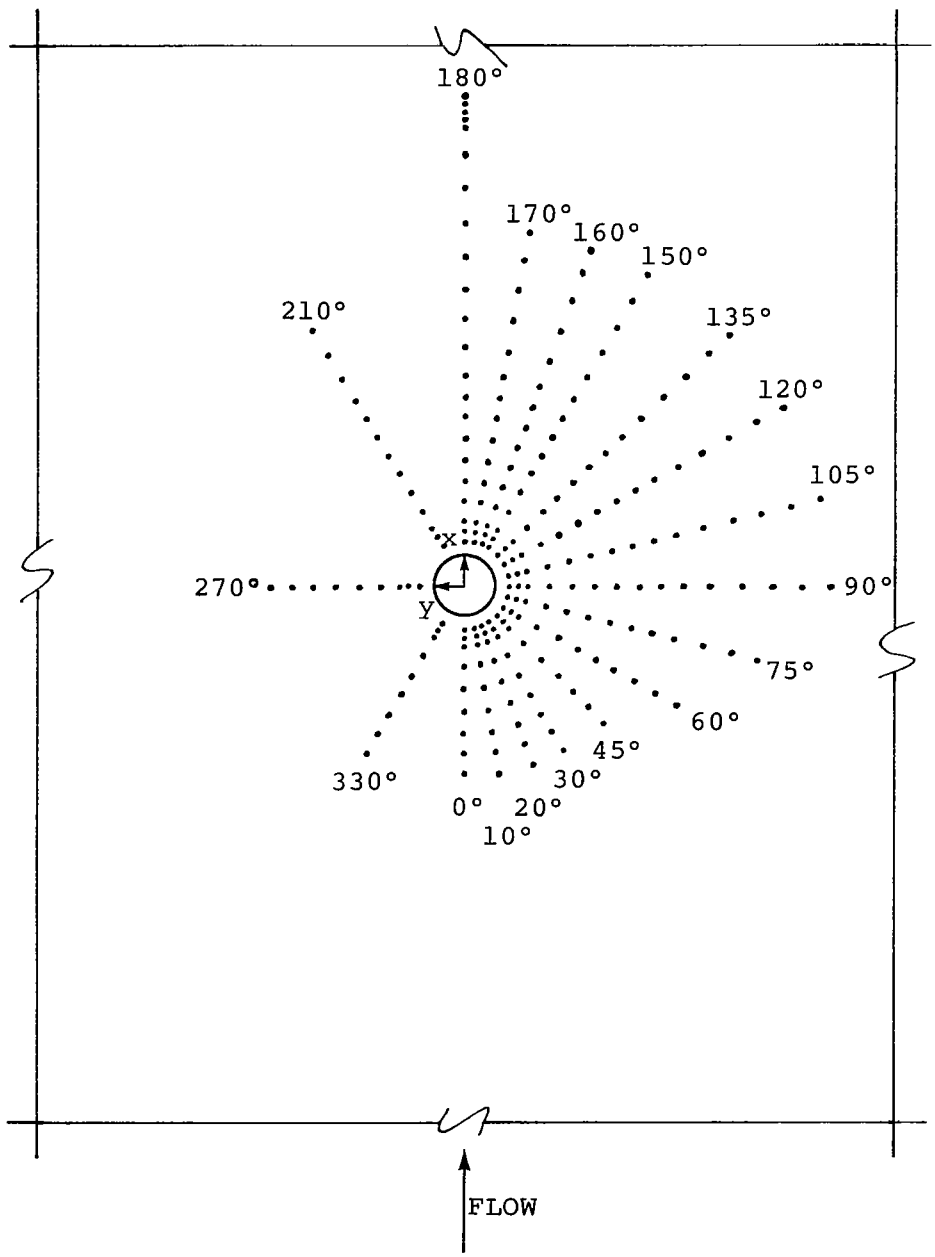

Figure 2. Plate pressure port distribution.

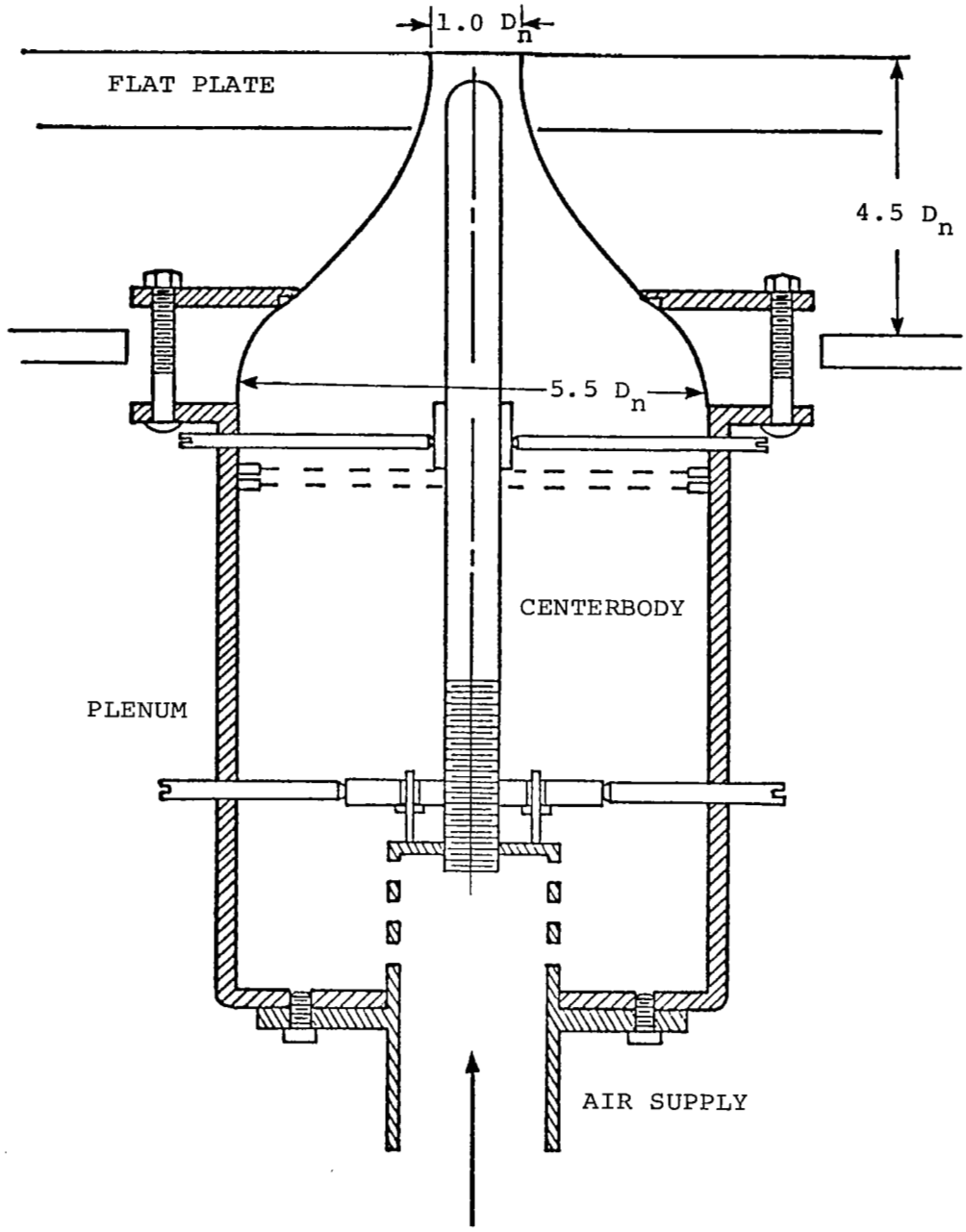

Figure 3. Cross-sectional view of jet nozzle, plenum, and centerbody.

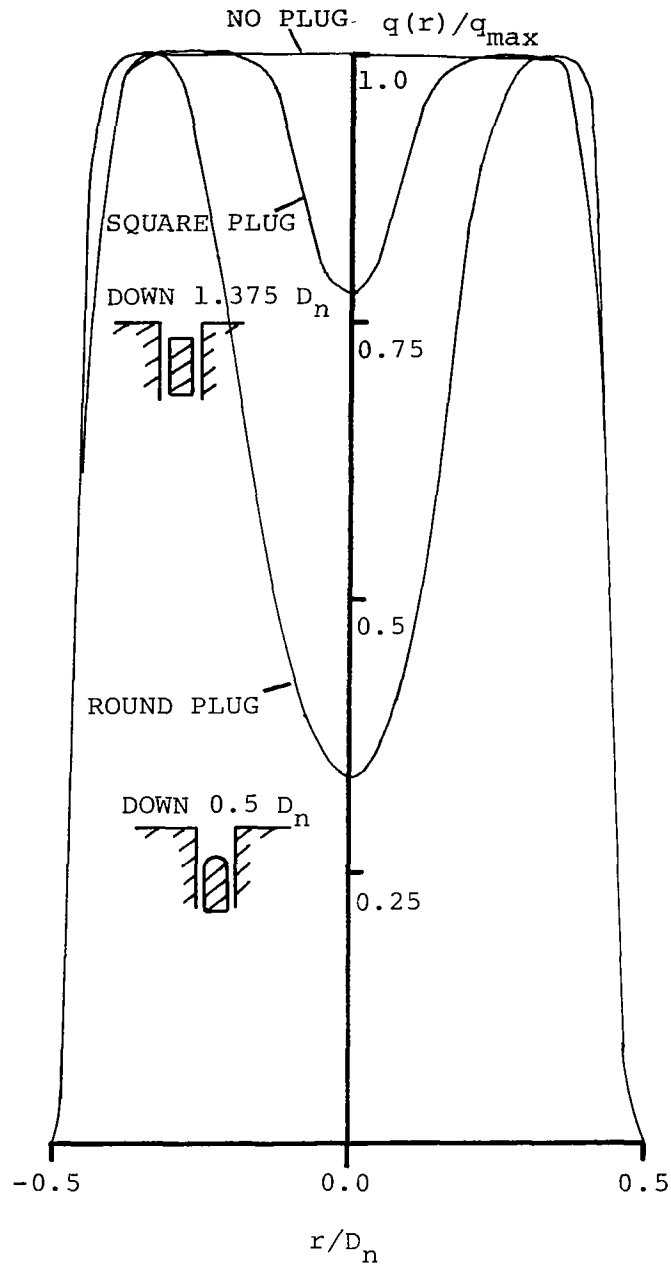

Figure 4. Examples of nondimensional jet exit plane dynamic pressure profiles, no crossflow.

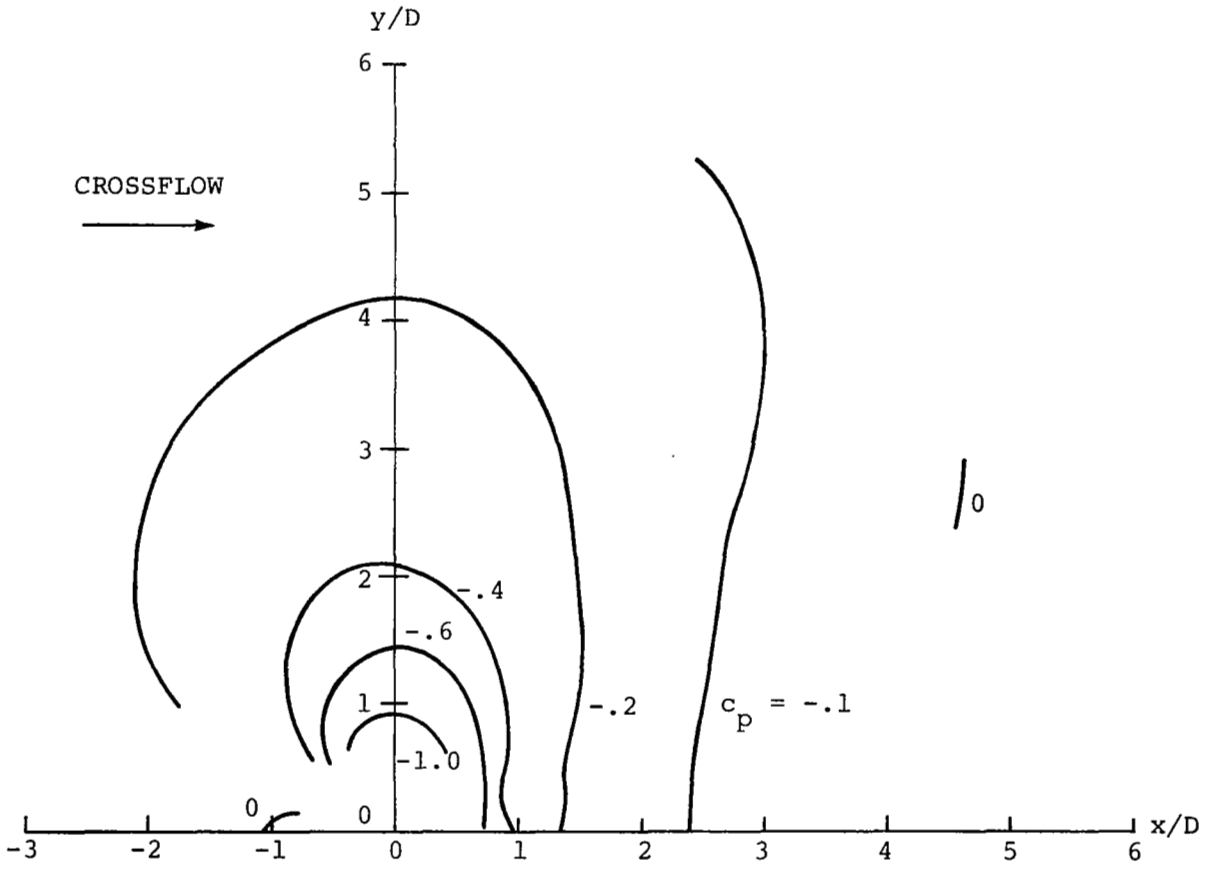

Figure 5. Constant pressure contour data; no plug, R = 9.11.

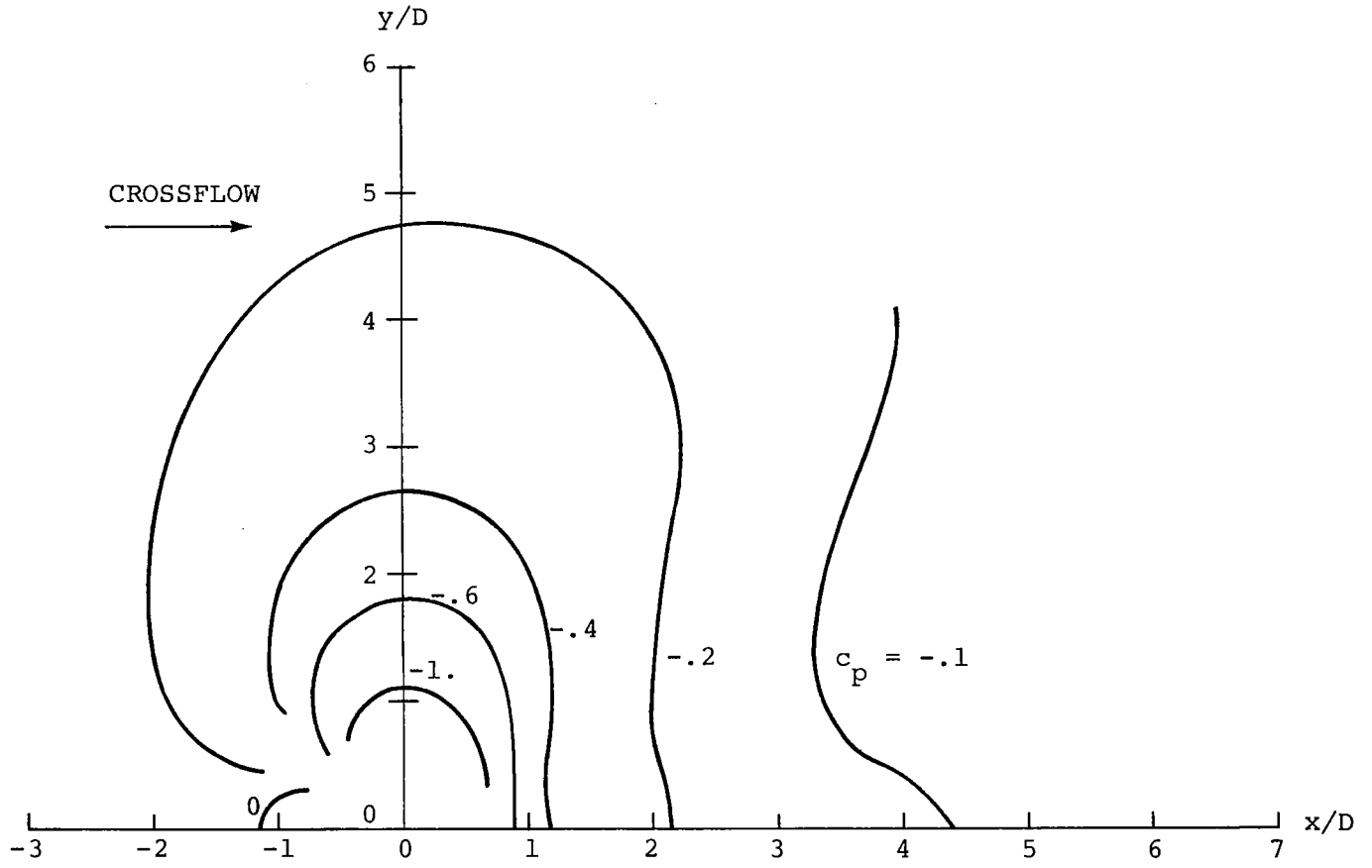

Figure 6. Constant pressure contour data; no plug, R = 7.81.

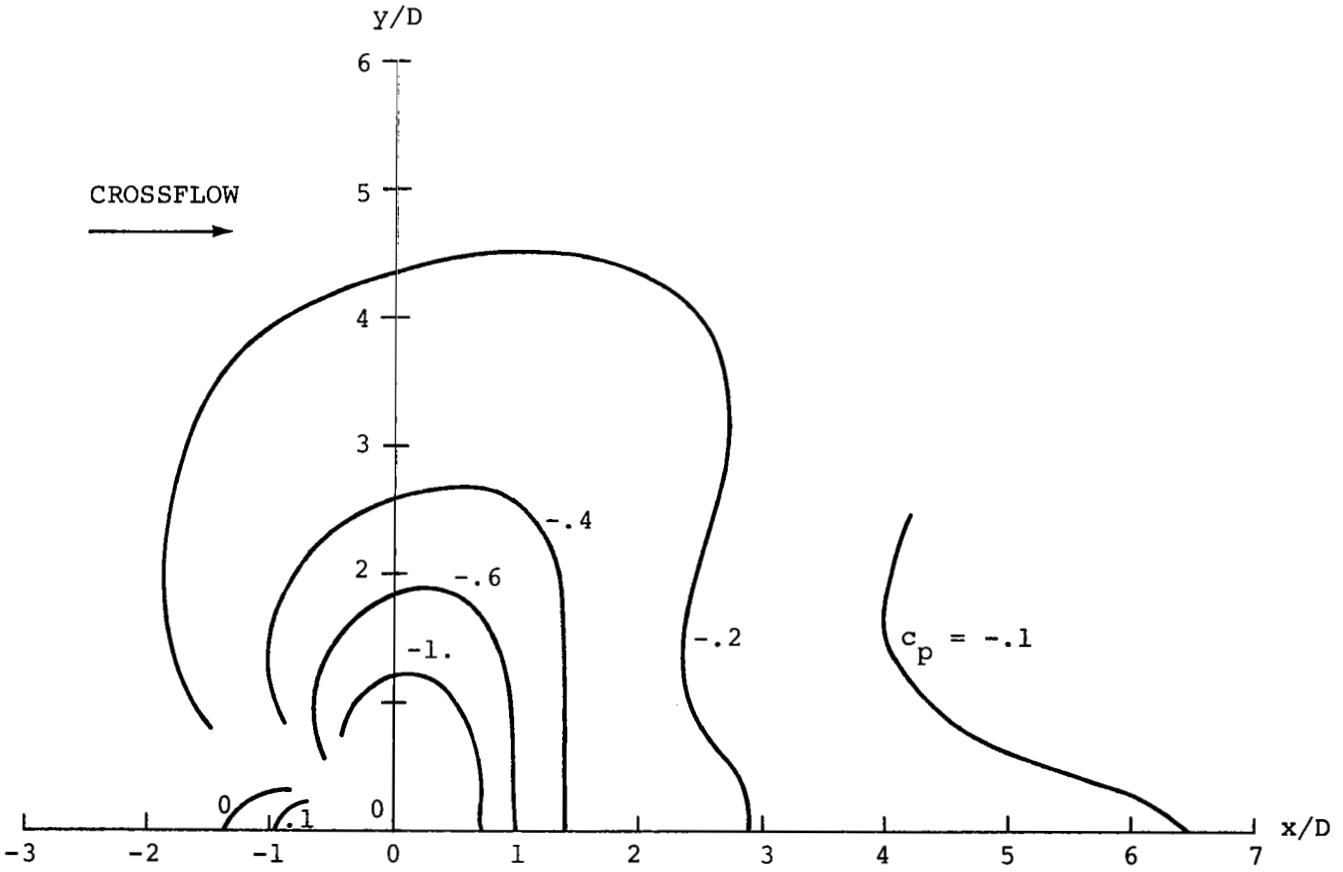

Figure 7. Constant pressure contour data; no plug, R = 6.51.

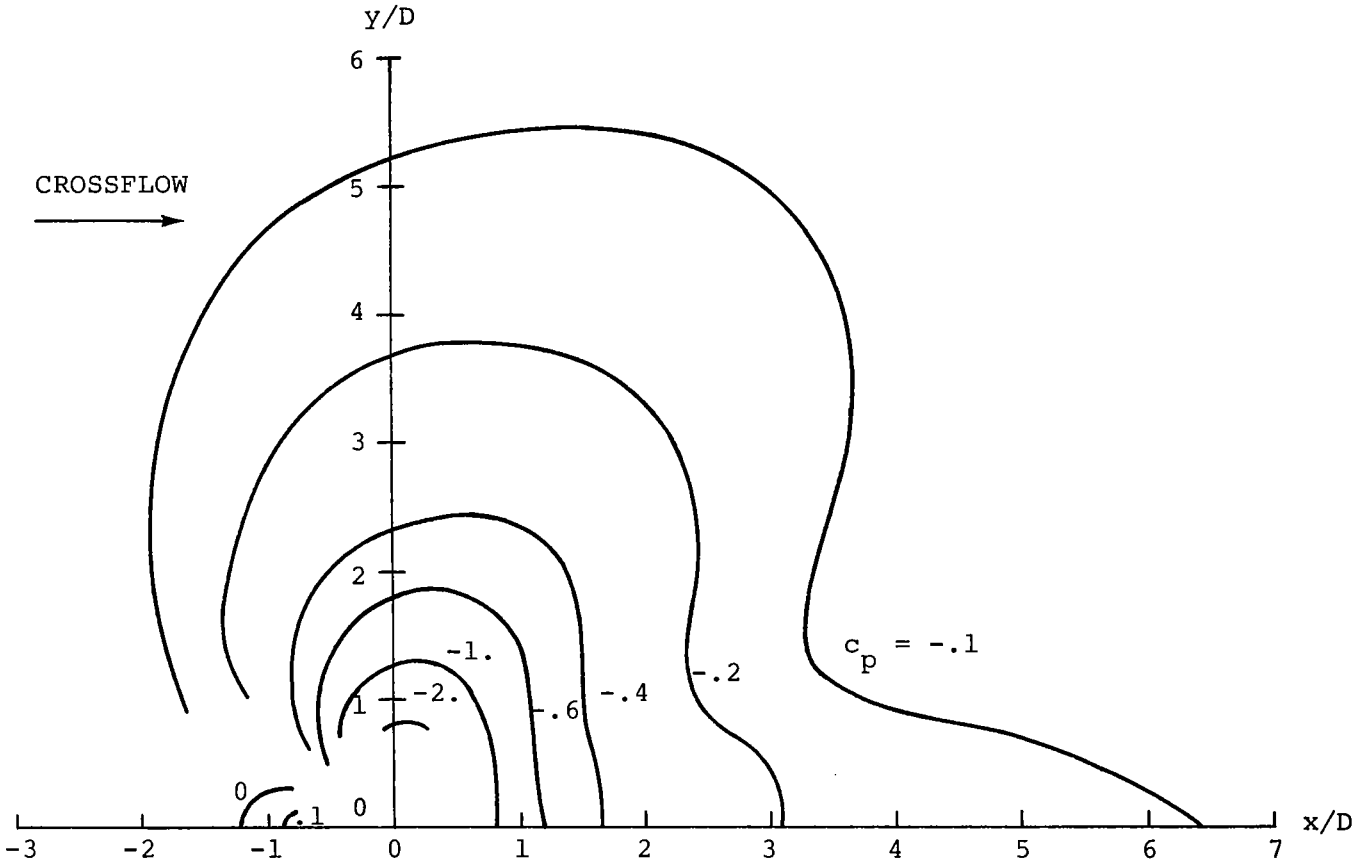

Figure 8. Constant pressure contour data; no plug, R = 5.20.

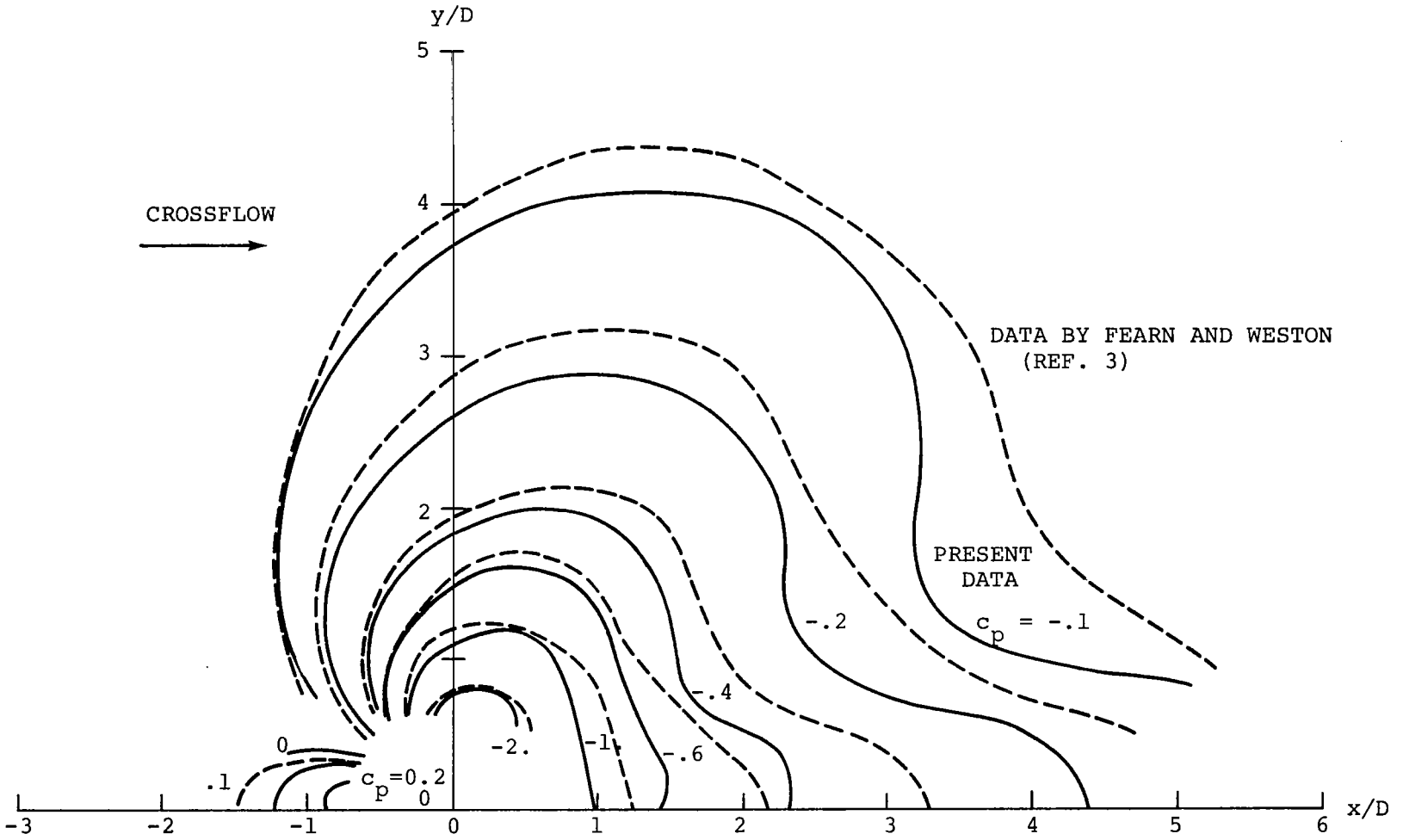

Figure 9. Constant pressure contour data; no centerbody in nozzle, R = 3.9.

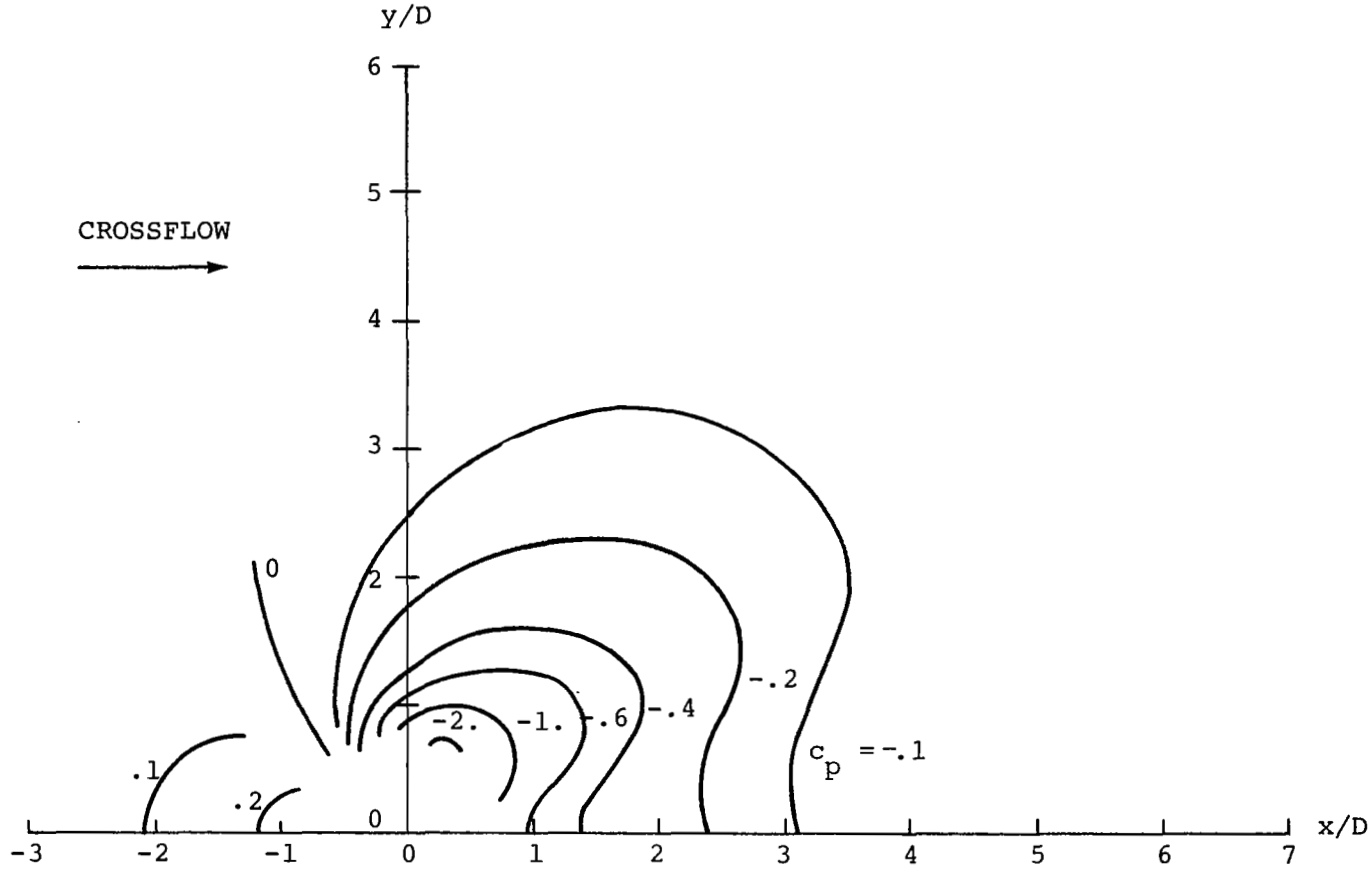

Figure 10. Constant pressure contour data; no plug, R = 2.60.

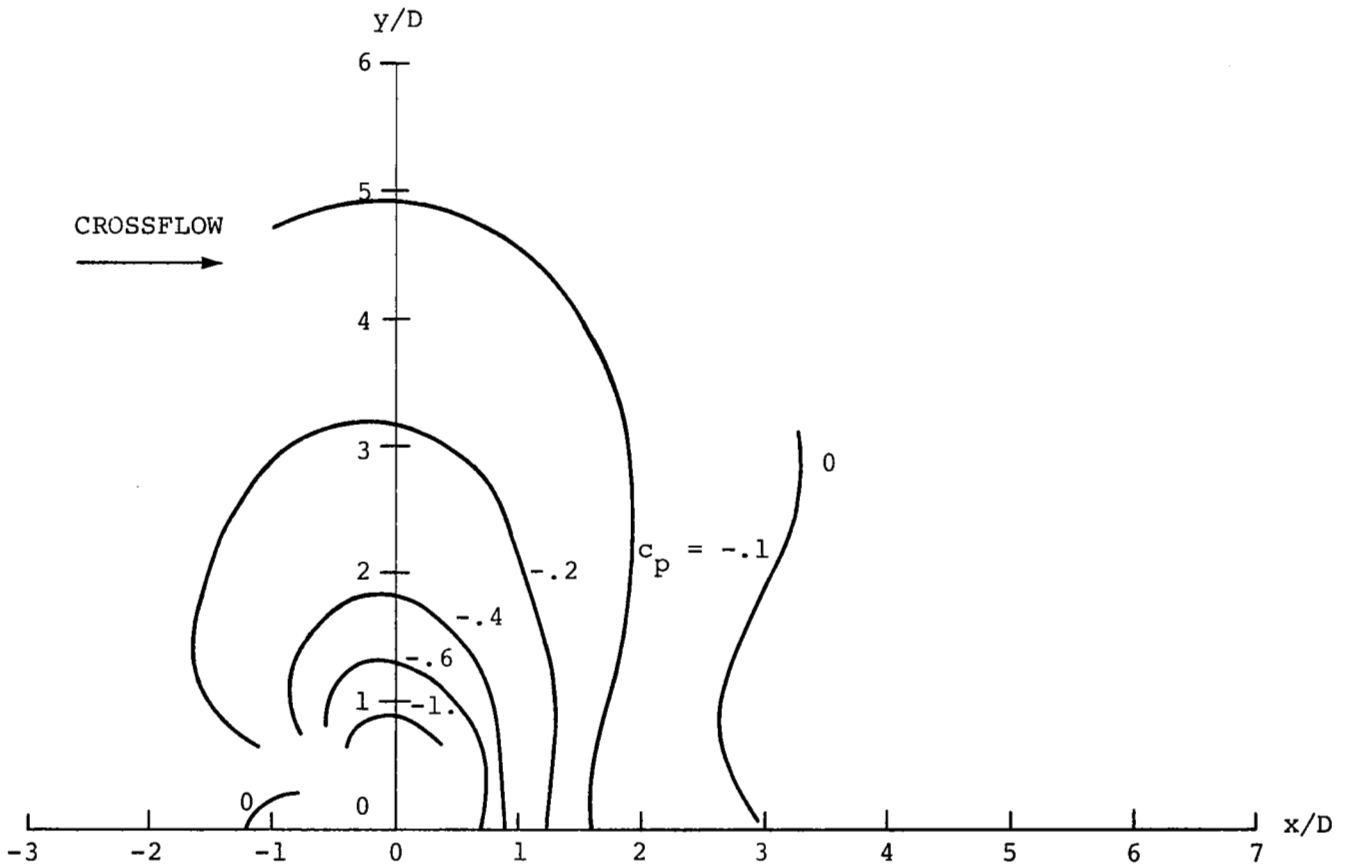

Figure 11. Constant pressure contour data; round plug down 1.0 D_n, R = 9.96.

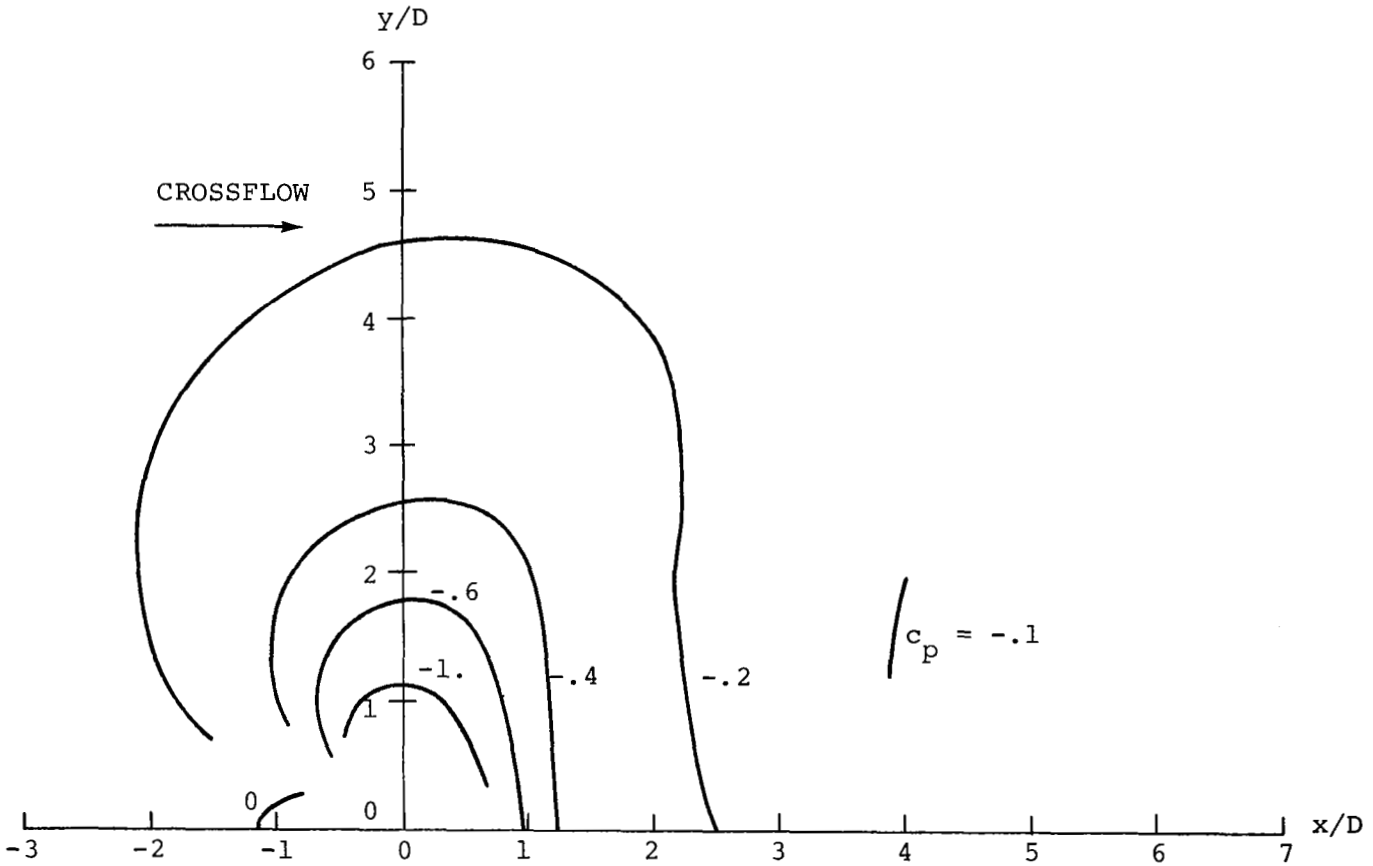

Figure 12. Constant pressure contour data; round plug down 1.0 D_n, R = 7.47.

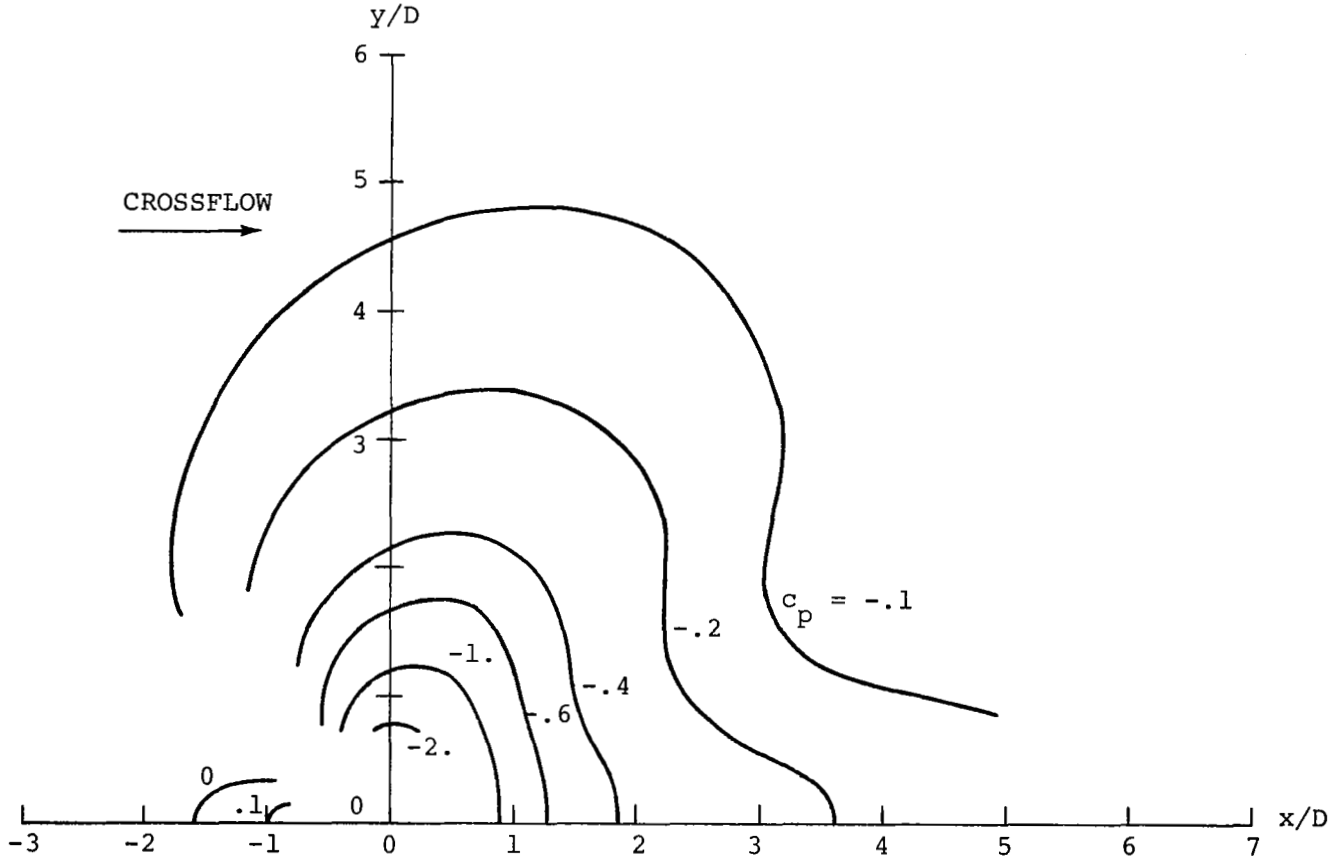

Figure 13. Constant pressure contour data; round plug, down 1.0 D_n, R = 4.98.

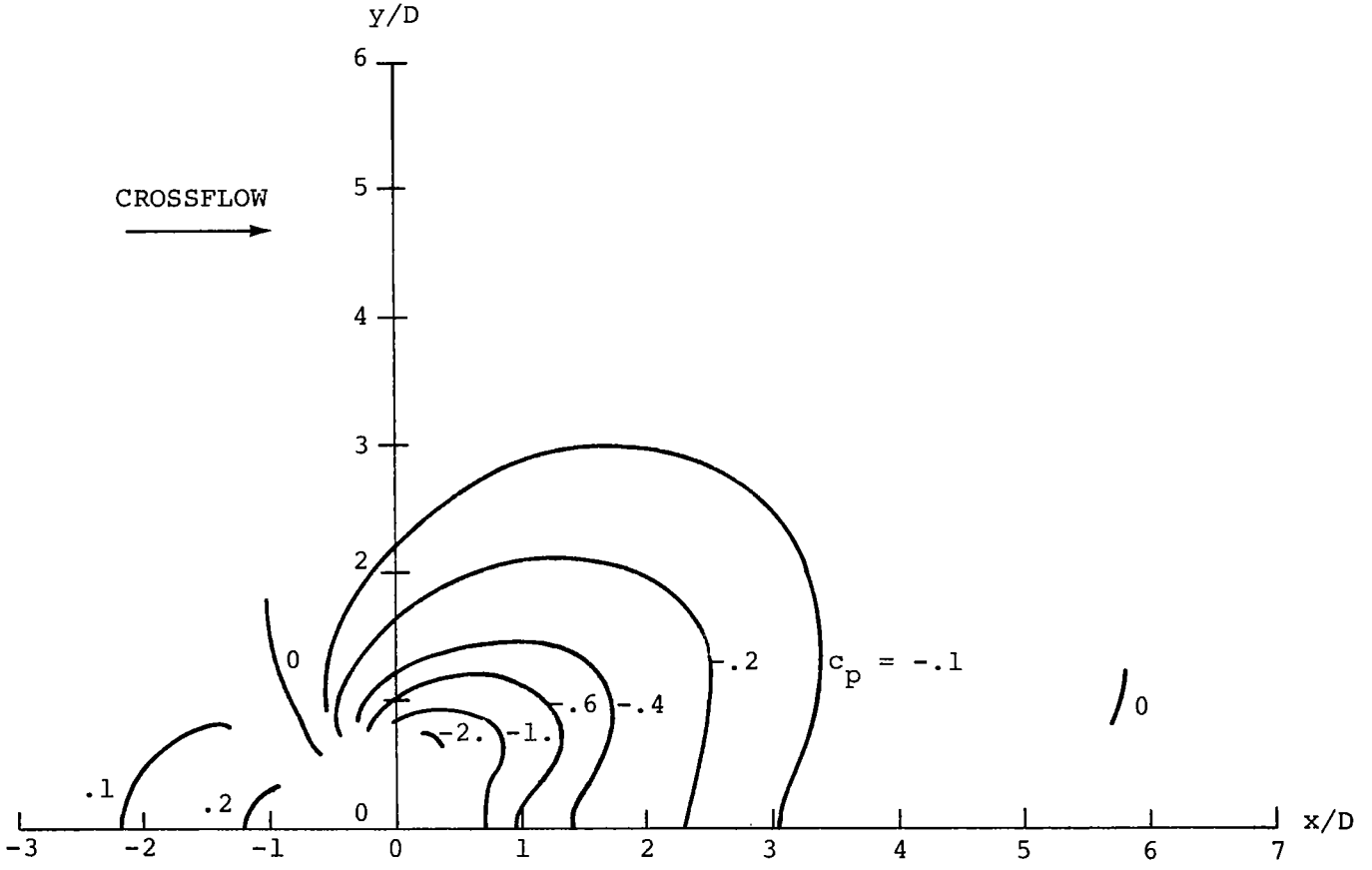

Figure 14. Constant pressure contour data; round plug down 1.0 D_n, R = 2.49.

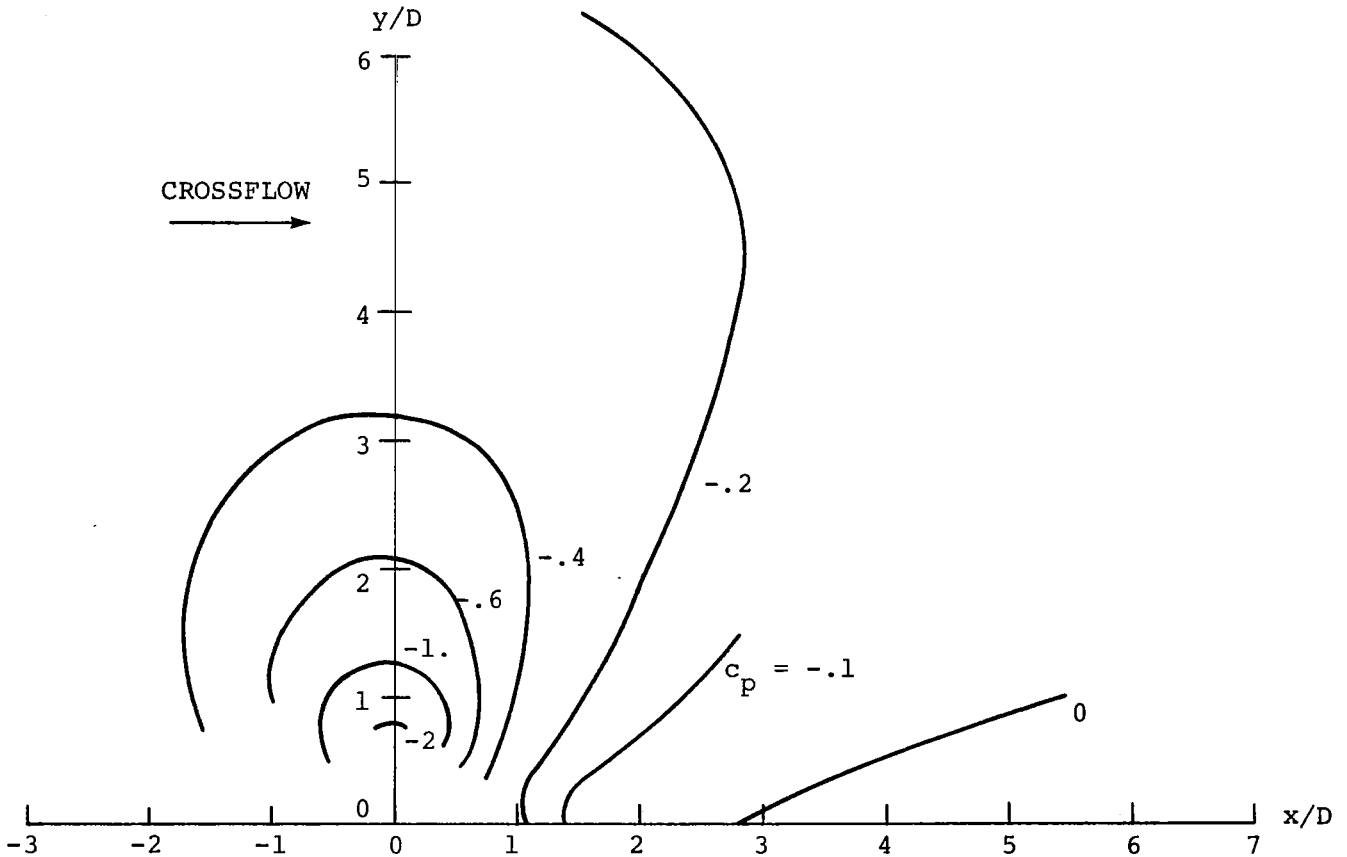

Figure 15. Constant pressure contour data; round plug down 0.5 D_n, R = 10.35.

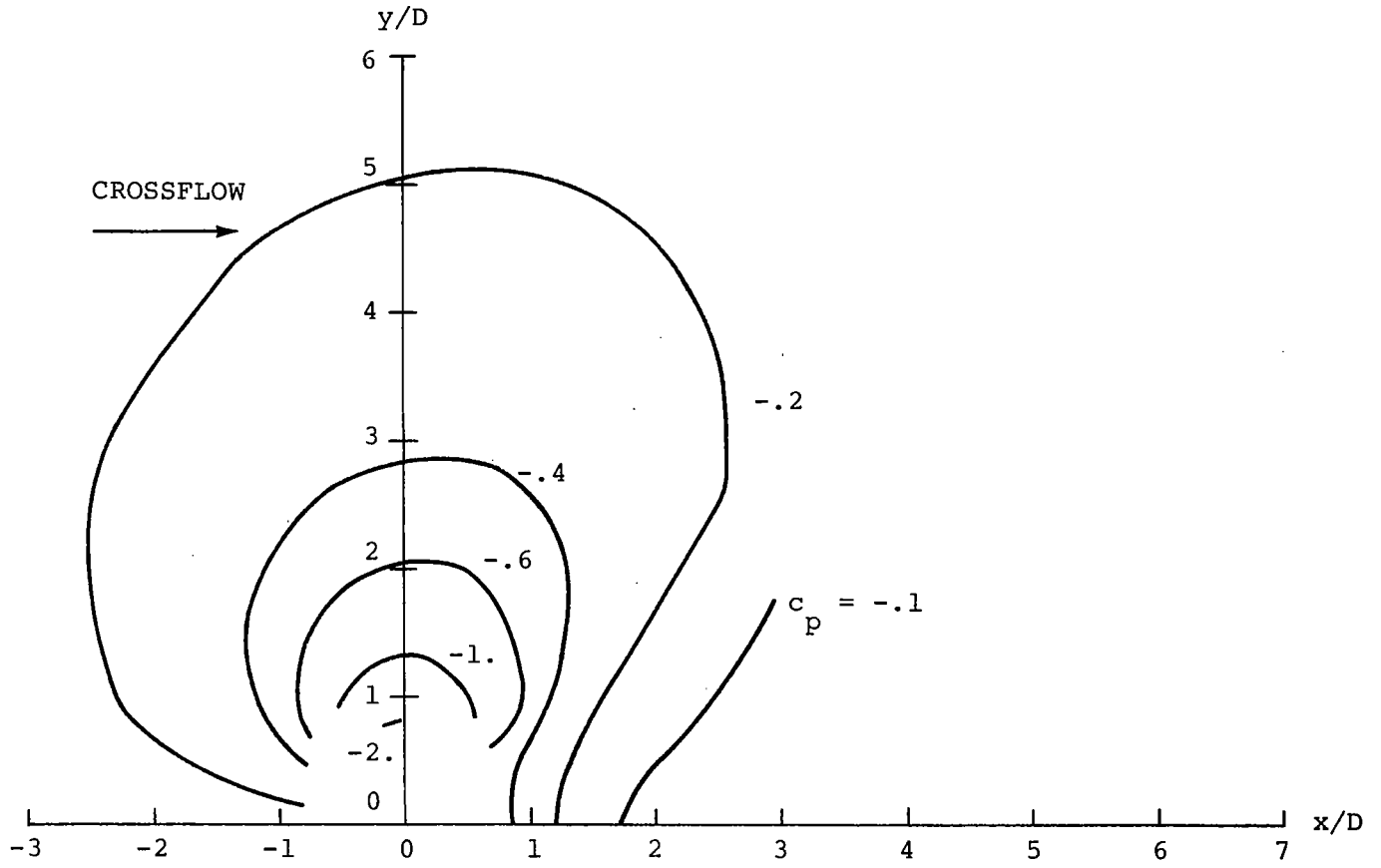

Figure 16. Constant pressure contour data; round plug down 0.5 D_n, R = 7.76.

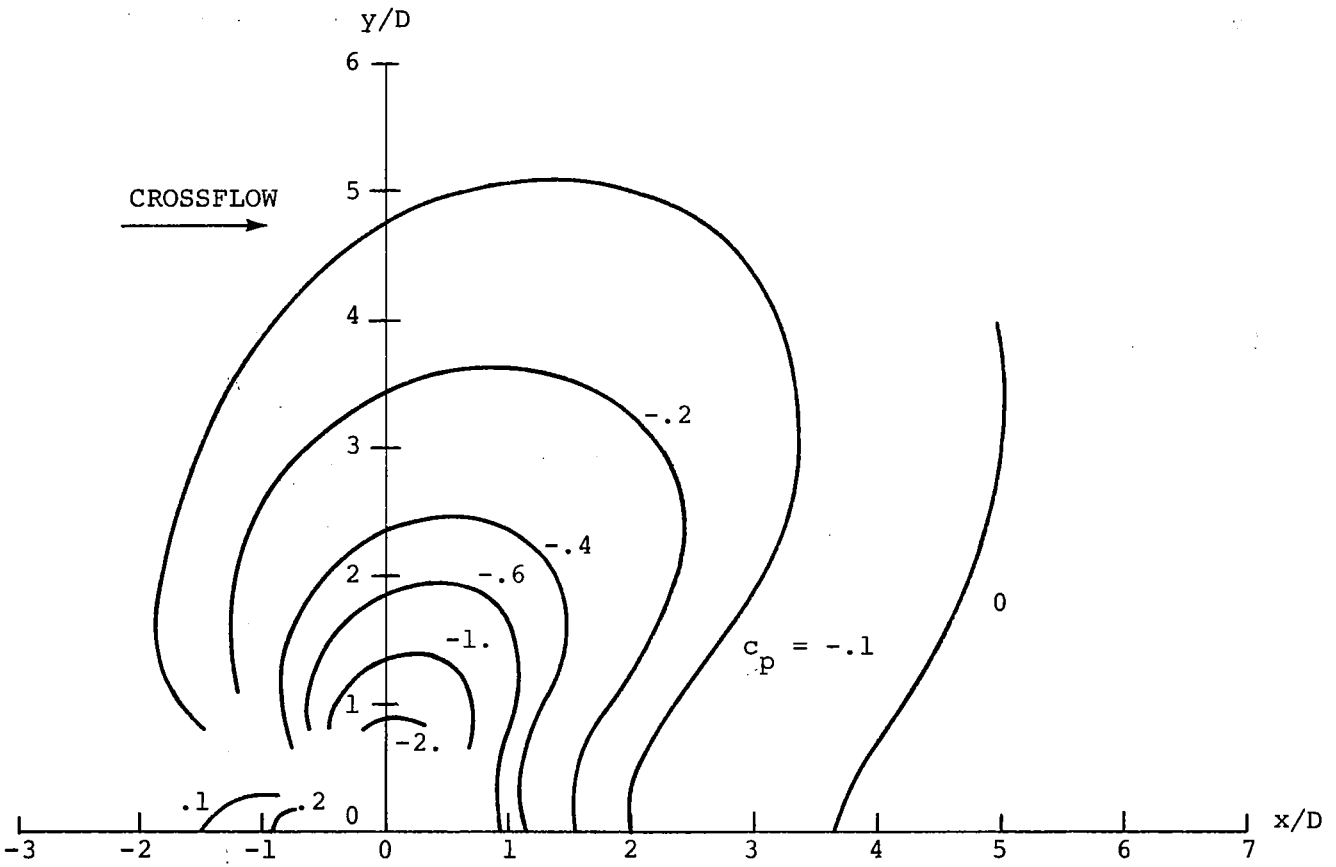

Figure 17. Constant pressure contour data; round plug down 0.5 D_n, R = 5.18.

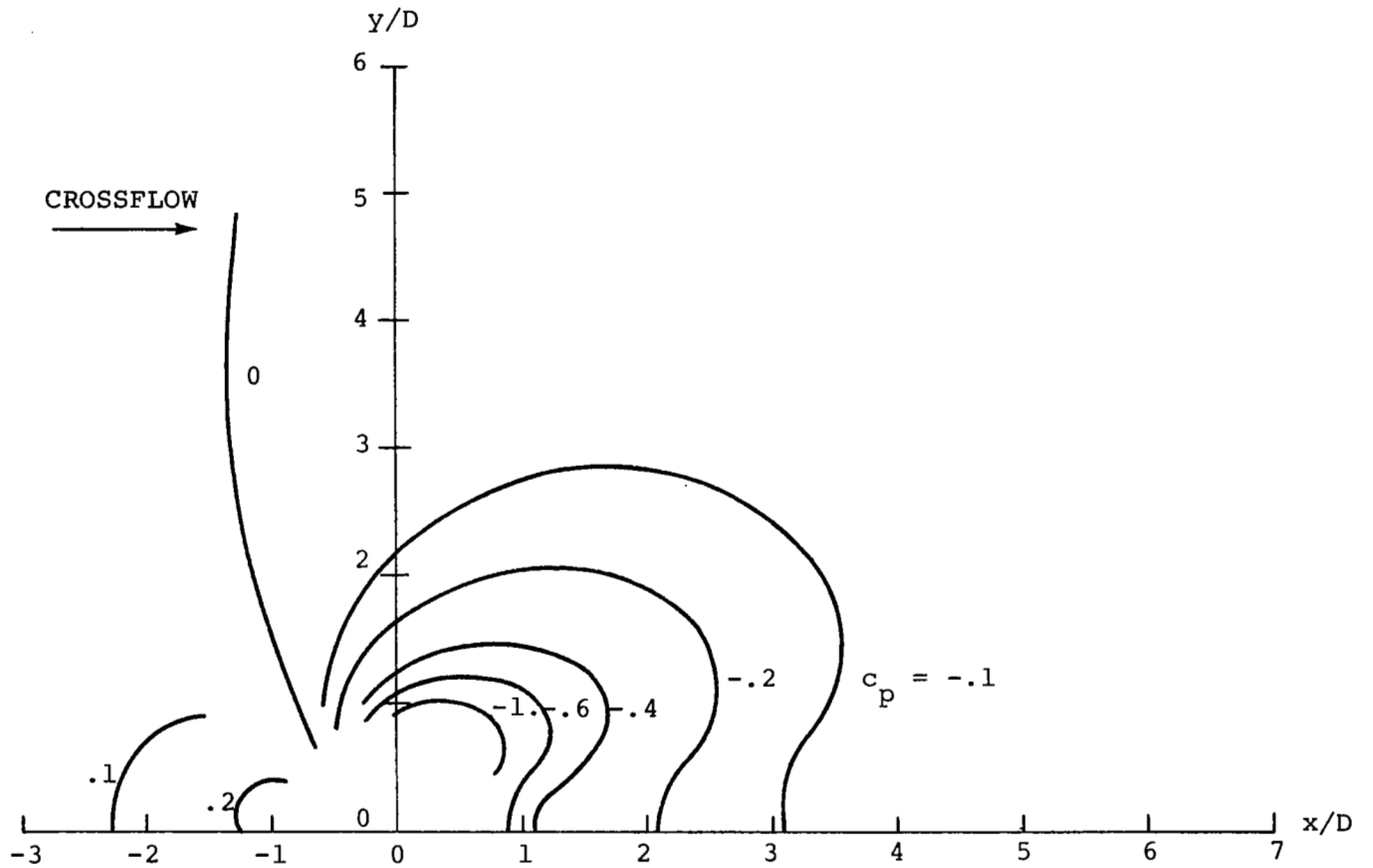

Figure 18. Constant pressure contour data; round plug down 0.5 D_n, R = 2.59.

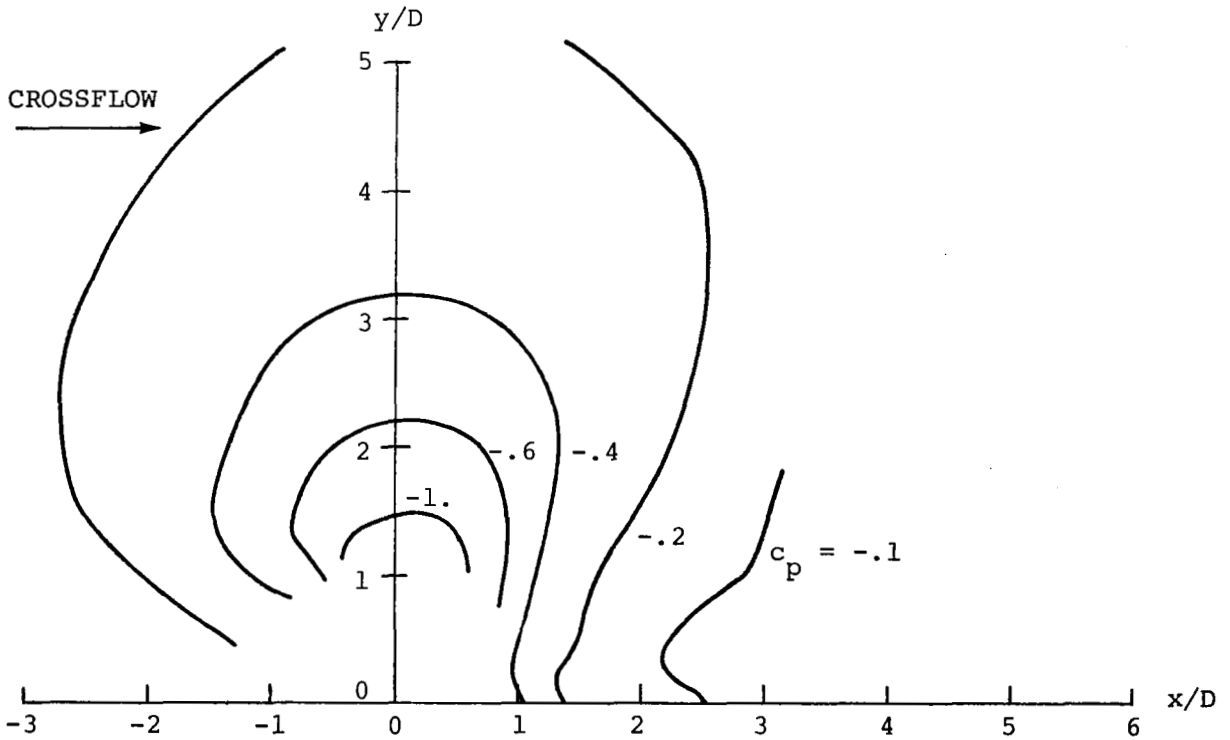

Figure 19. Constant pressure contour data; round plug flush, R = 9.08.

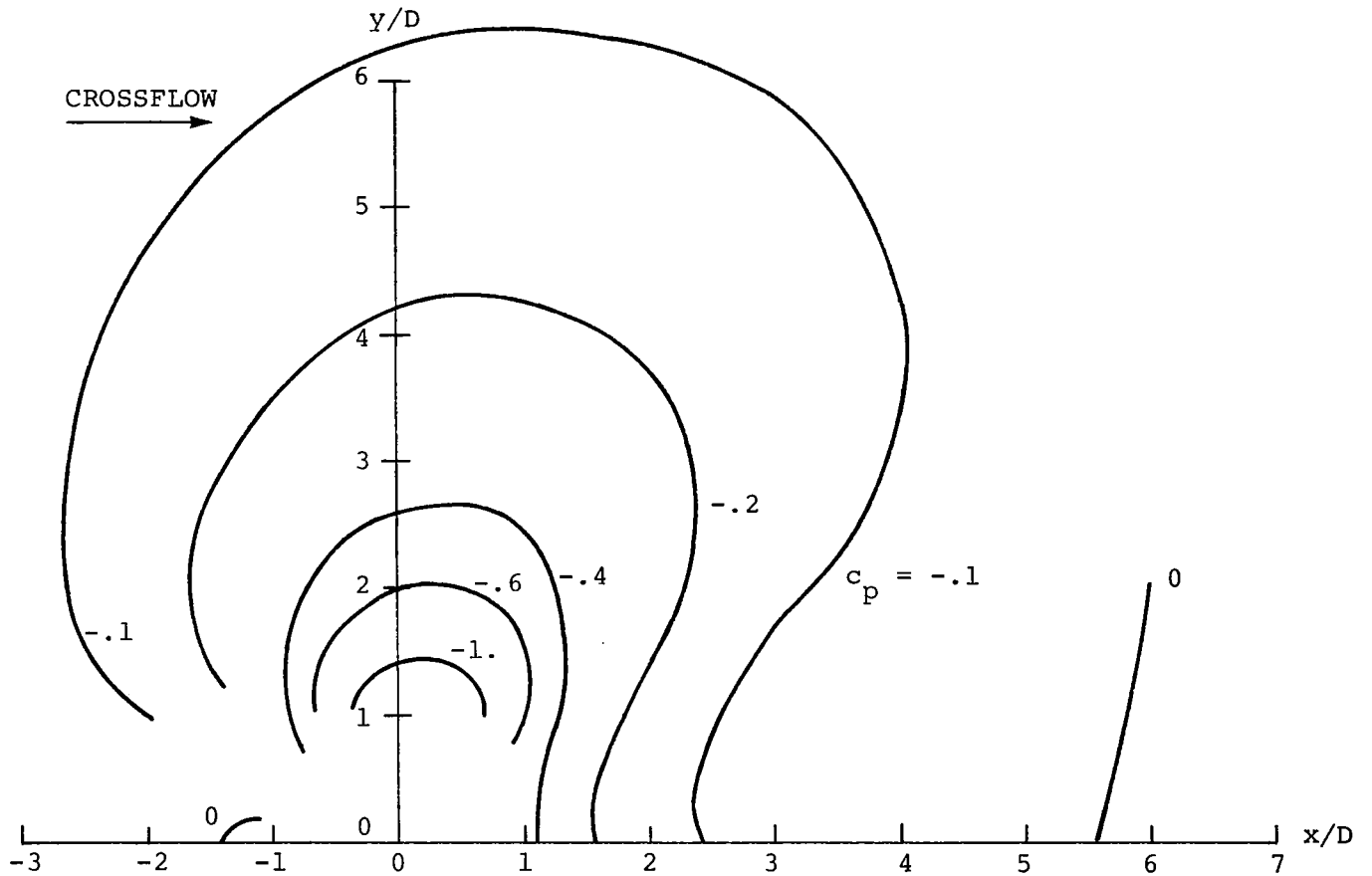

Figure 20. Constant pressure contour data; round plug flush, R = 6.81.

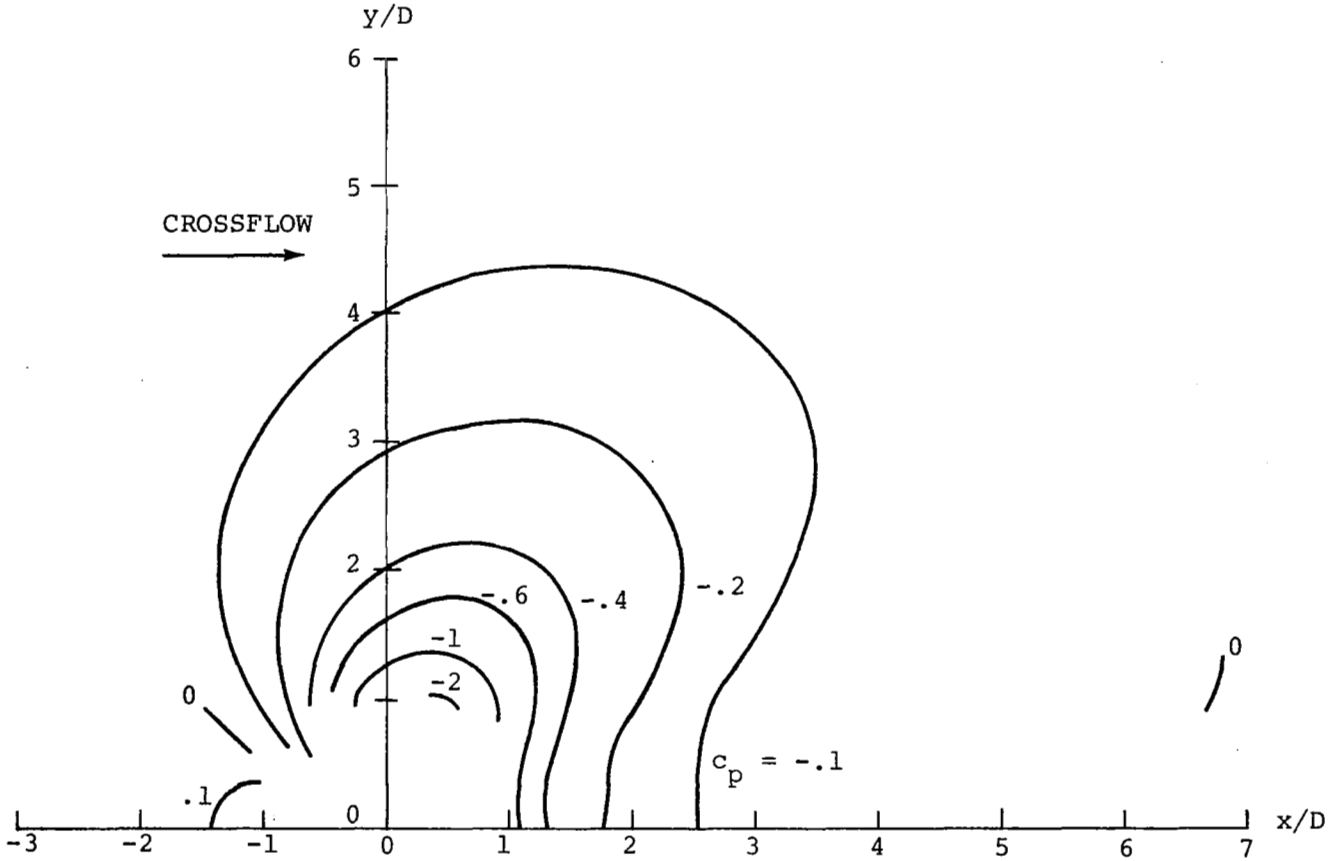

Figure 21. Constant pressure contour data; round plug flush, R = 4.54.

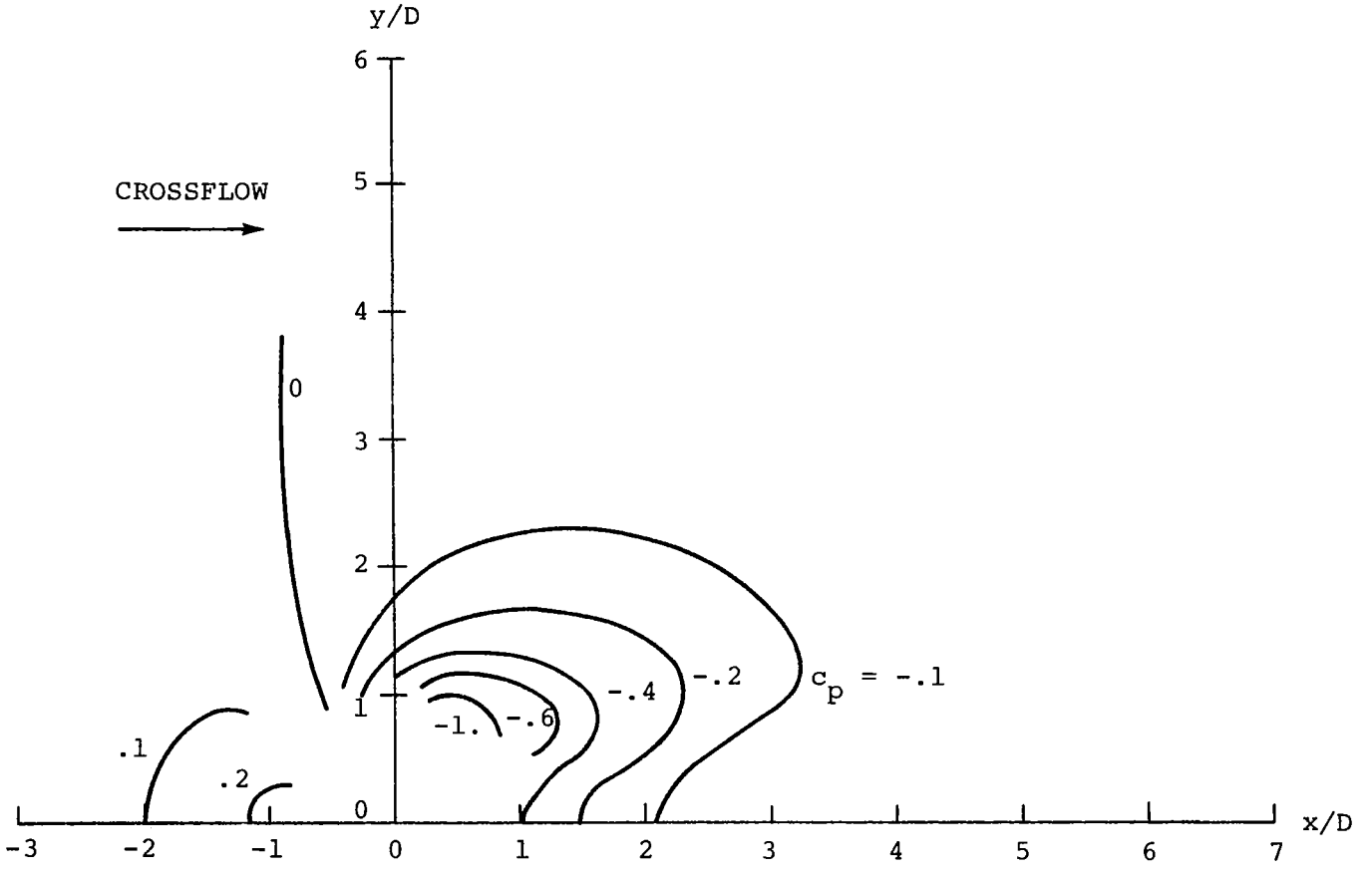

Figure 22. Constant pressure contour data; round plug flush, R = 2.27.

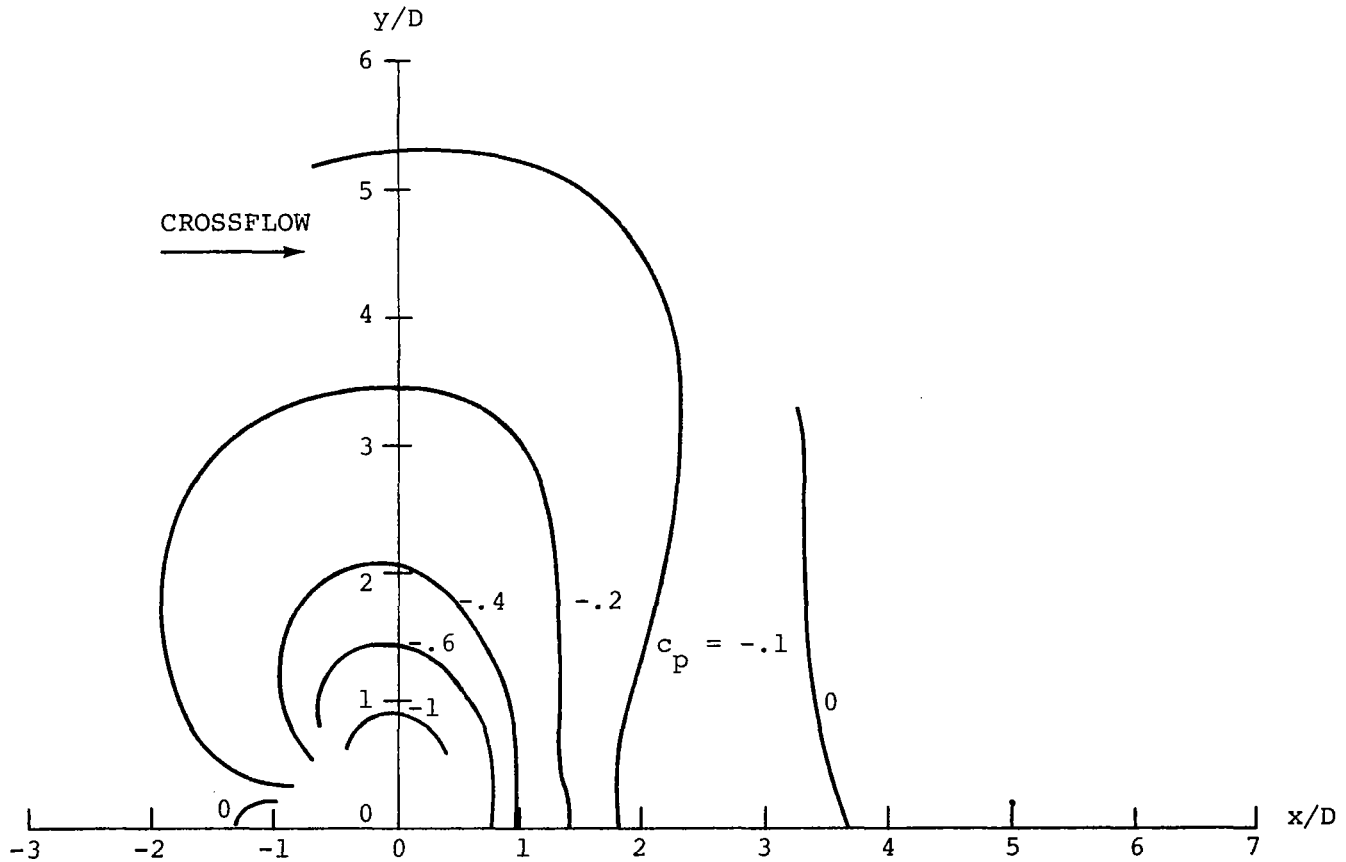

Figure 23. Constant pressure contour data; flat ended plug down 1.375 D_n, R = 9.48.

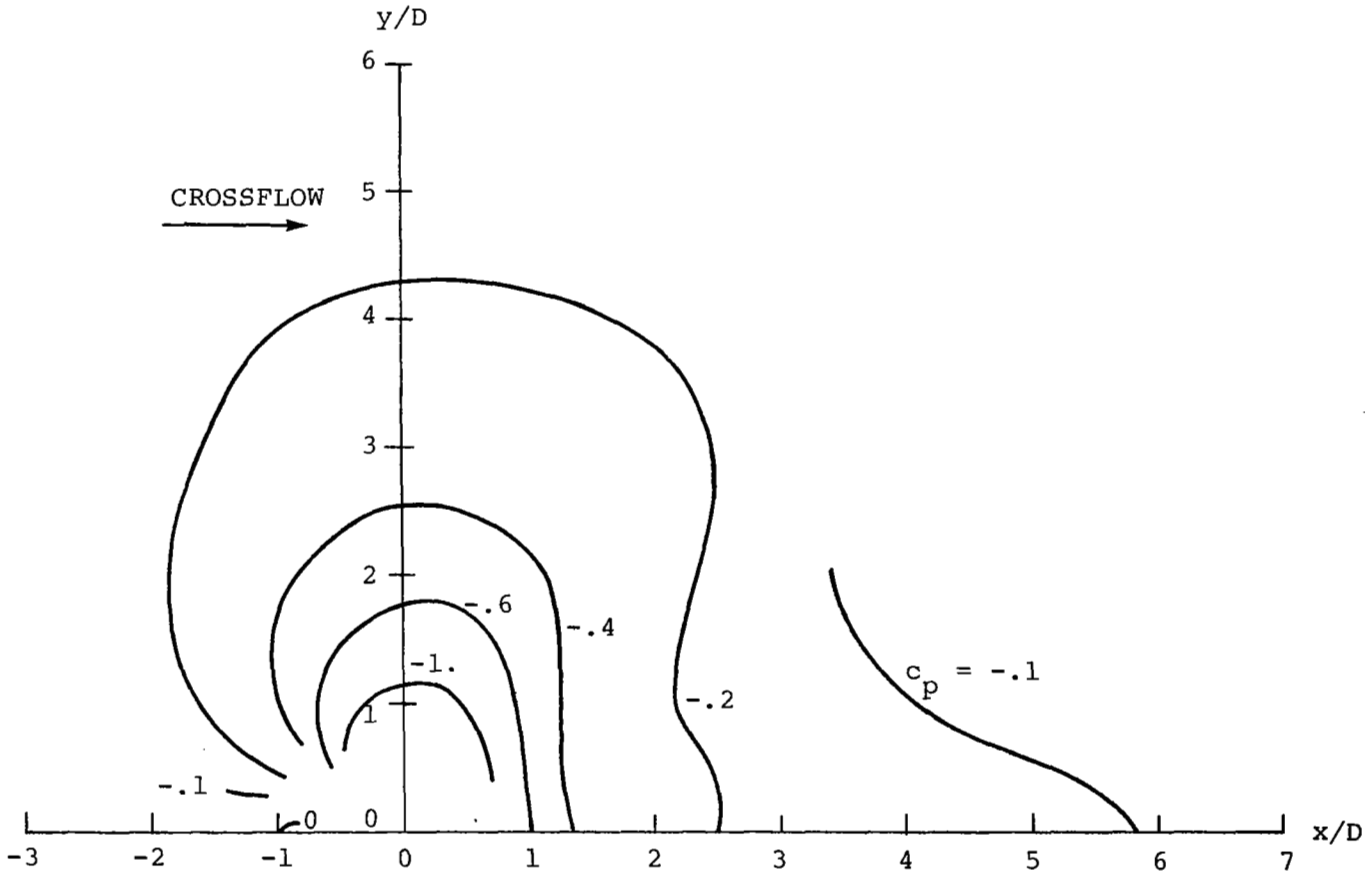

Figure 24. Constant pressure contour data; flat ended plug down 1.375 D_n, R = 7.10.

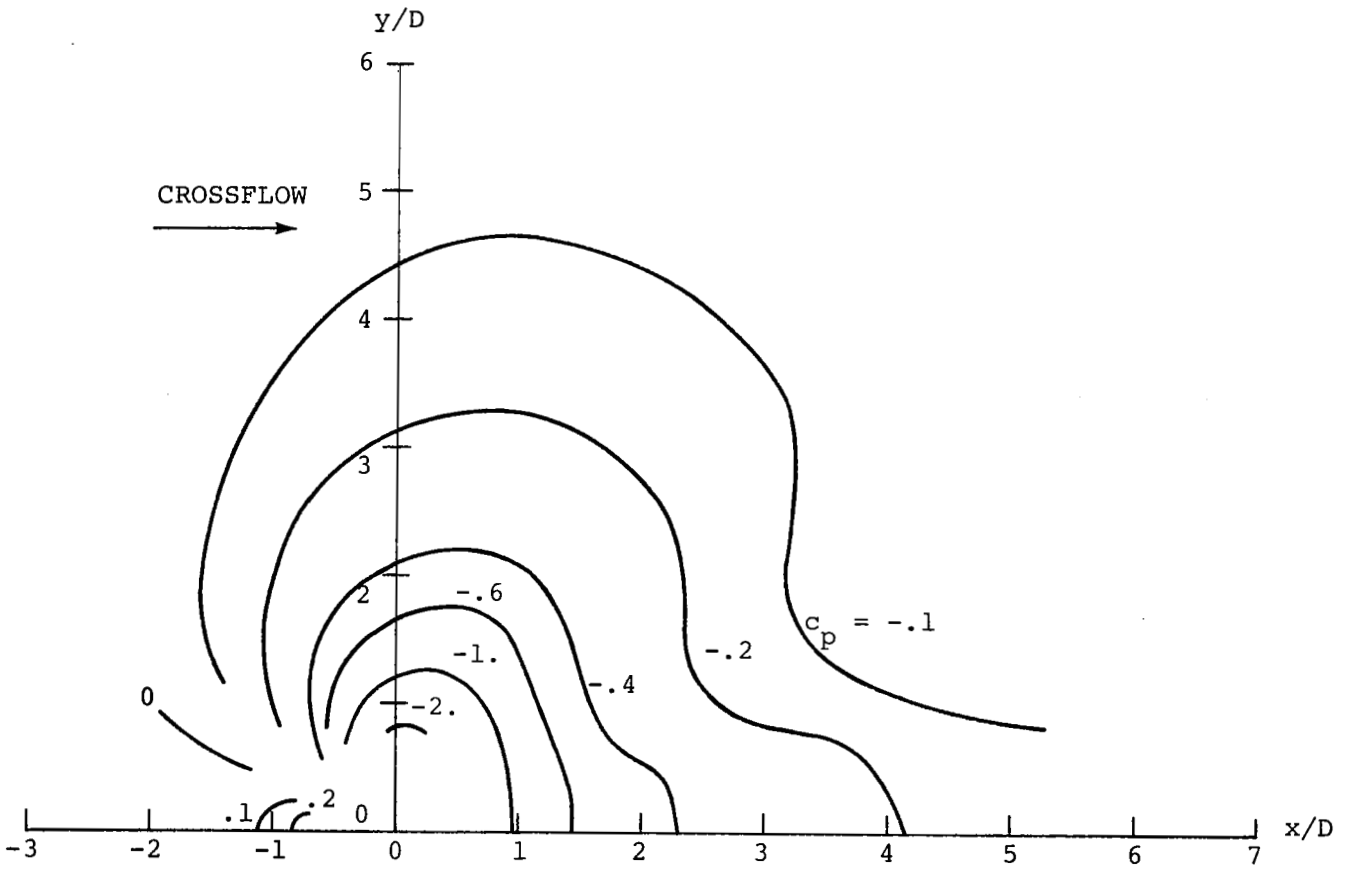

Figure 25. Constant pressure contour data; flat ended plug down 1.375 D_n, R = 4.74.

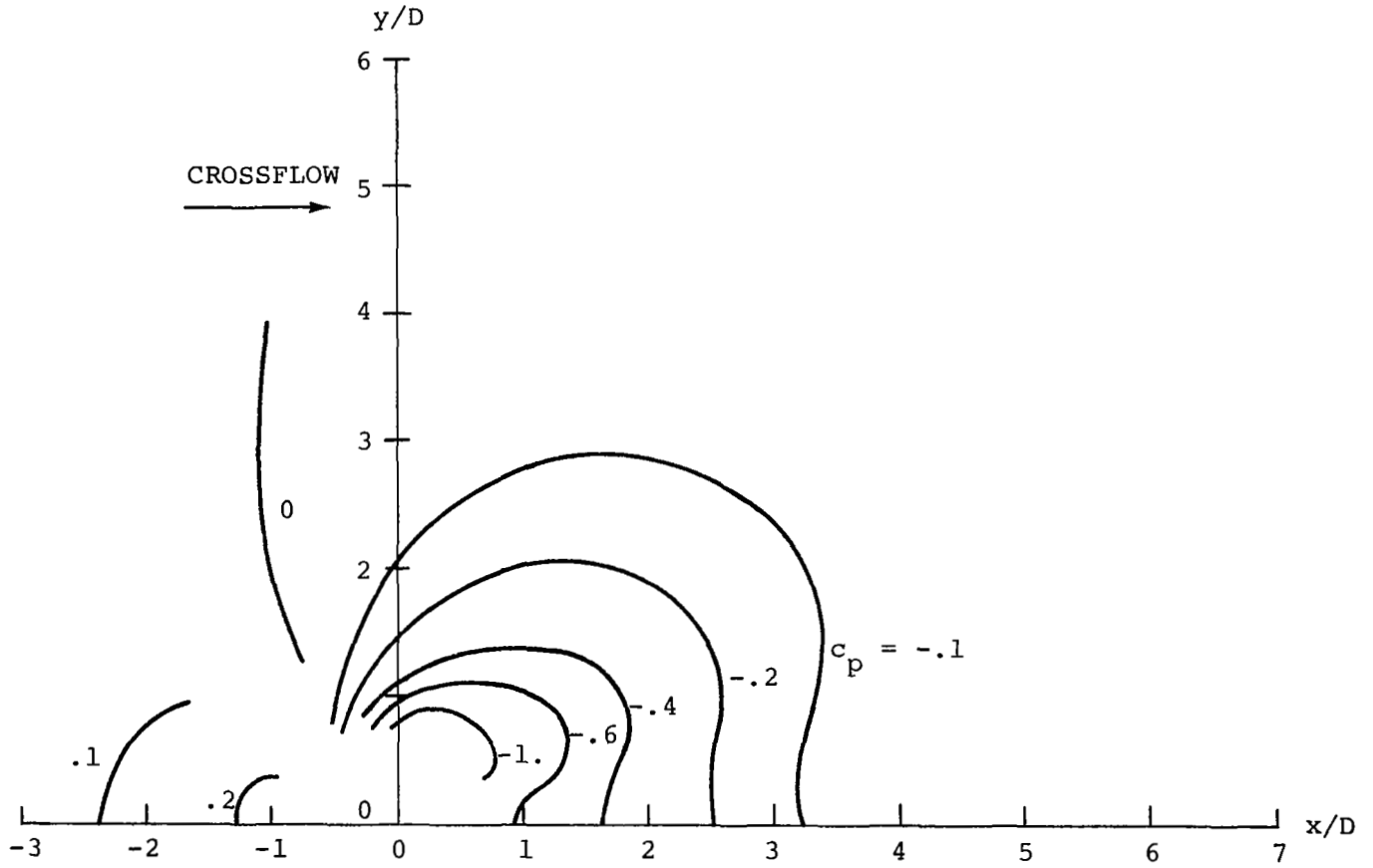

Figure 26. Constant pressure contour data; flat ended plug down 1.375 D_n, R = 2.37.

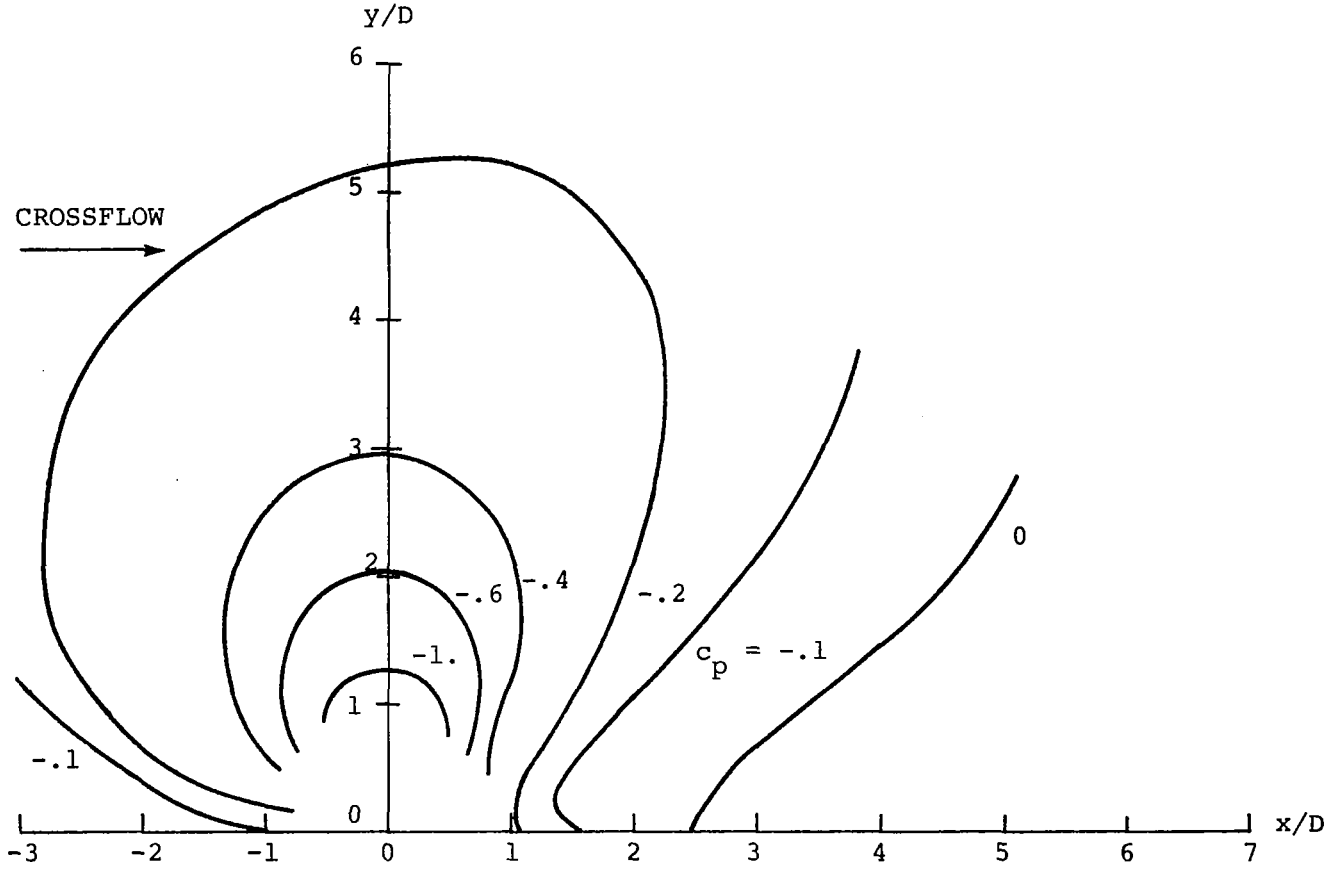

Figure 27. Constant pressure contour data; flat ended plug down 0.875 D_n, R = 9.36.

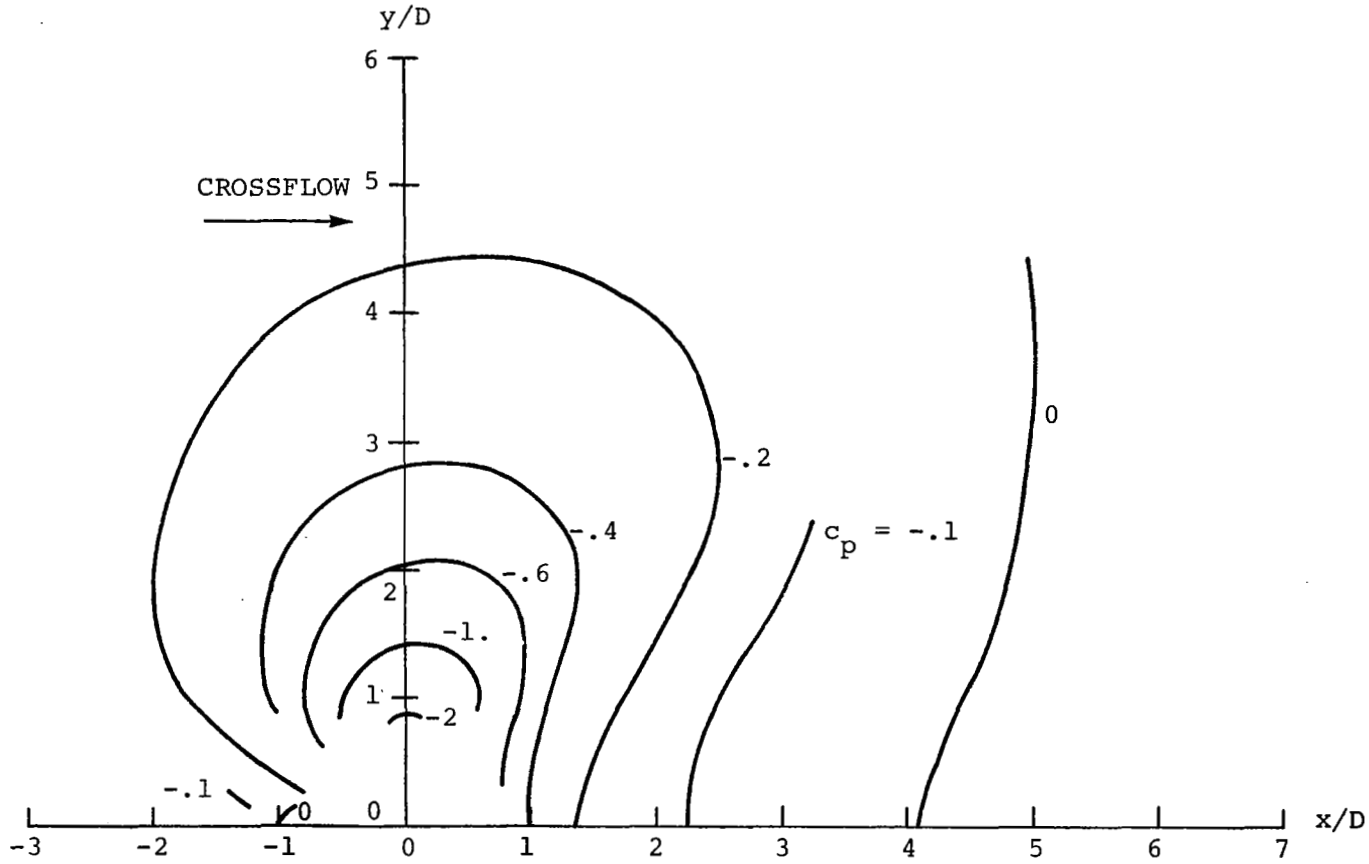

Figure 28. Constant pressure contour data; flat ended plug down 0.875 D_n, R = 7.01.

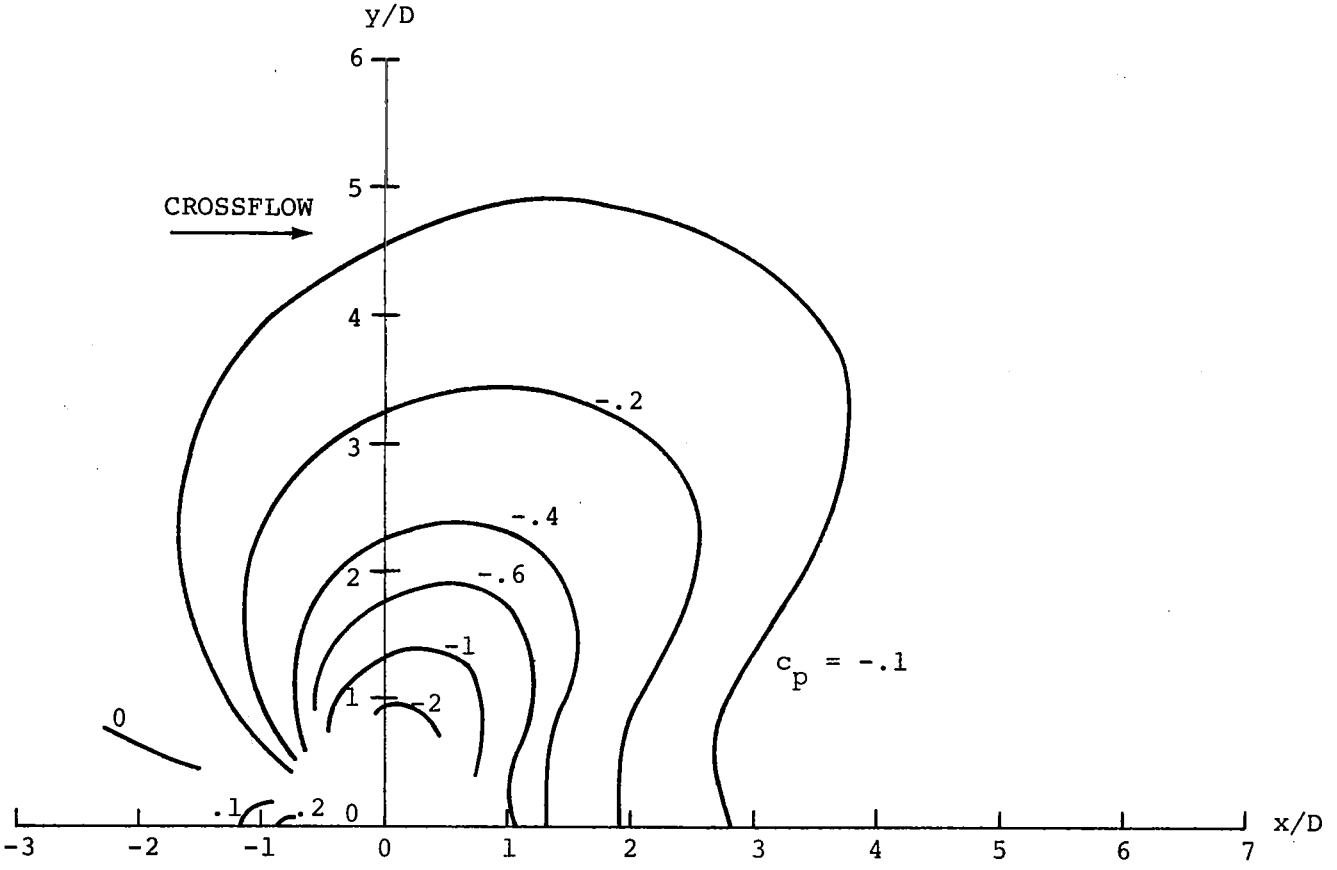

Figure 29. Constant pressure contour data; flat ended plug down 0.875 D_n, R = 4.67.

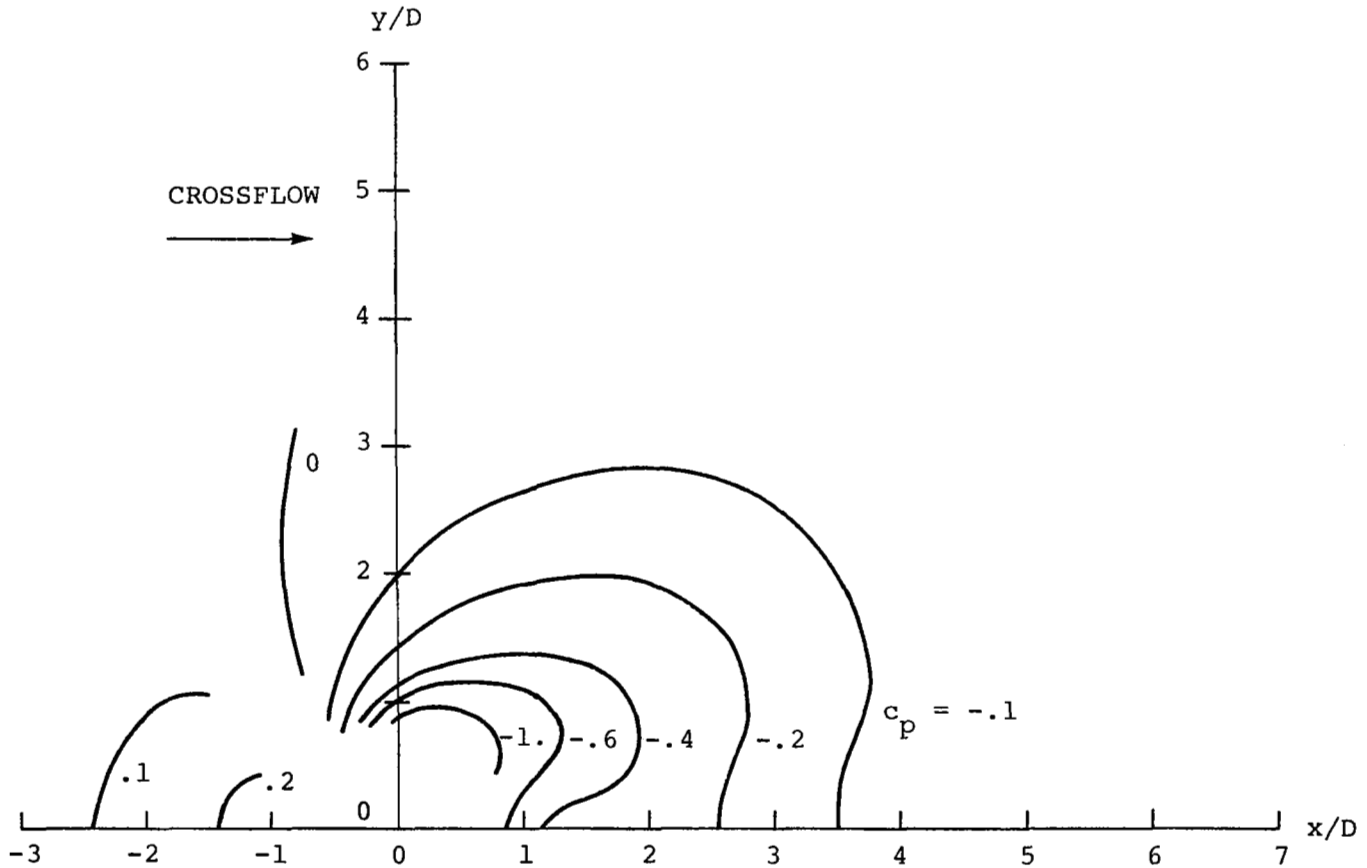

Figure 30. Constant pressure contour data; flat ended plug down 0.875 D_n, R = 2.34.

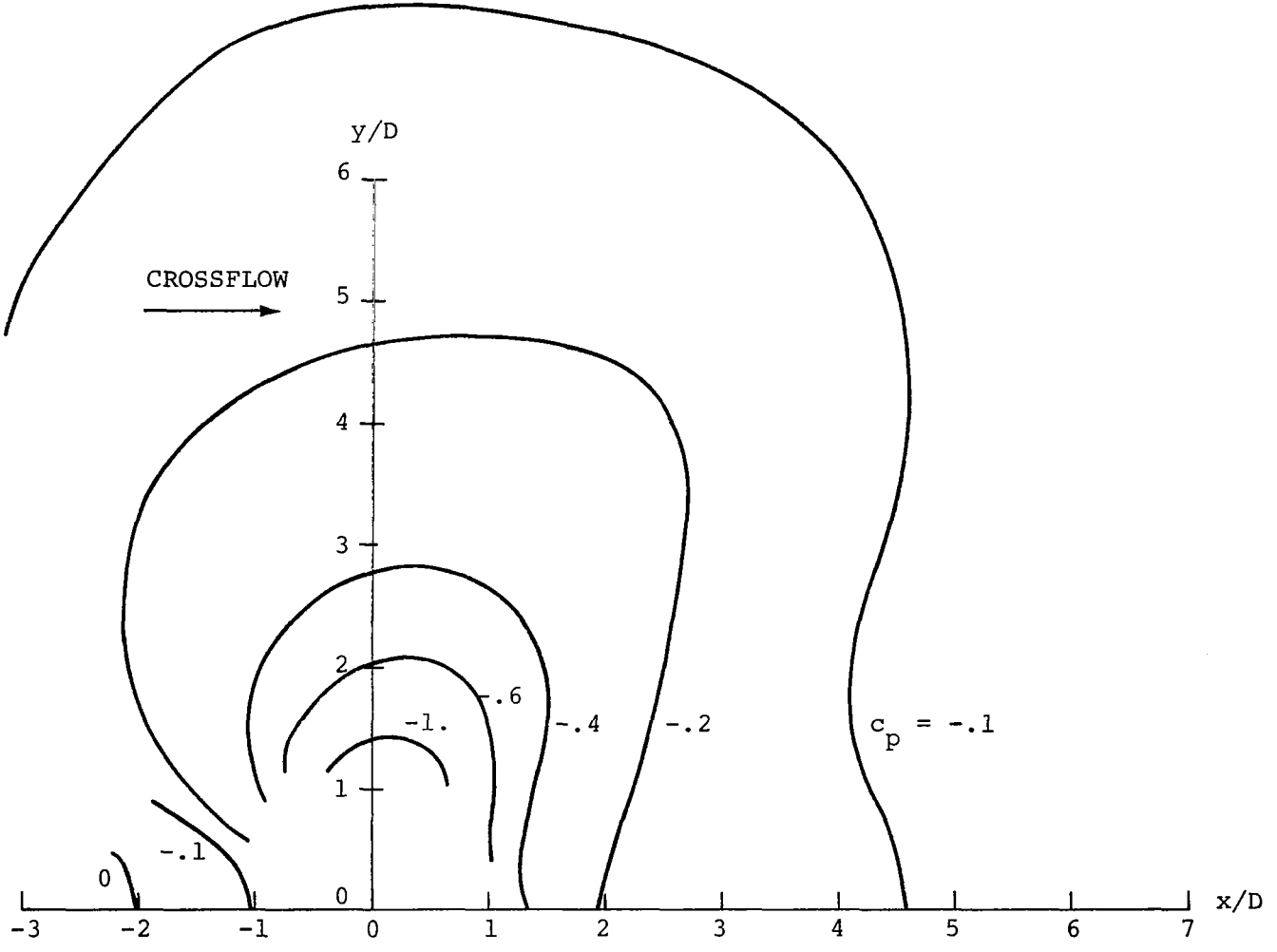

Figure 31. Constant pressure contour data; flat ended plug down 0.375 D_n, R = 8.74.

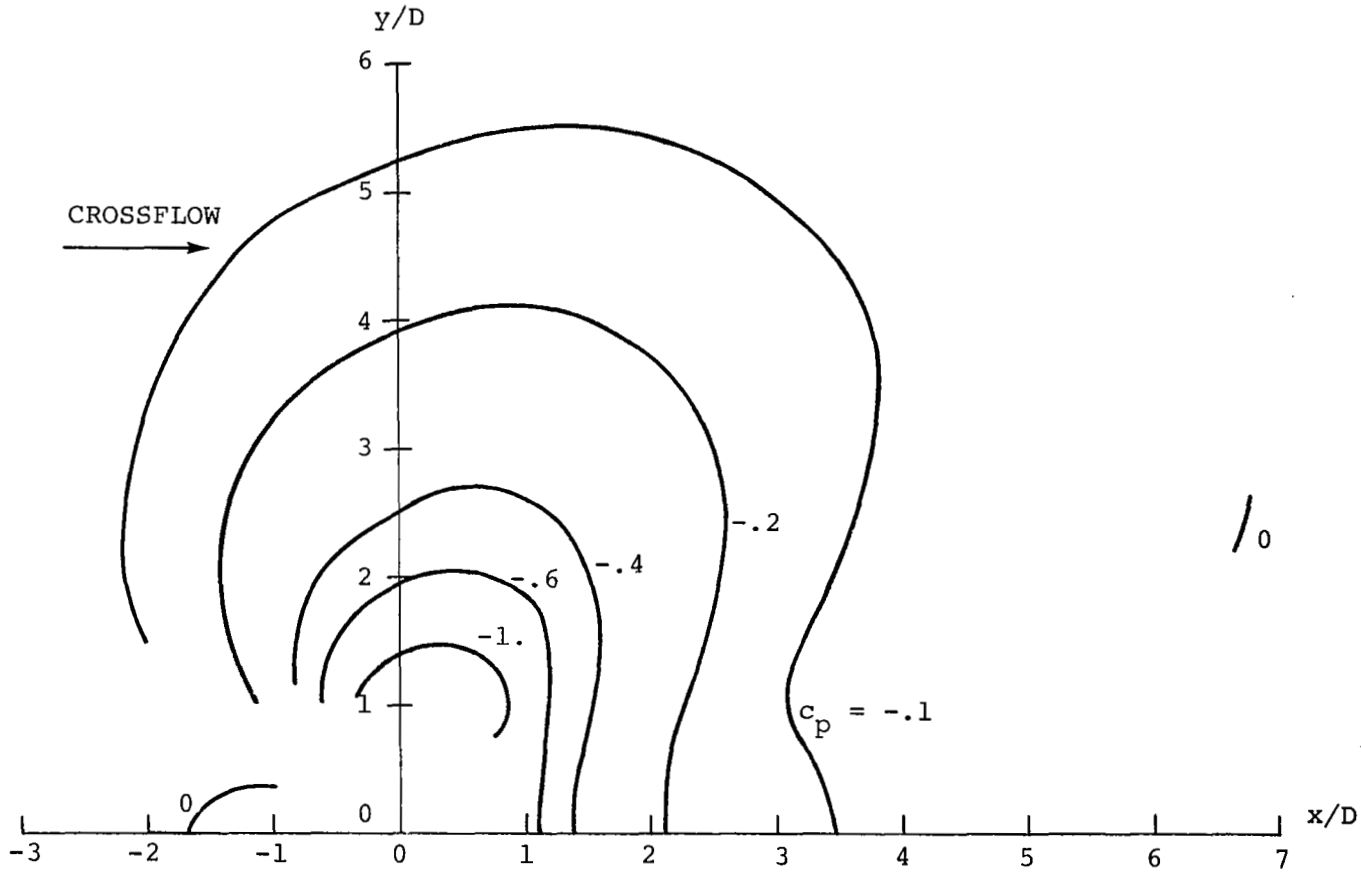

Figure 32. Constant pressure contour data; flat ended plug down 0.375 D_n, R = 6.55.

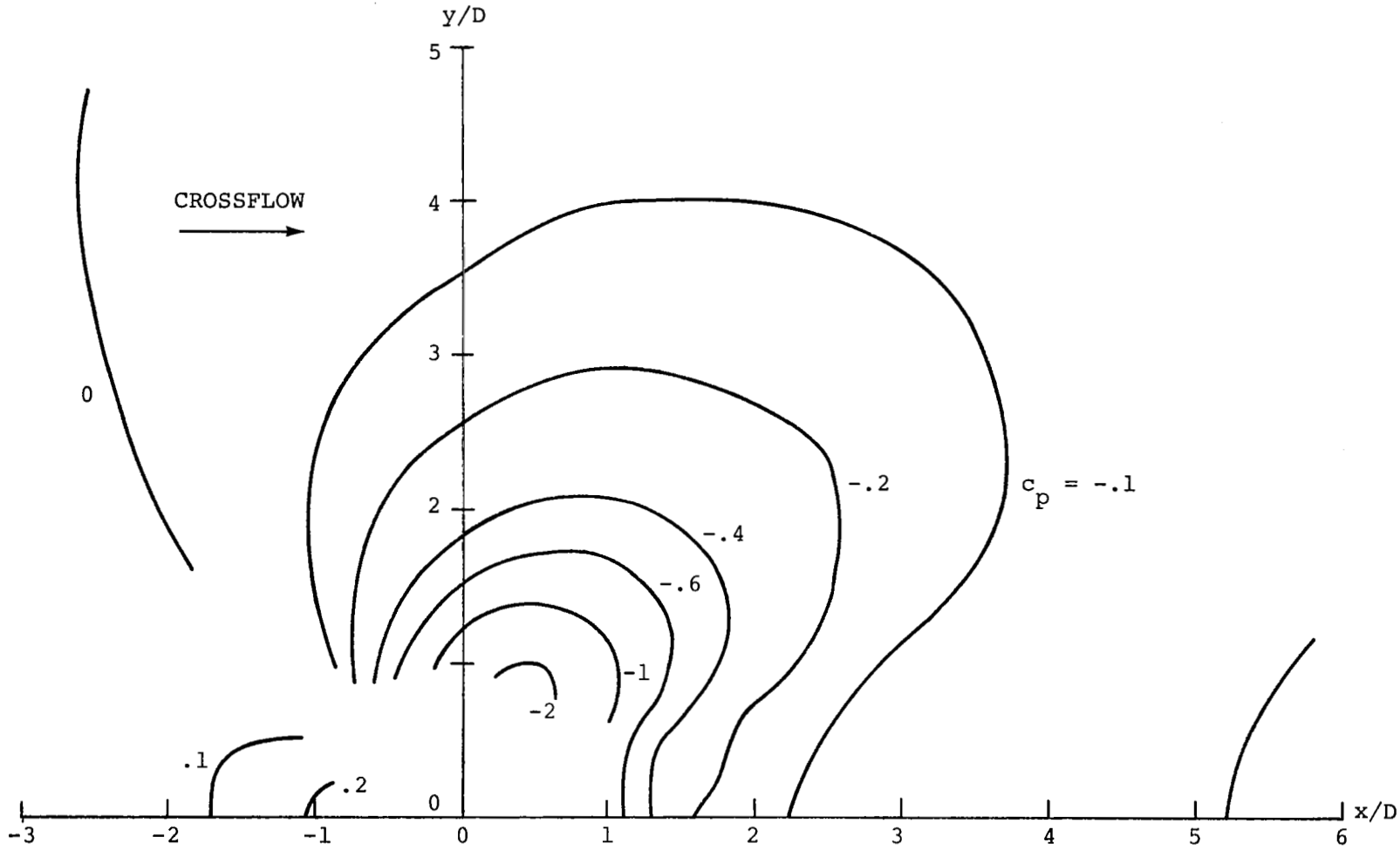

Figure 33. Constant pressure contour data; flat ended plug down 0.375 D_n, R = 4.36.

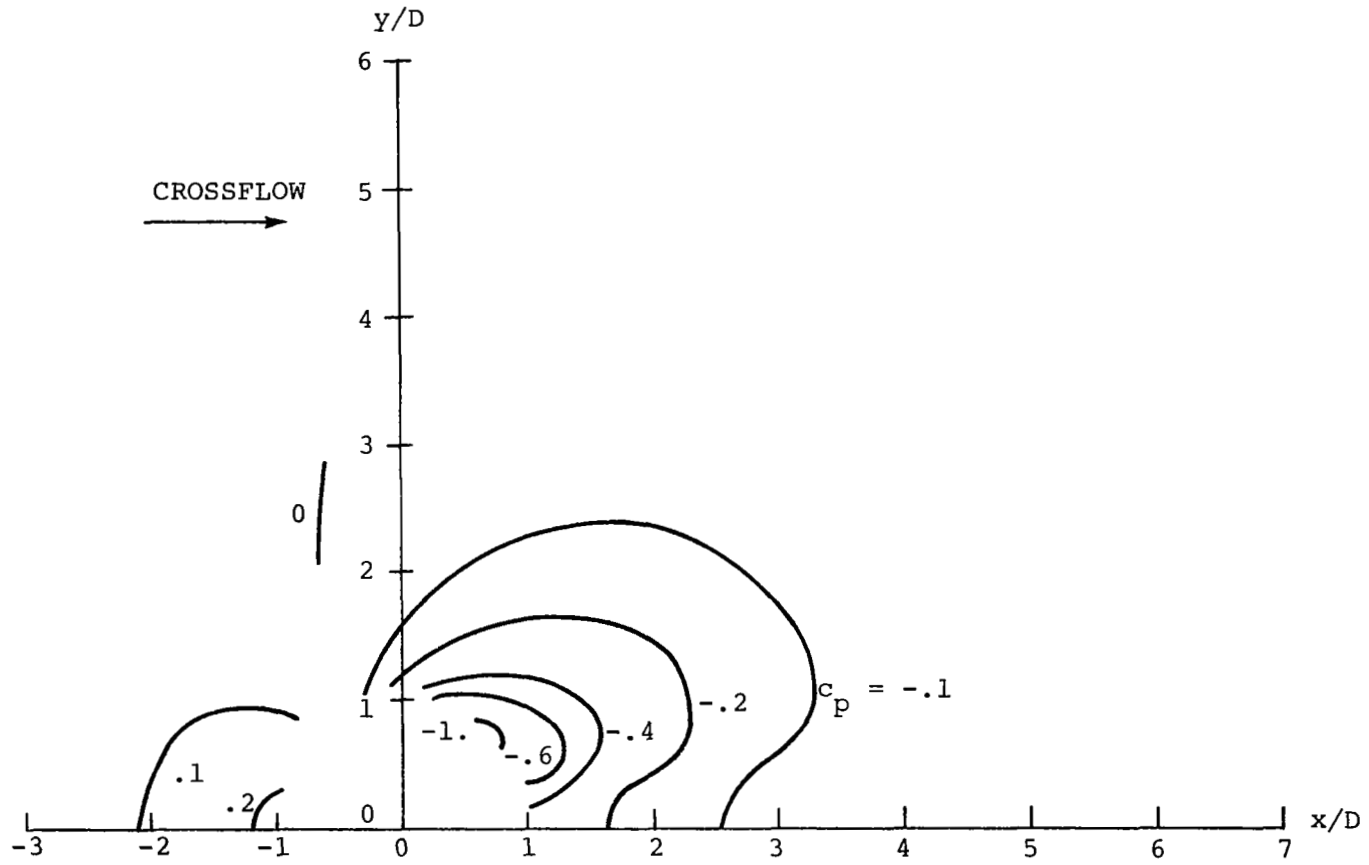

Figure 34. Constant pressure contour data; flat ended plug down 0.375 D_n, R = 2.18.

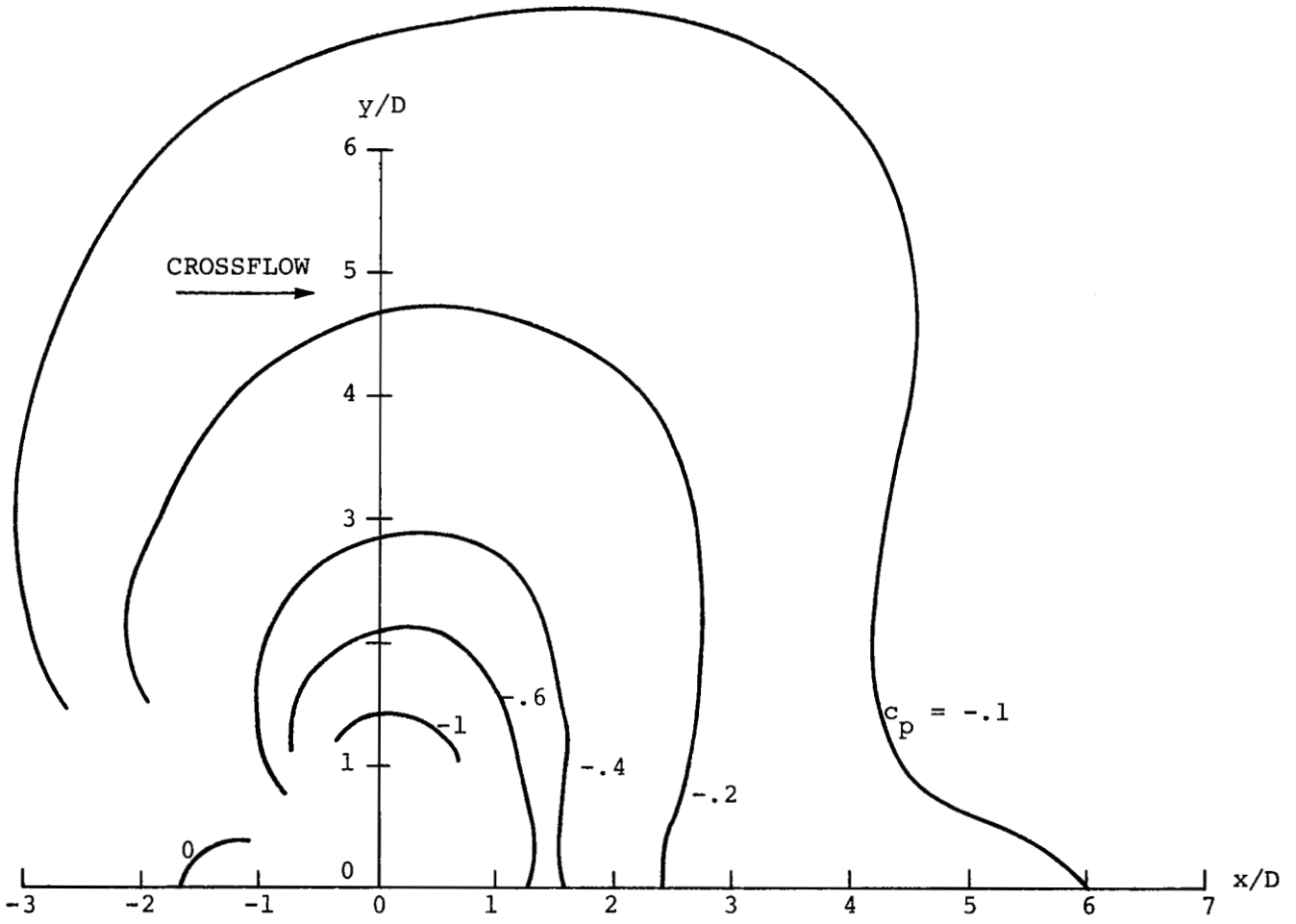

Figure 35. Constant pressure contour data; flat ended plug flush, R = 8.78.

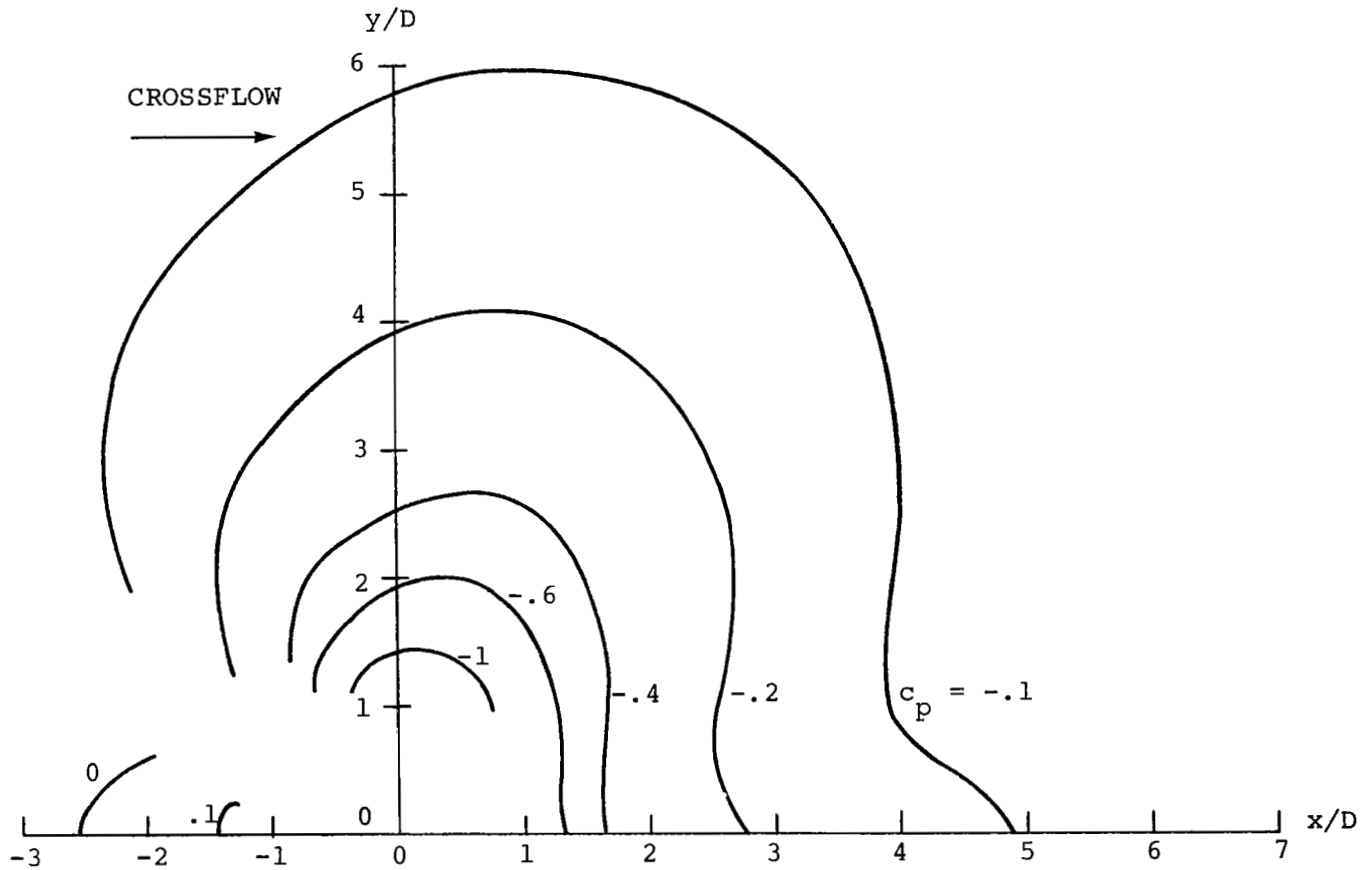

Figure 36. Constant pressure contour data; flat ended plug flush, R = 6.58.

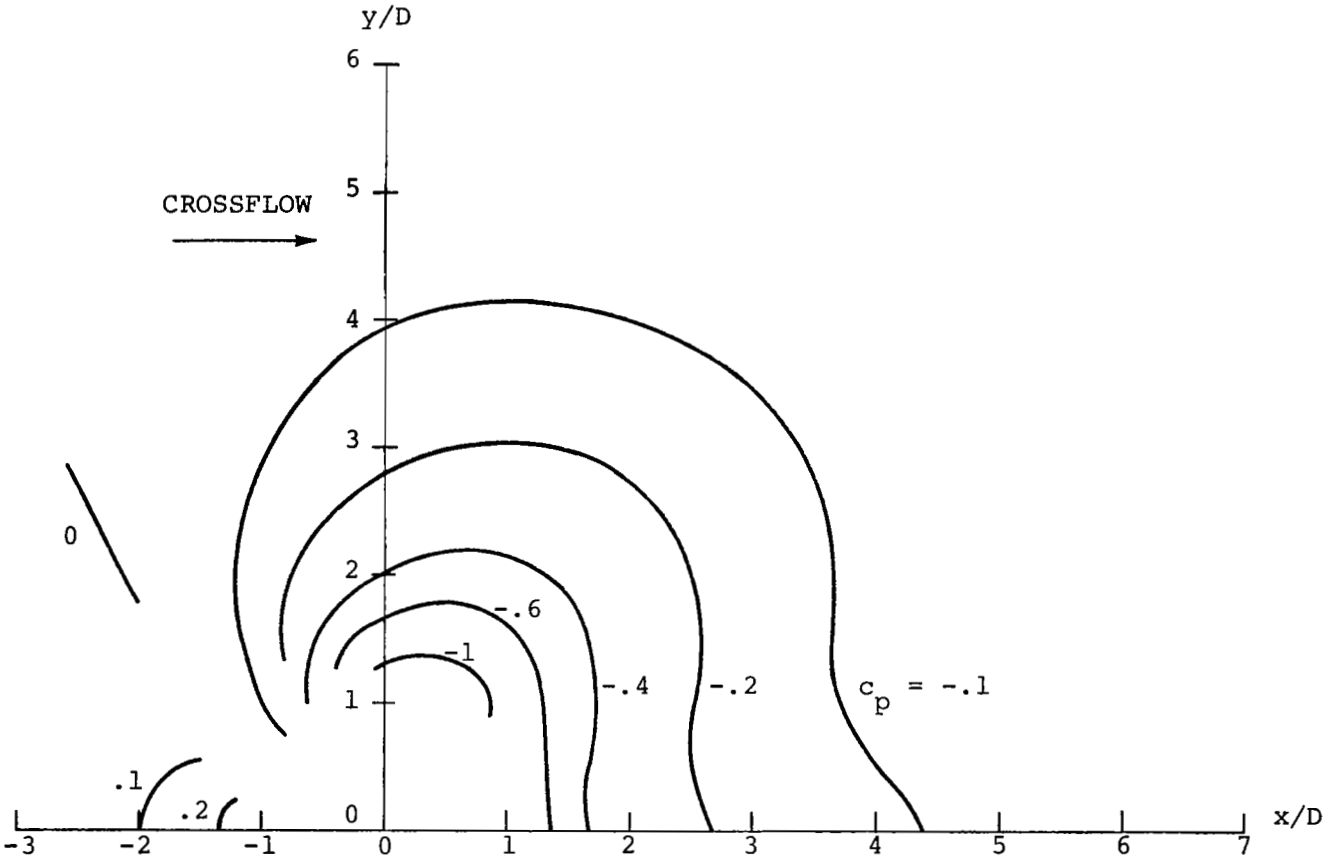

Figure 37. Constant pressure contour data; flat ended plug flush, R = 4.39.

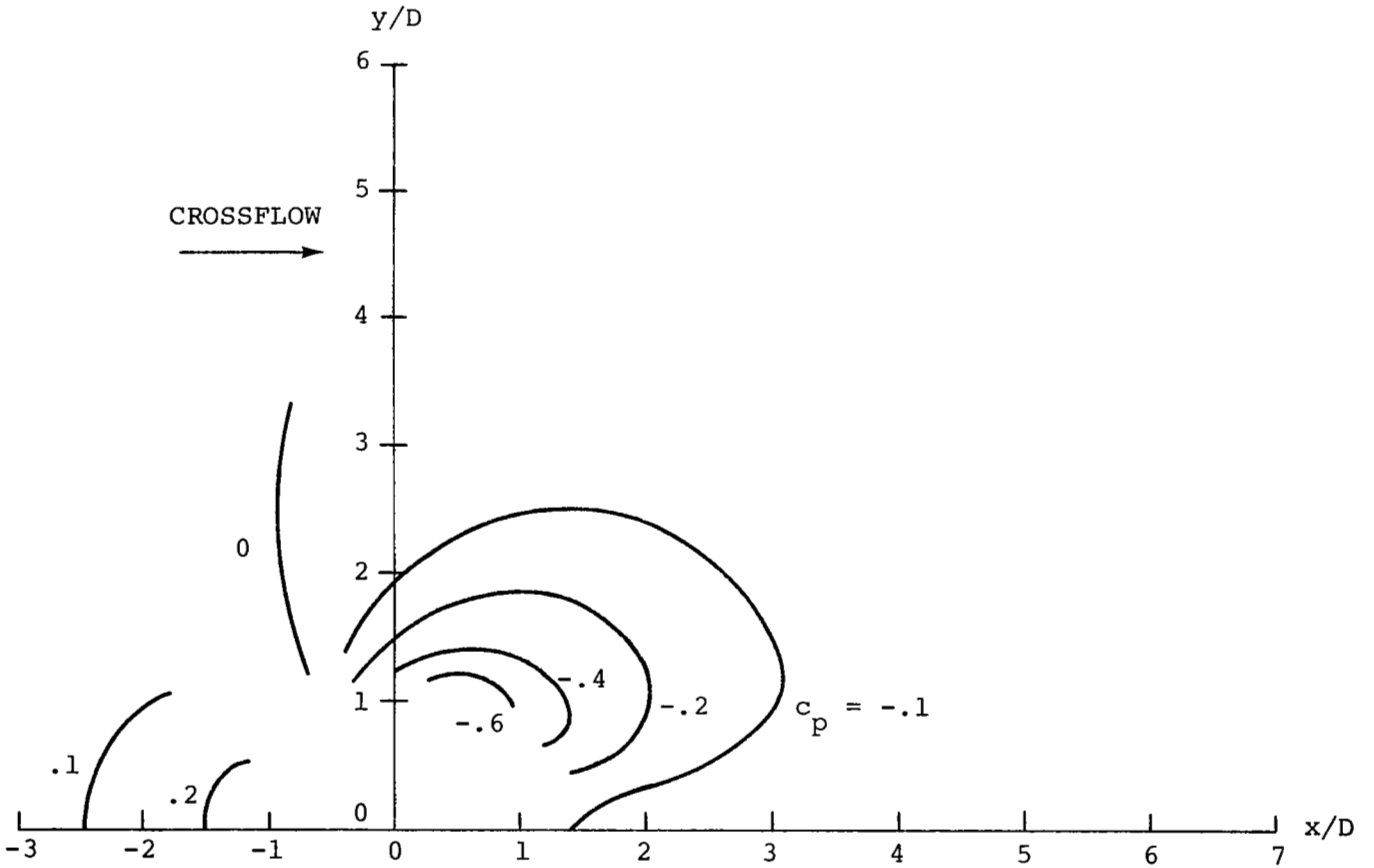

Figure 38. Constant pressure contour data; flat ended plug flush, R = 2.19.

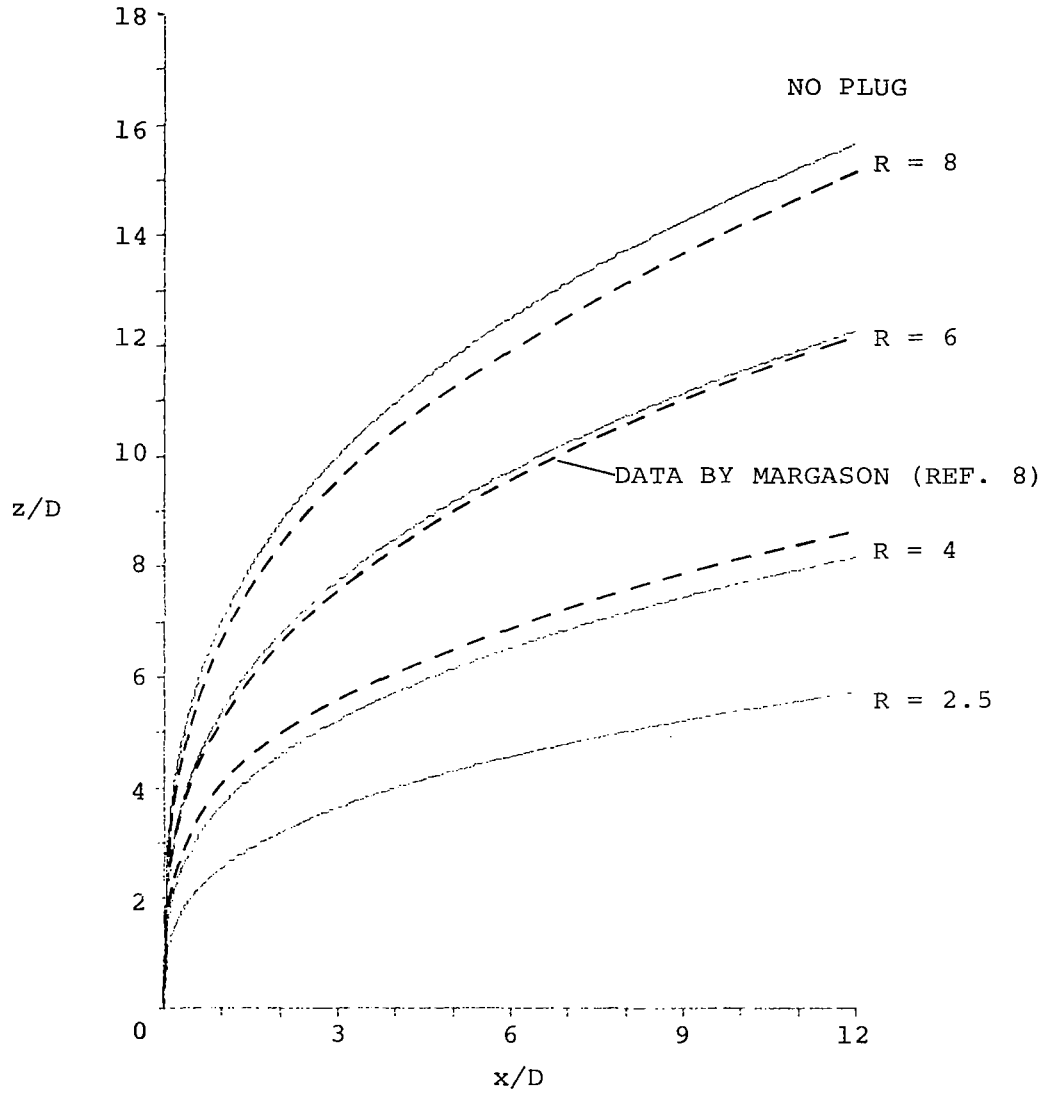

Figure 39. Jet centerline trajectories for configurations with no centerbody.

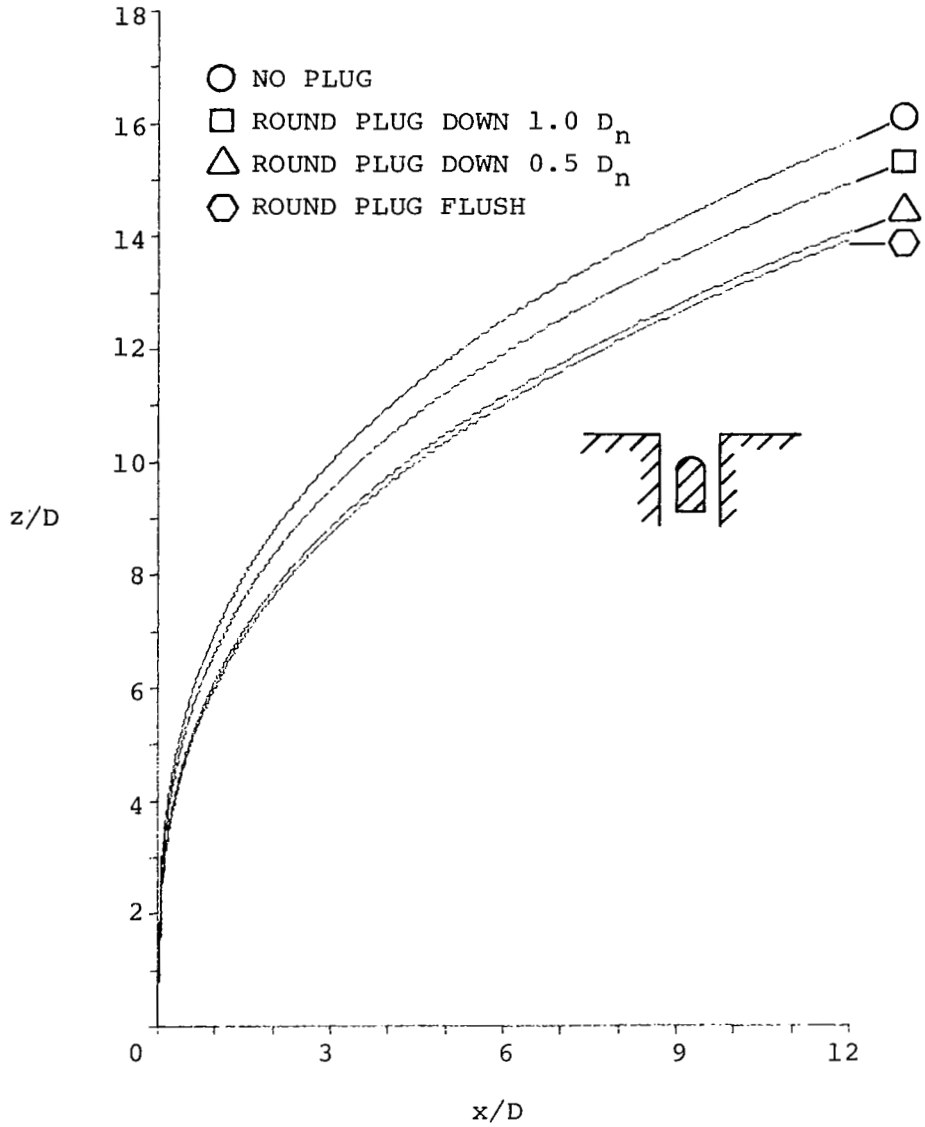

Figure 40. Jet centerline trajectories for configurations with round-ended centerbodies, R = 8.

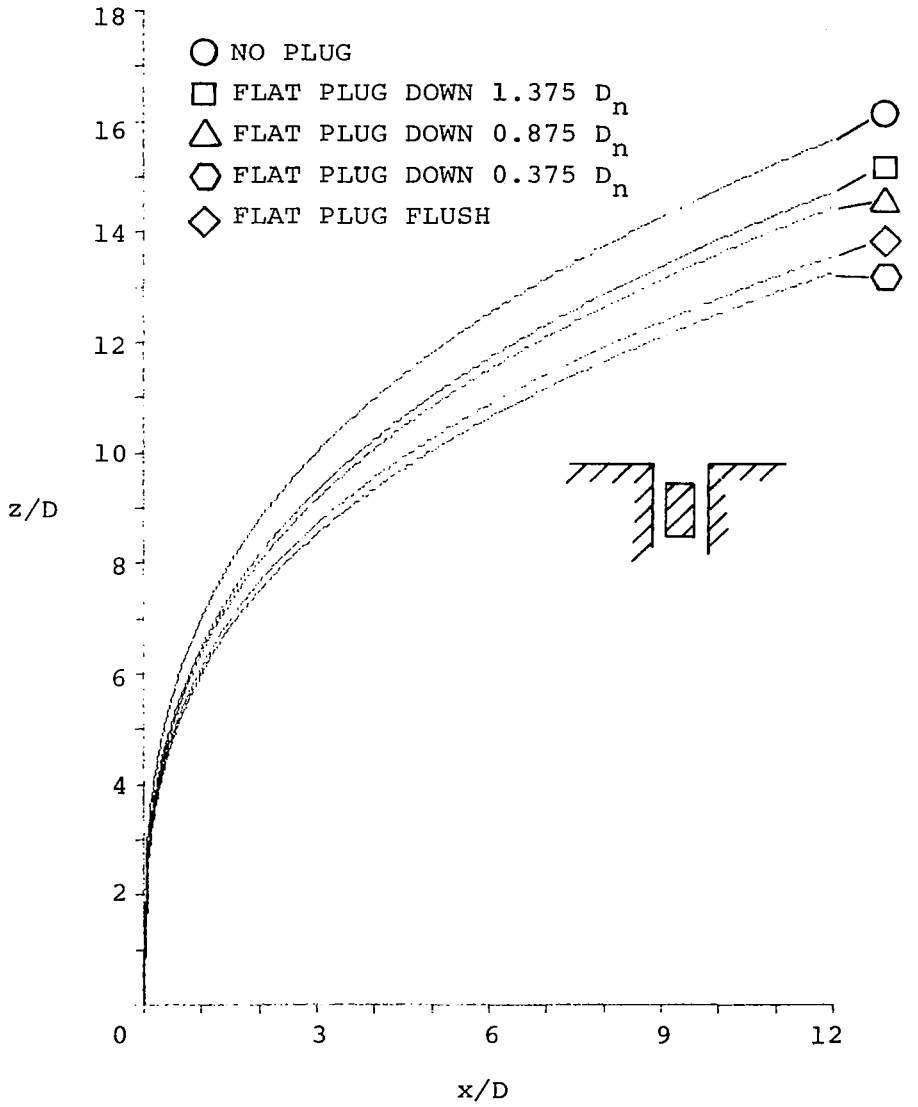

Figure 41. Jet centerline trajectories for configurations with flat ended centerbodies, R = 8.

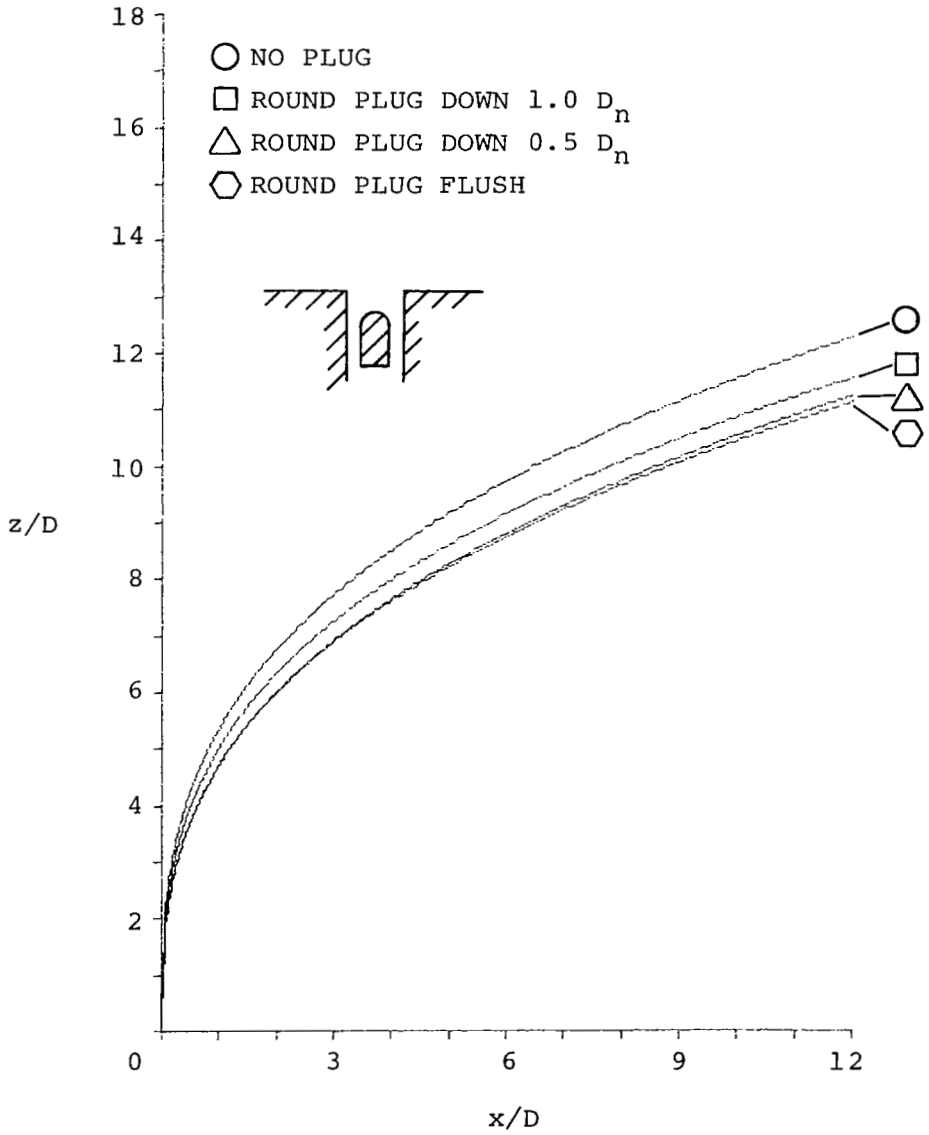

Figure 42. Jet centerline trajectories for configurations with round ended centerbodies, R = 6.

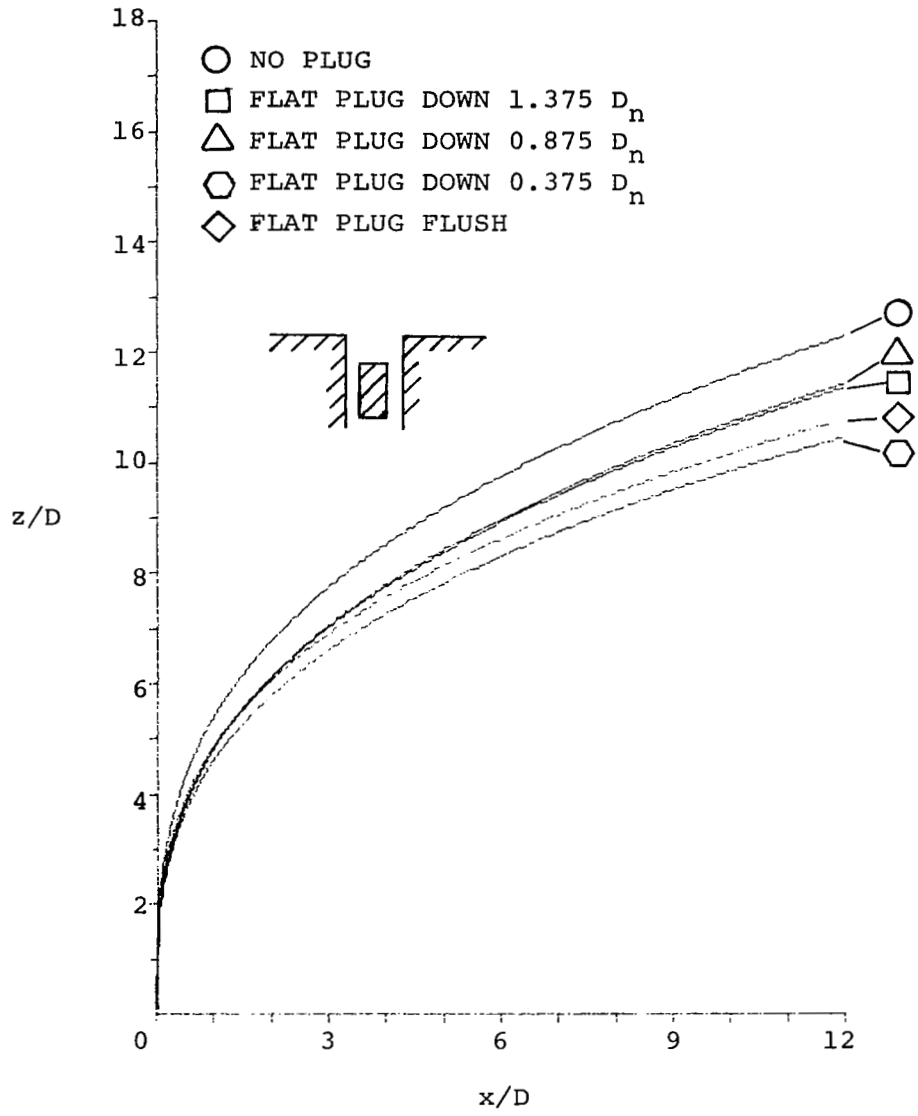

Figure 43. Jet centerline trajectories for configurations with flat ended centerbodies, R = 6.

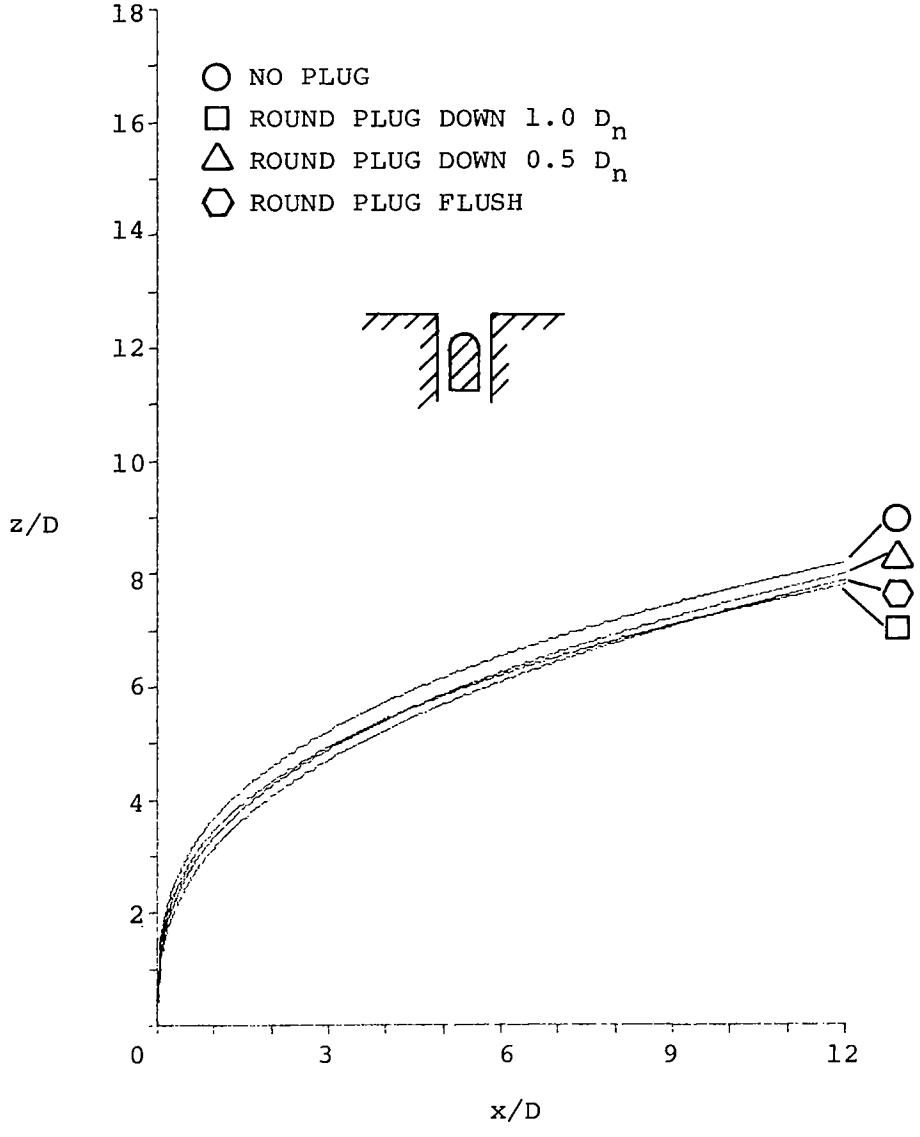

Figure 44. Jet centerline trajectories for configurations with round ended centerbodies, R = 4.

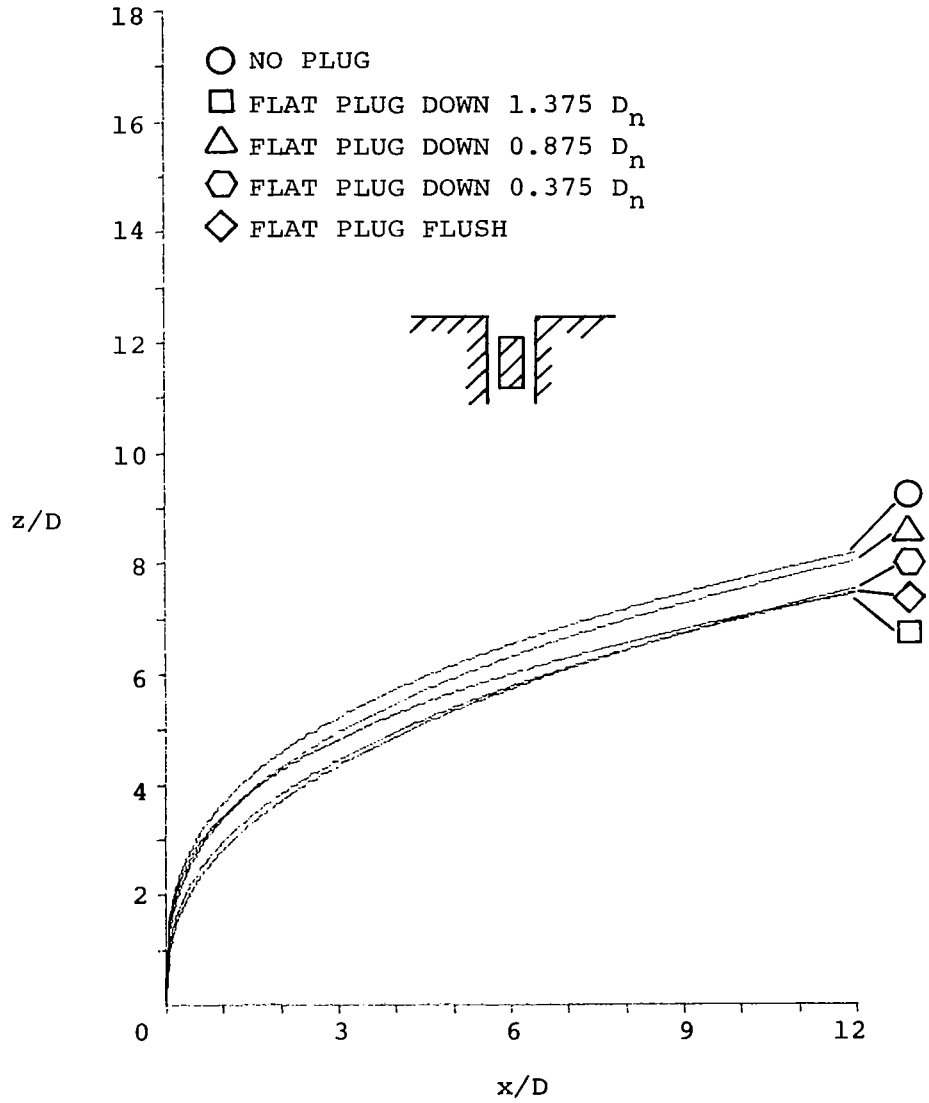

Figure 45. Jet centerline trajectories for configurations with flat ended centerbody, R = 4.

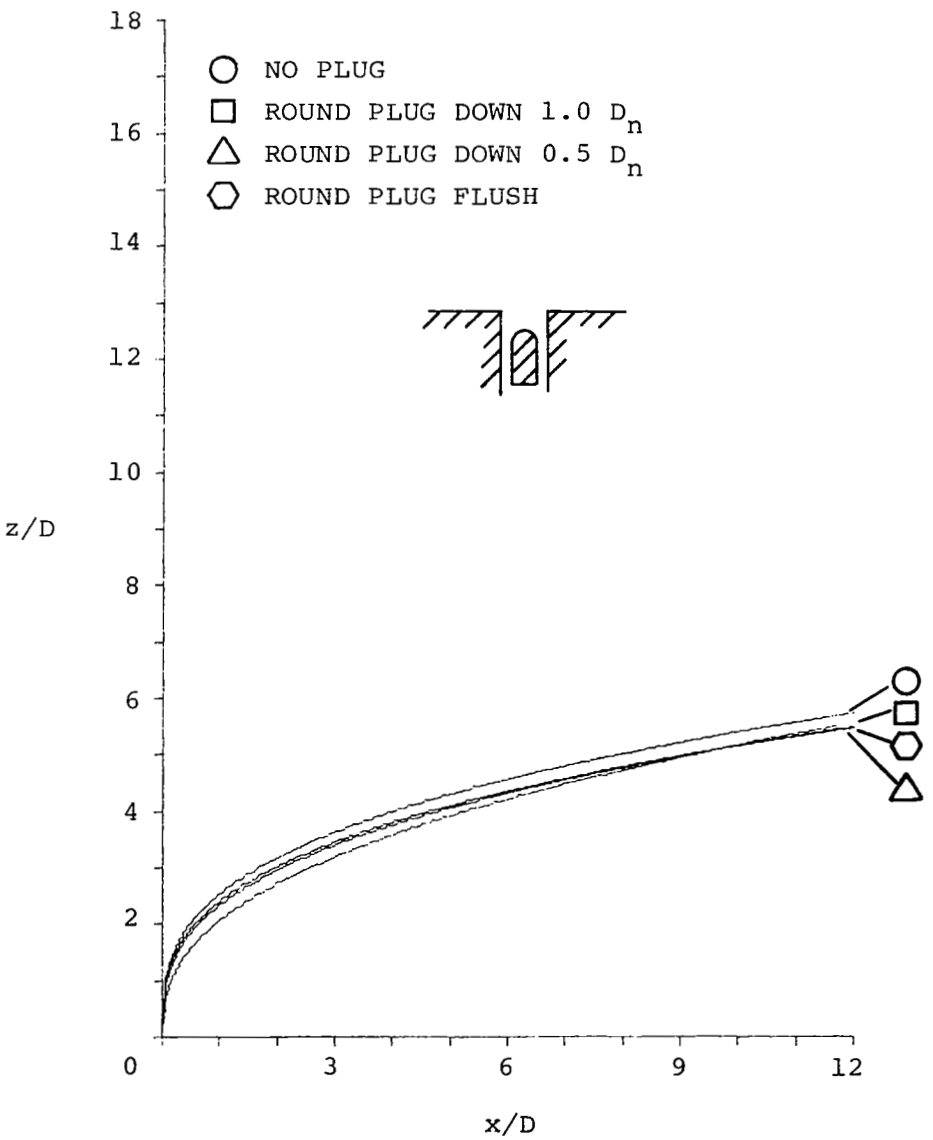

Figure 46. Jet centerline trajectories for configurations with round ended centerbodies, R = 2.5.

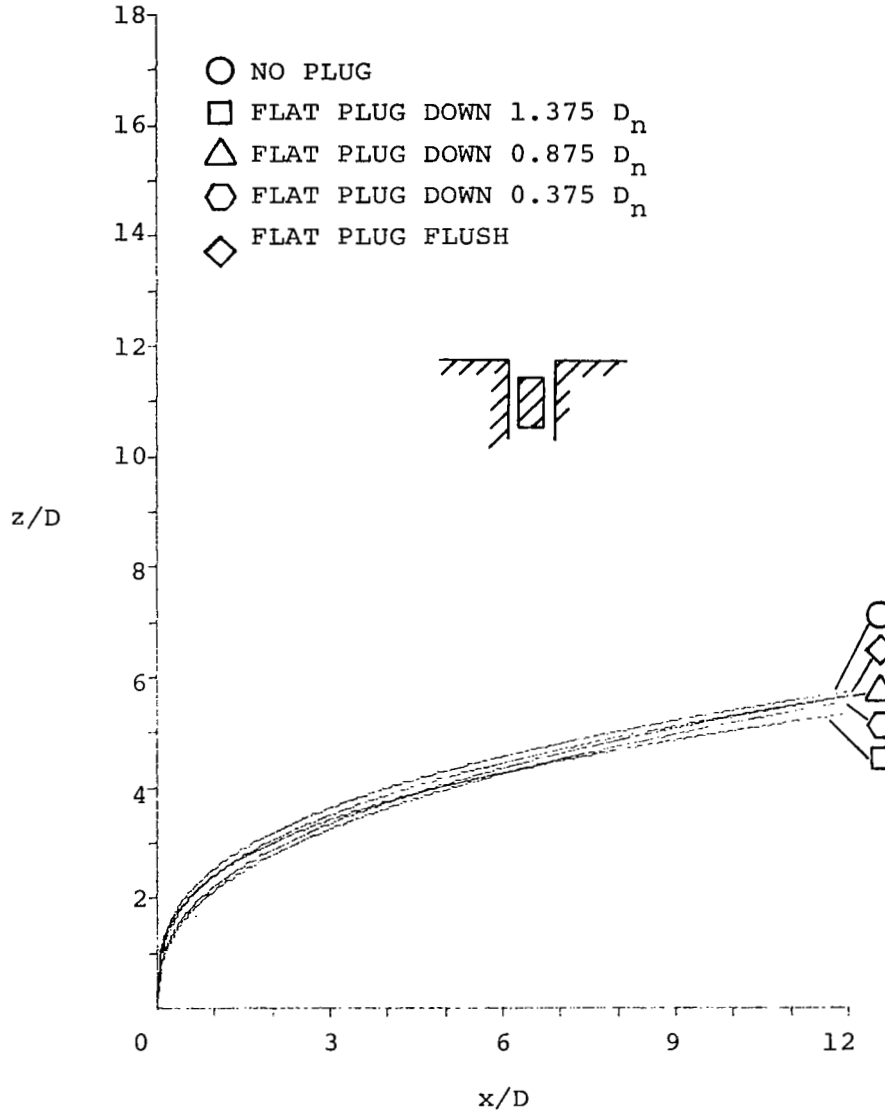

Figure 47. Jet centerline trajectories for configurations with flat-ended centerbodies, R = 2.5.

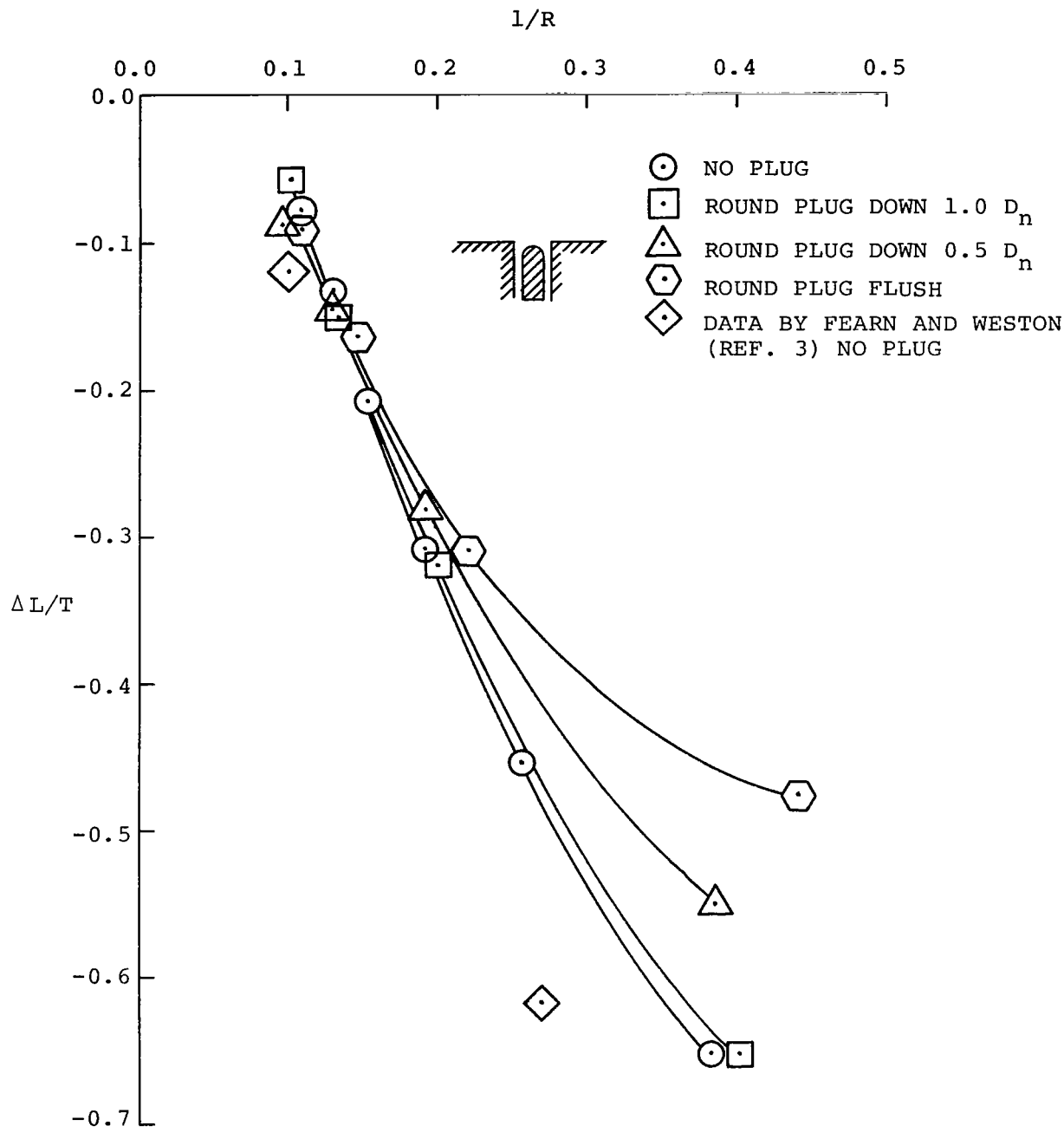

Figure 48. Integrated lift loss for round ended plug configurations compared with unplugged jets.

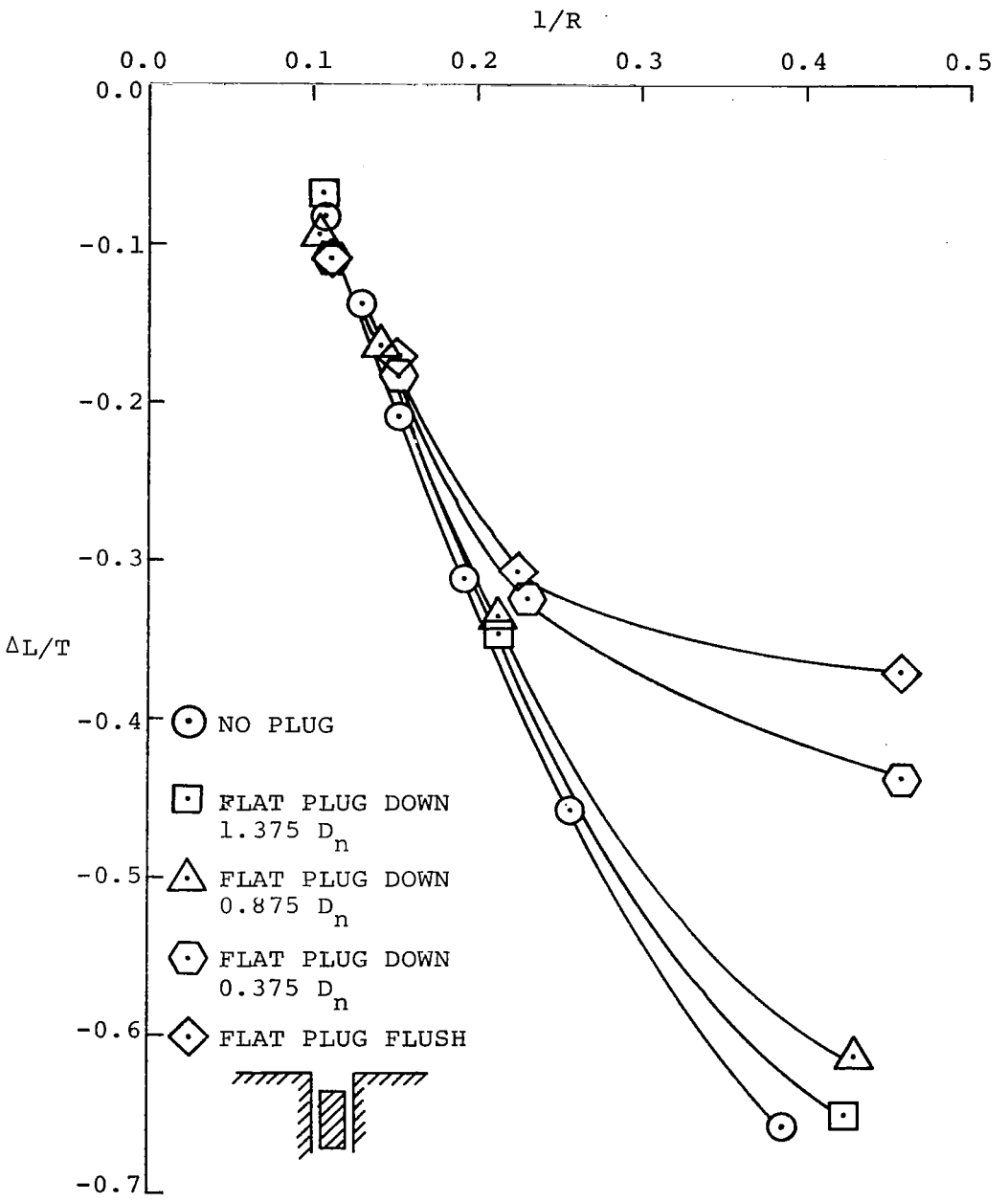

Figure 49. Integrated lift loss for flat tipped plug configurations compared with unplugged jets.

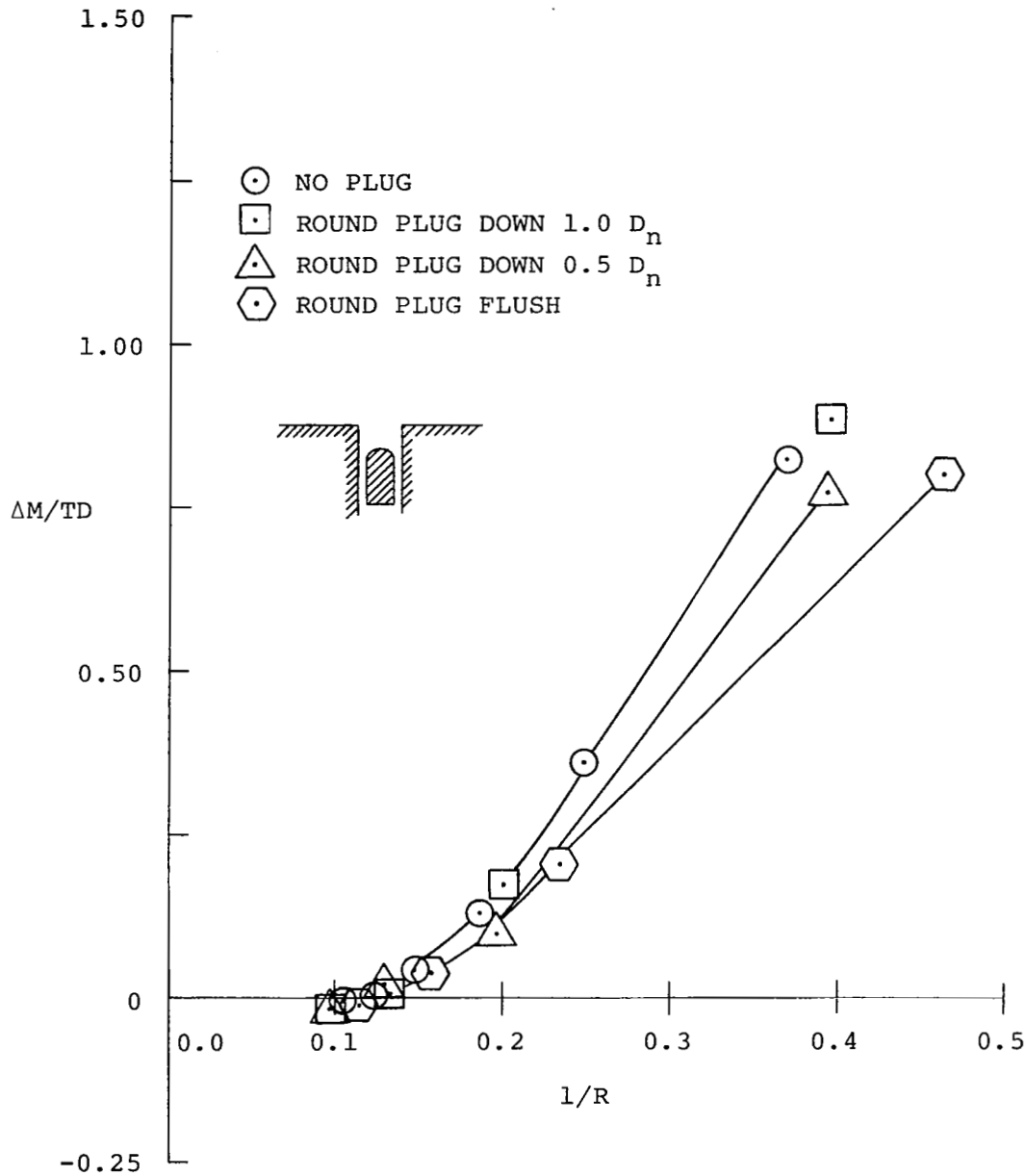

Figure 50. Pitching moment for round ended centerbodies compared with unplugged configurations.

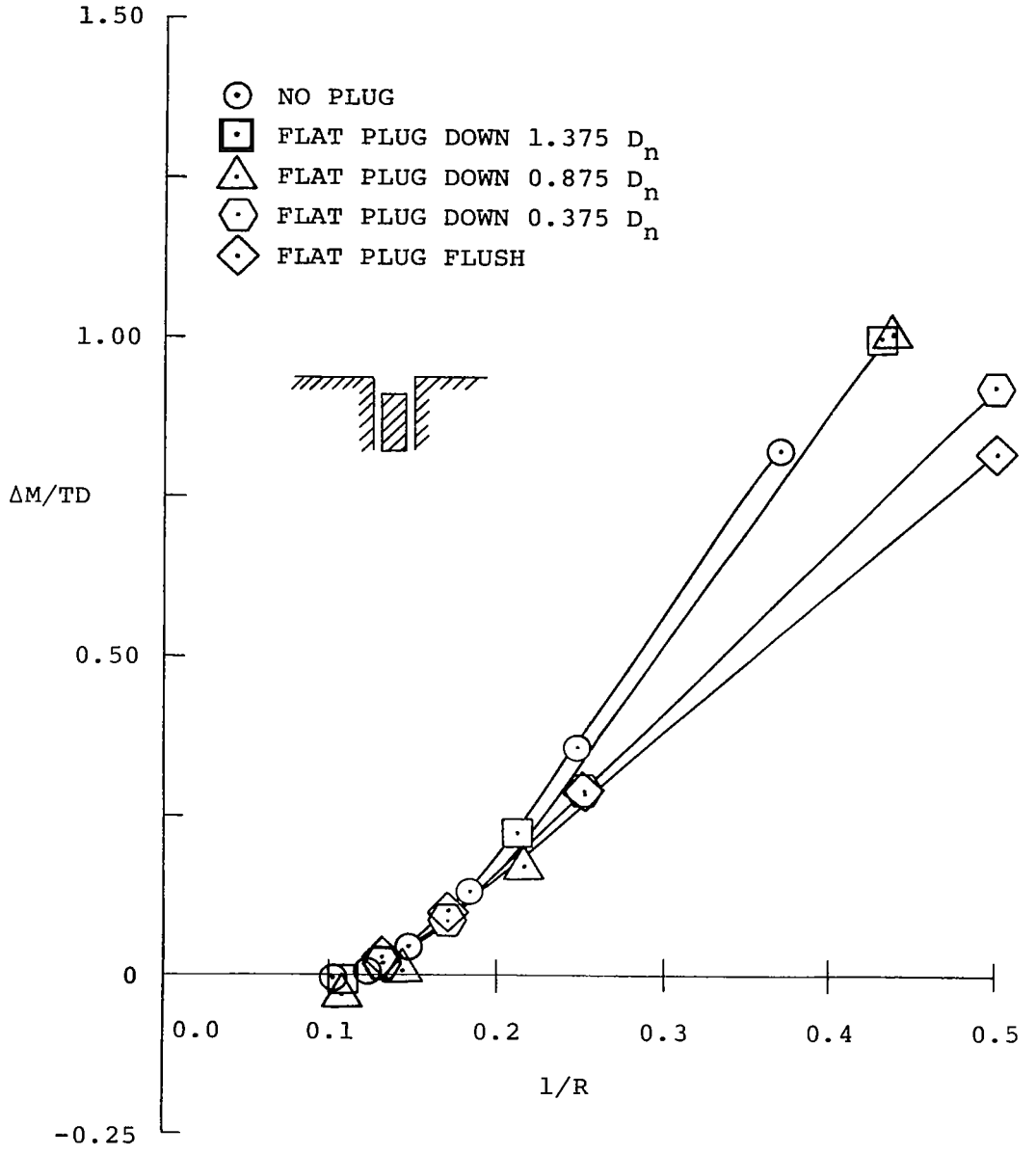

Figure 51. Pitching moment for flat ended centerbodies compared with unplugged configurations.

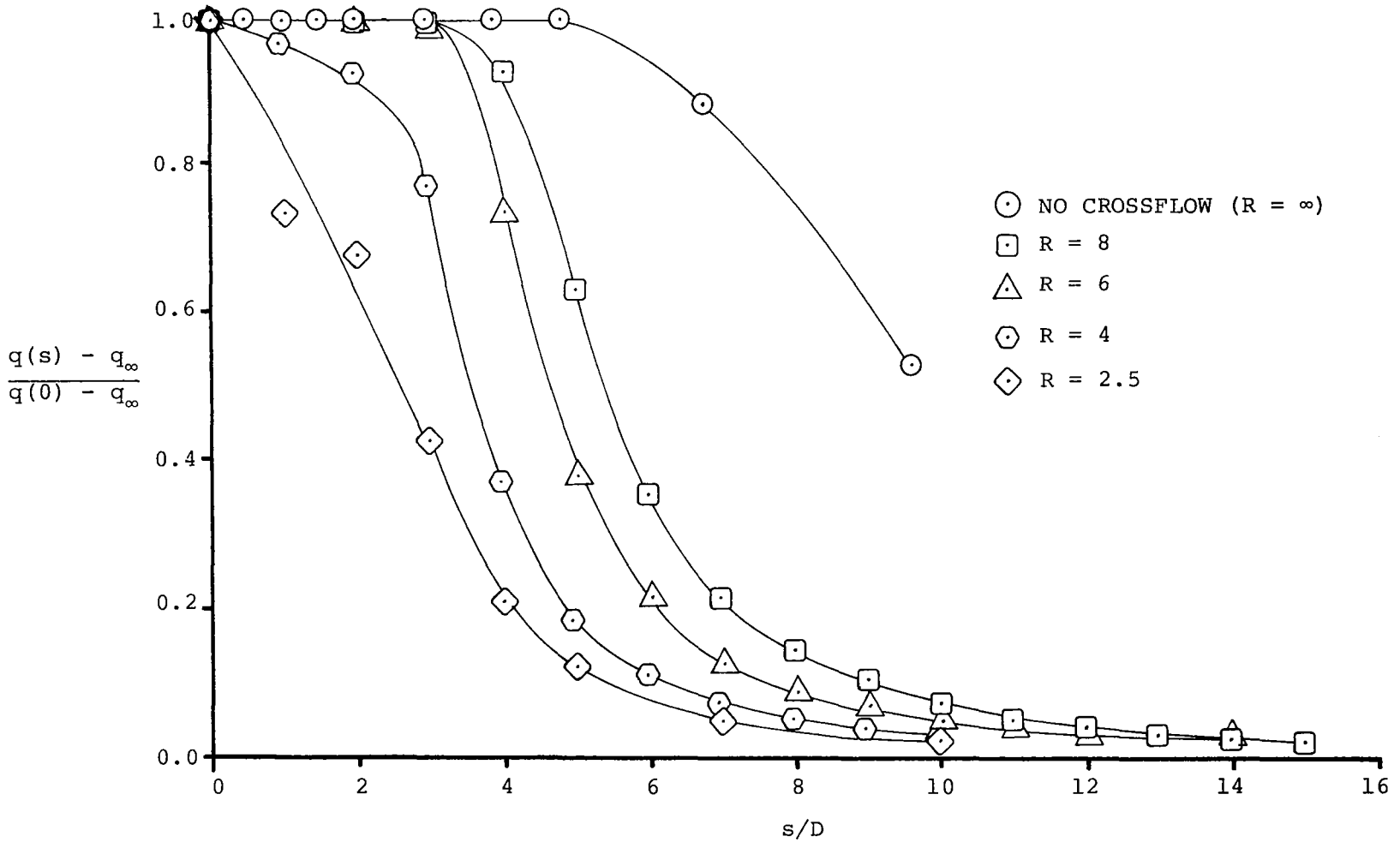

Figure 52. Dynamic pressure decay along jet trajectory. No centerbody in nozzle.

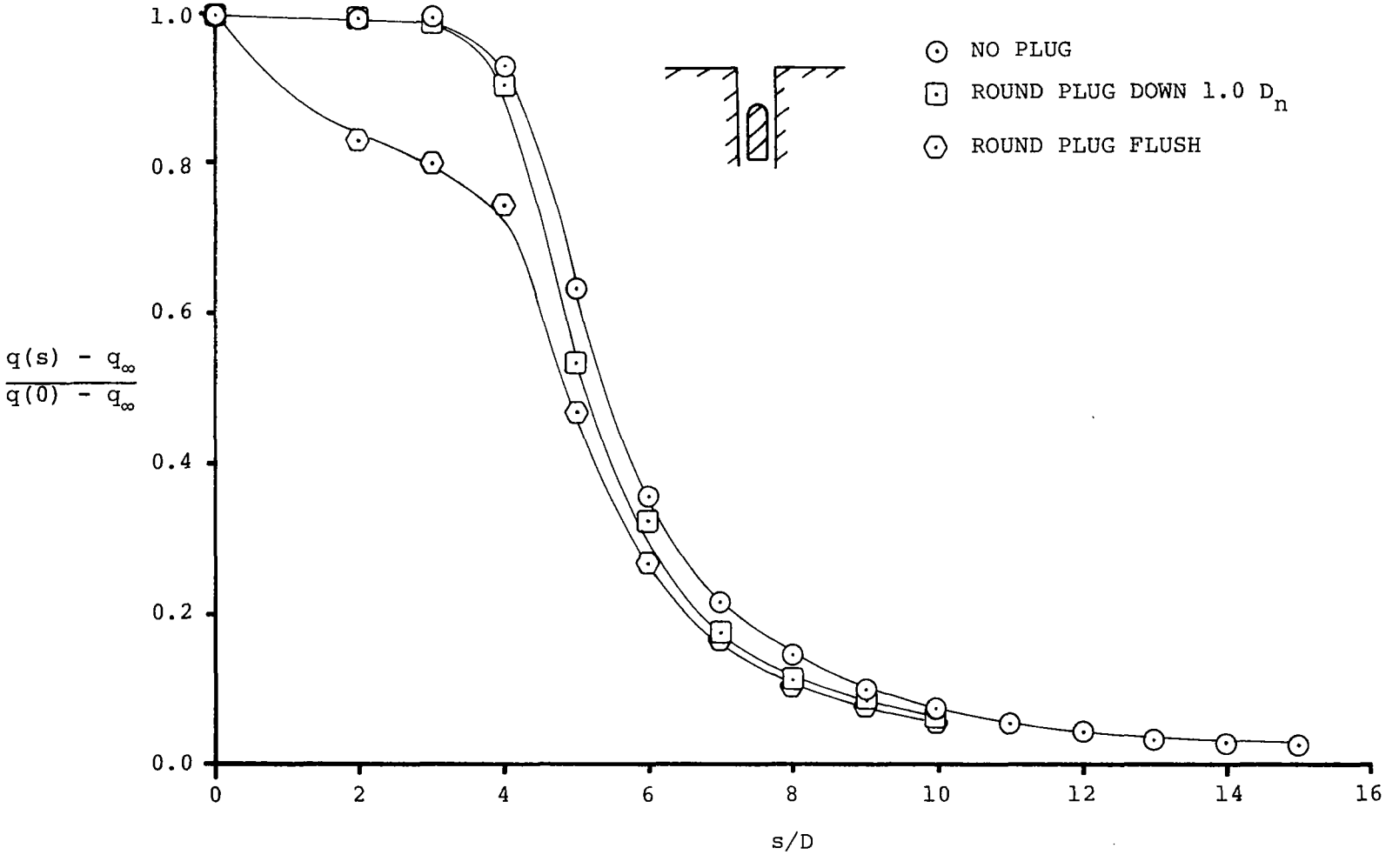

Figure 53. Dynamic pressure decay along jet trajectory R = 8.

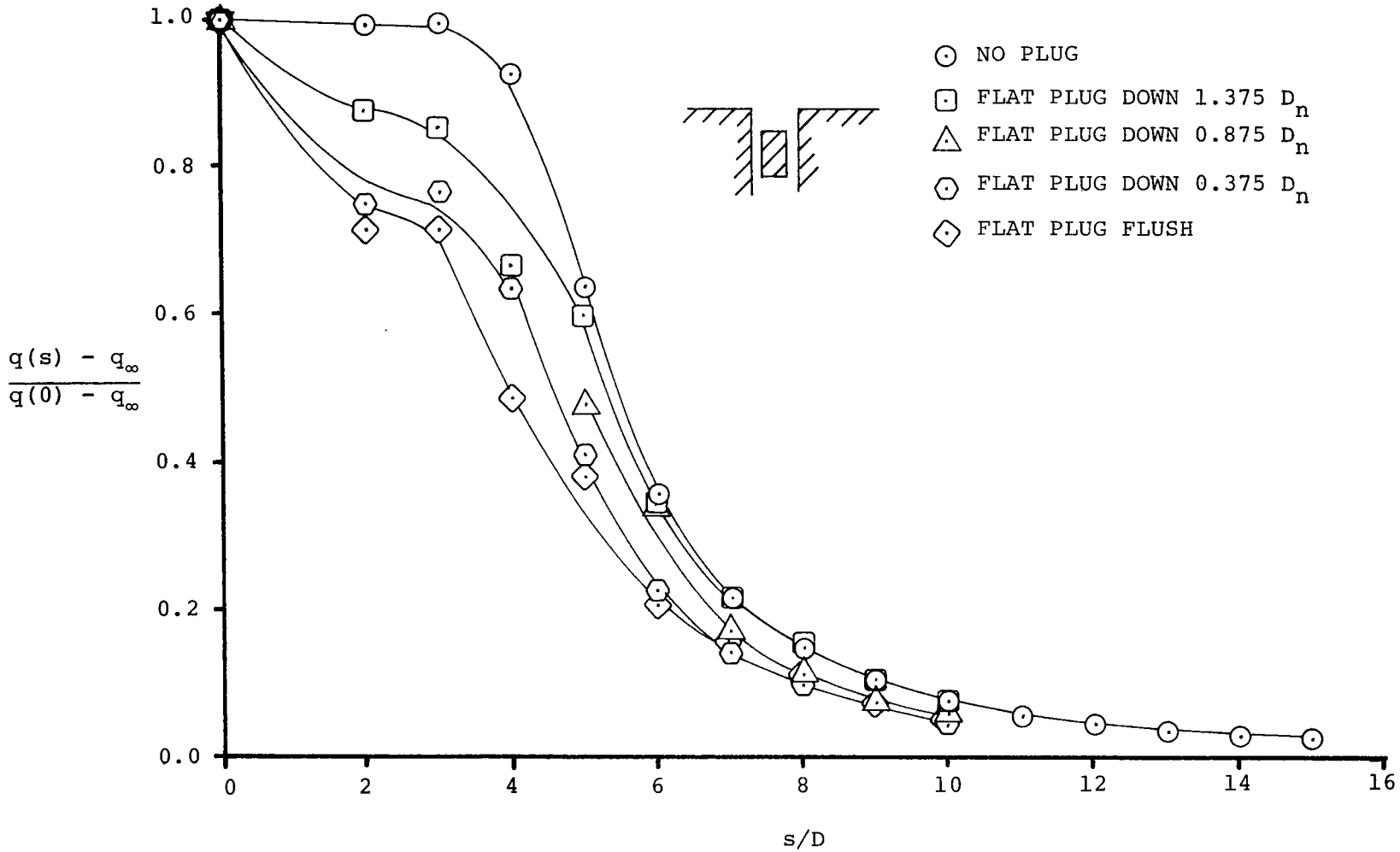

Figure 54. Dynamic pressure decay along jet trajectory R = 8.

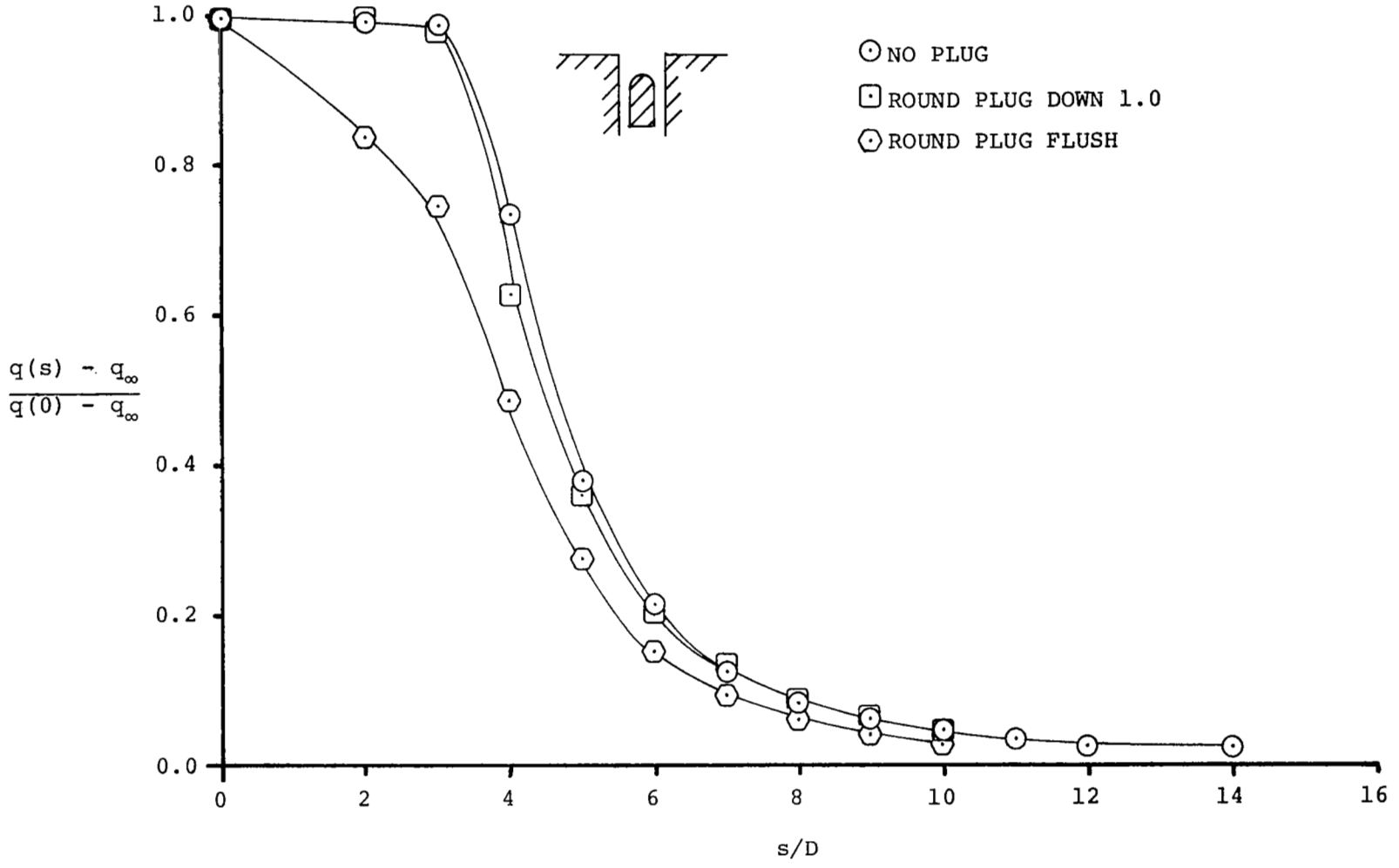

Figure 55. Dynamic pressure decay along jet trajectory R = 6.

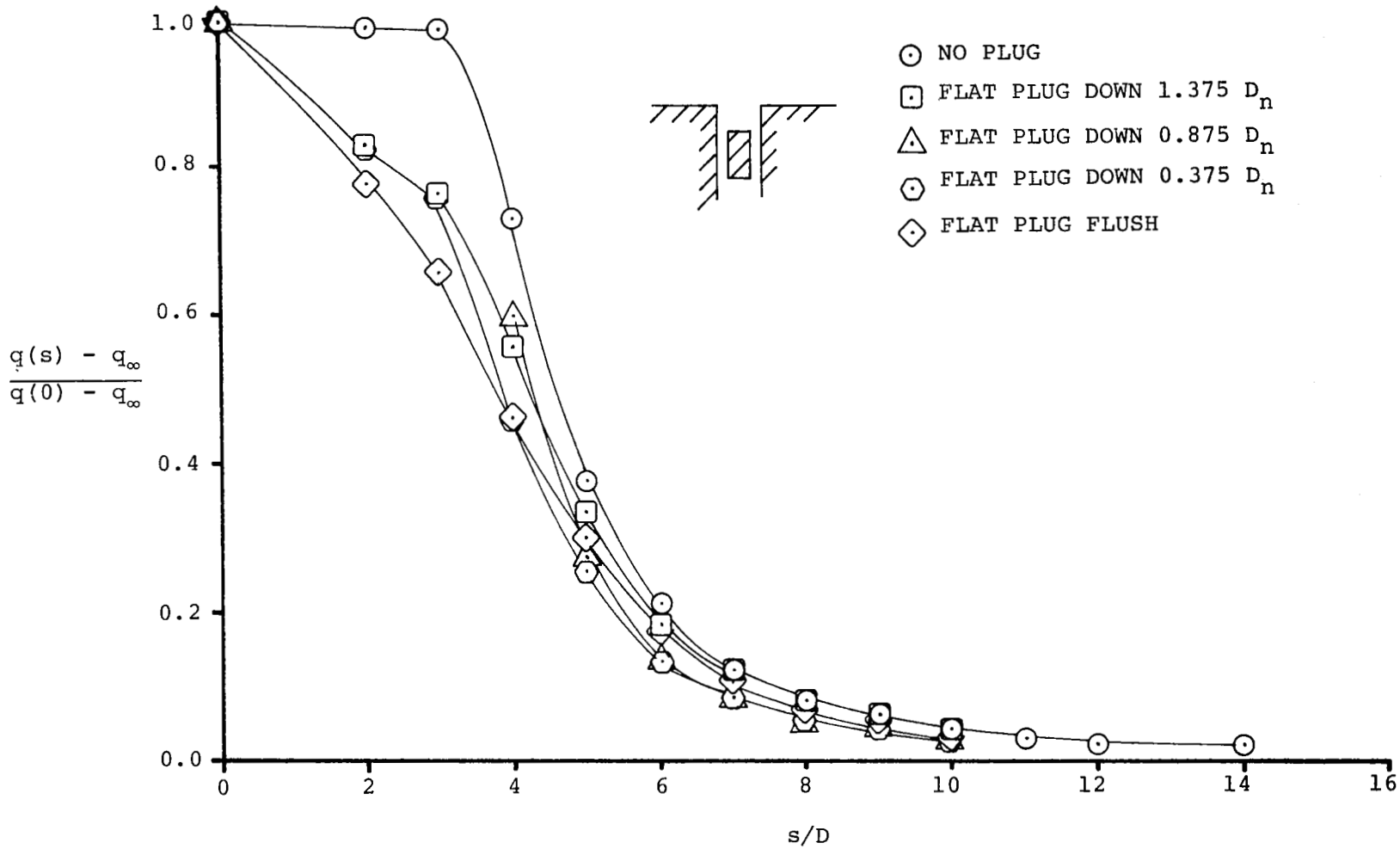

Figure 56. Dynamic pressure decay along jet trajectory R = 6.

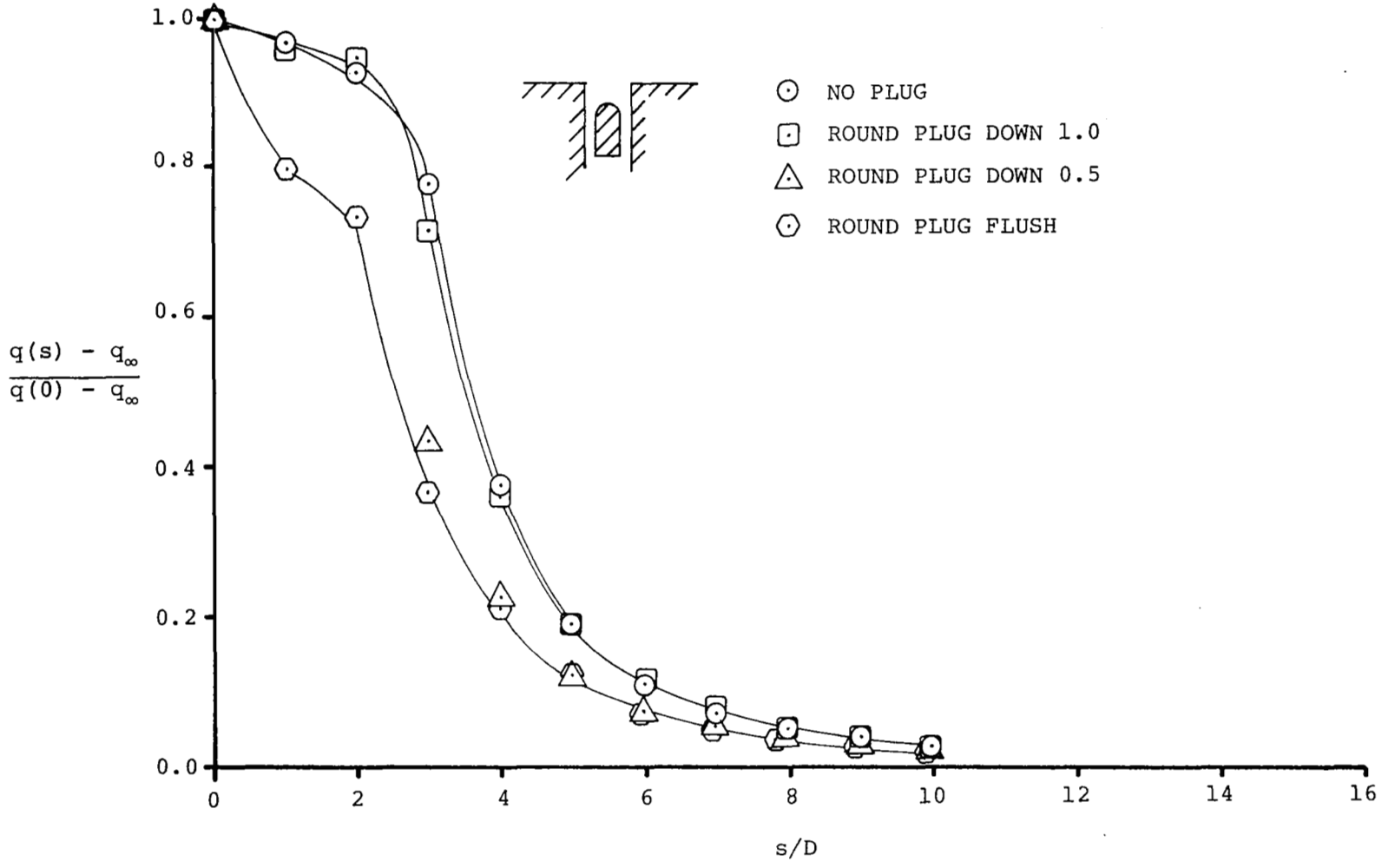

Figure 57. Dynamic pressure decay along jet trajectory R = 4.

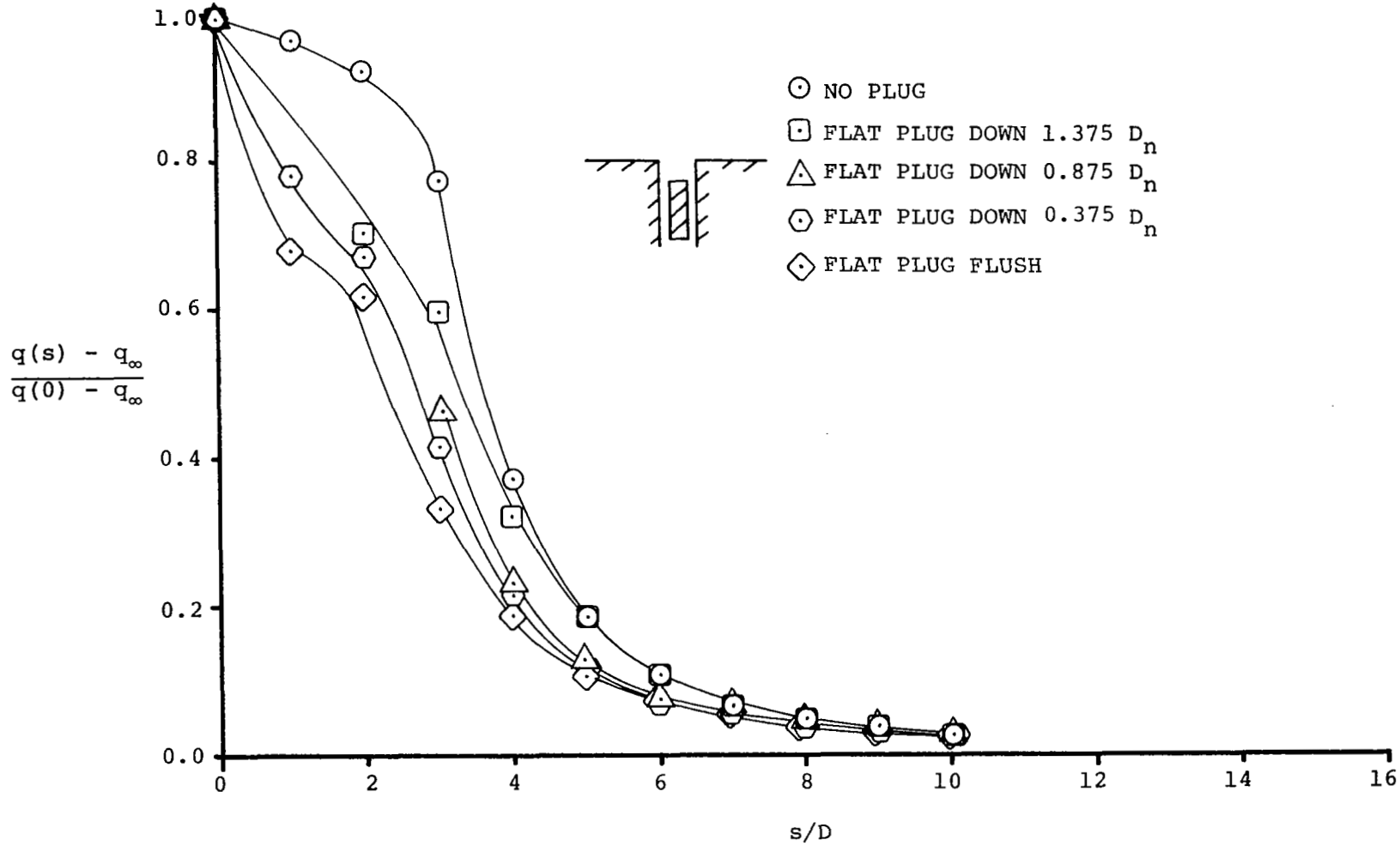

Figure 58. Dynamic pressure decay along jet trajectory R = 4.

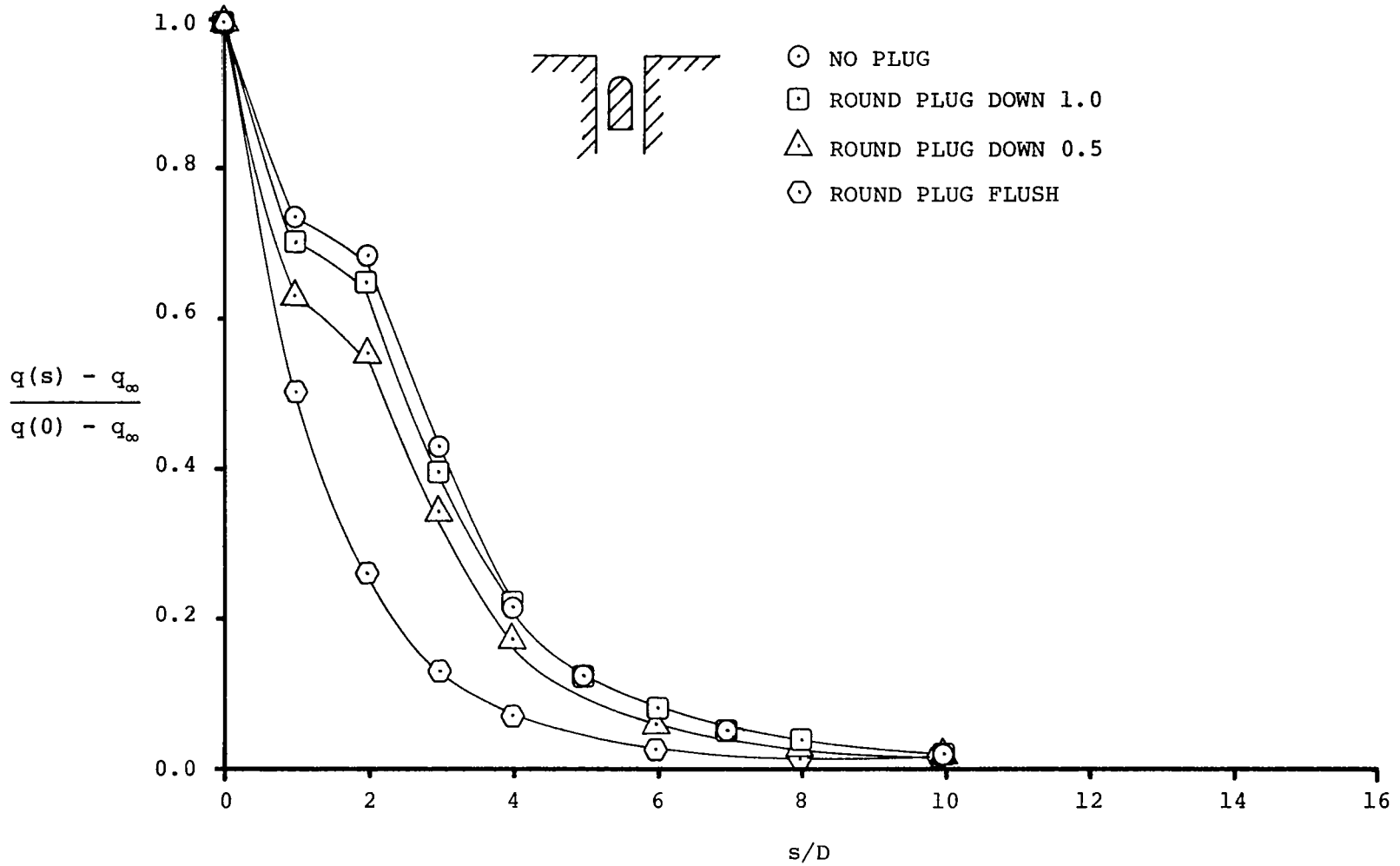

Figure 59. Dynamic pressure decay along jet trajectory R = 2.5.

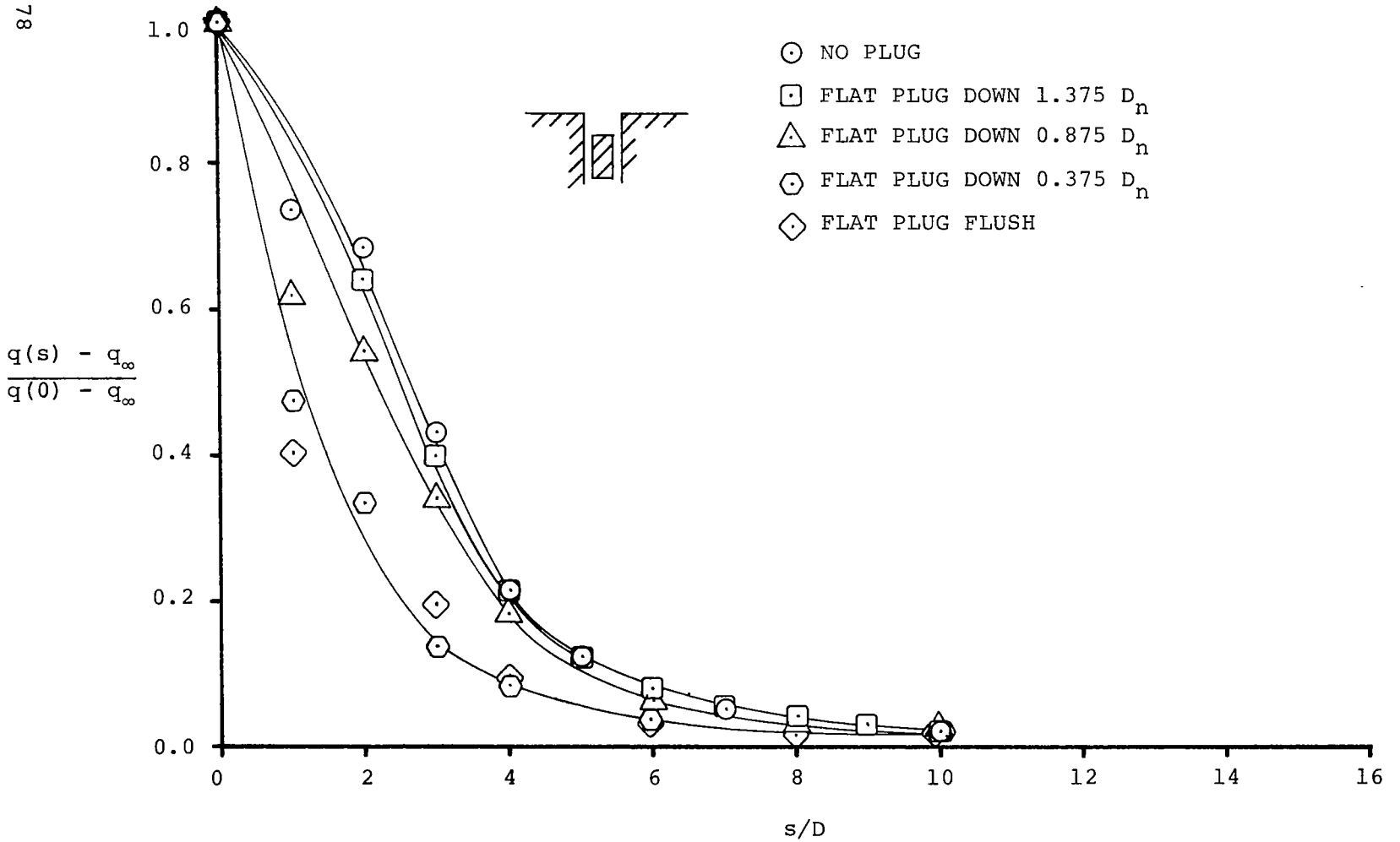

Figure 60. Dynamic pressure decay along jet trajectory R = 2.5.

1. Report No.	2. Government Accession No.	3. Recipient's Catalog No.
NASA CR-2979		

4. Title and Subtitle	5. Report Date
EXPERIMENTAL INVESTIGATION OF EFFECT OF JET DECAY RATE ON JET-INDUCED PRESSURES ON A FLAT PLATE	April 1978
	6. Performing Organization Code
7. Author(s) John M. Kuhlman, Don S. Ousterhout, and Ronald W. Warcup	8. Performing Organization Report No.
9. Performing Organization Name and Address Old Dominion University Research Foundation Norfolk, Virginia 23508	10. Work Unit No.
	11. Contract or Grant No. NGL 47-003-039
12. Sponsoring Agency Name and Address National Aeronautics and Space Administration Washington, DC 20546	13. Type of Report and Period Covered Contractor Report
	14. Sponsoring Agency Code

15. Supplementary Notes

Langley Technical Monitor: Richard J. Margason
Final Report

16. Abstract

An experimental study of the interaction between a lift jet and an aircraft wing for a jet VTOL aircraft was performed for the simplified model of an unheated, subsonic, circular jet exiting at right angles to a flat plate into a uniform subsonic crosswind. The effects of jet dynamic pressure decay rate upon the jet location and jet-induced pressure distribution on the plate were studied over a range of jet-to-crossflow velocity ratios of $2.2 \leq R \leq 10$. Jet decay rate was varied through use of cylindrical centerbodies with flat or hemispherical tips submerged in the jet nozzle at various depths below the jet exit plane.

Quicker jet dynamic pressure decay, caused by the presence of a centerbody, resulted in reductions in the jet-induced lift loss by as much as 45 percent relative to values for jets with no centerbody. These reductions in lift loss were observed at the larger values of crossflow velocity.

17. Key Words (Selected by Author(s))	18. Distribution Statement
Jet in a crossflow, Jet-induced pressures, Jet decay rate, Jet VTOL aircraft	Unclassified-Unlimited Subject Category 05

19. Security Classif. (of this report)	20. Security Classif. (of this page)	21. No. of Pages	22. Price*
Unclassified	Unclassified	78	$6.00

*For sale by the National Technical Information Service, Springfield, Virginia 22151

NASA-Langley, 1978